Journal of
Big Data & Smart City

A Geometry-Grounded Framework for Explainable Symmetry Quantification and Asymmetry Localization in Robotic CAD Parts
Najla Al Amri

AI Based Adaptive Behavioral Monitoring for Handicap Persons Using Smart Glove
Noor Aldeen Mohamed Zaidan, Dr. Muhammad Nauman Bashir, Arsalan Asif

Automatic Sleep Stage Classification and Sleep Quality Assessment Using EEG Signals and Convolutional Neural Networks
Khalid Al Jassasi , Jayasankar Srilla

AI-Based Smart Child Life Detection and Rescue System in Vehicles
Alkawthar Moosa Al Ruqaishi, Ajitha Sajan

An Embedded AI System for Skin Cancer Screening Using MobileNetV2 and Edge Inference
Rudaina Fahad Al-Farsi, Mohammed Izaan Kari, Shaik Asif Hussain

EMG-Controlled Prosthetic Arm for Upper-Limb Amputees
Malak Marhoon Al Harrasi, Shaik Asif Hussain

ISSN (Print) : 2706-7912
ISSN (Online) : 2788-4112

2026

VOLUME 6
ISSUE 2
SPRING 2026

www.mjbdsc.org

Journal of
Big Data &
Smart City

Message from the Editor in Chief

On behalf of my co-editors (Prof. Ahmed Nawaz Hakro & Prof. Anupam Srivastav) and other members of Editorial Board, I am delighted to bring this Volume 6, Issue 2 of the Journal of Big Data and Smart City (JBDSC). This Issue, like its predecessor issues, is an open access journal, with an Arabic translation of the Abstract of every paper published.

The Journal of Big Data and Smart City (JBDSC) is providing an exciting platform to scholars, researchers, other related professionals, policy makers, and especially to the students, to showcase their scholarly ideas and research in Smart City applications, building on Big Data technologies. The journal has been accessible, engaging and motivating to the young researchers, as all the 6 papers in this Issue are joint work with students.

The journal has been successful in fulfilling its objective to publish original interdisciplinary research. All the published papers, which cover the areas of Expert Systems, IoT, Mobile Applications, etc, have been subjected to a double-blind review process. The multidisciplinary collaborative work combining multiple fields in wider possible contexts, published in this issue integrates theoretical, experimental, and computational approaches, providing solutions towards smart city/ information and communication technologies themes.

I am thankful to those who submitted papers, both individually or collaboratively from academia and industry. I take this opportunity to also thank all those who contributed in bringing out this issue of the Journal. I am extremely thankful for the continuous support of MoHERI and MoI for allowing this scholarly publication.

Special thanks to all the members of the Editorial Board for dedicating their valuable time and energy which made it possible for this issue to be published well in time.
Wishing the readers of the articles of this journal making a fruitful contribution in their future research pursuits.

Dr. Alya Al Farsi
Editor in Chief
Journal of Big Data and Smart City

ISSN (Print) : 2706-7912
ISSN (Online) : 2788-4112

VOLUME 6
ISSUE 2
SPRING 2026
www.mjbdsc.org

Journal of Big Data & Smart City

VOLUME 6 ISSUE 2 SPRING 2026

ISSN (Print) : 2706-7912
ISSN (Online) : 2788-4112

Editorial

www.mjbdsc.org

Journal of
Big Data & Smart City

Editorial

VOLUME 6
ISSUE 2
SPRING 2026

ISSN (Print) : 2706-7912
ISSN (Online) : 2788-4112

A Geometry-Grounded Framework for Explainable Symmetry Quantification and Asymmetry Localization in Robotic CAD Parts
Najla Al Amri, Page: 1 - 8

AI Based Adaptive Behavioral Monitoring for Handicap Persons Using Smart Glove
Noor Aldeen Mohamed Zaidan, Dr. Muhammad Nauman Bashir, Arsalan Asif, Page: 9 - 20

Automatic Sleep Stage Classification and Sleep Quality Assessment Using EEG Signals and Convolutional Neural Networks
Khalid Al Jassasi , Jayasankar Srilla, Page: 21 - 28

AI-Based Smart Child Life Detection and Rescue System in Vehicles
Alkawthar Moosa Al Ruqaishi, Ajitha Sajan, Page: 29 - 38

An Embedded AI System for Skin Cancer Screening Using MobileNetV2 and Edge Inference
Rudaina Fahad Al-Farsi, Mohammed Izaan Kari, Shaik Asif Hussain, Page: 39 - 51

EMG-Controlled Prosthetic Arm for Upper-Limb Amputees
Malak Marhoon Al Harrasi, Shaik Asif Hussain, Page: 52 - 61

www.mjbdsc.org

A Geometry-Grounded Framework for Explainable Symmetry Quantification and Asymmetry Localization in Robotic CAD Parts

Najla Al Azri
Department of Computing and Electronics Engineering
Middle East College
Muscat, Sultanate of Oman
22F22887@mec.edu.om

Received: 2nd May 2026; Revised: 5th June 2026;

Accepted: 10th July 2026

***Abstract* — Symmetry analysis is important in robotic computer-aided design (CAD) because many parts are intended to be nearly balanced while still containing functional asymmetries such as holes, brackets, mounting surfaces, and cable-routing features. This paper presents a geometry-grounded framework for explainable symmetry quantification and asymmetry localization in robotic CAD parts. The method samples CAD meshes into normalized point clouds, evaluates reflection consistency along the engineering-aligned X, Y, and Z axes, computes scale-aware asymmetry scores, extracts compact invariant descriptors, and localizes high-deviation regions using heatmaps and worst-region bounding boxes. A lightweight classifier is used only as an optional axis-suggestion module; the final interpretation remains based on deterministic geometric validation. Experiments were conducted on seven robotic CAD parts, an extended 53-model CAD benchmark, and a NASA RASSOR case study. On the updated extended benchmark evaluation, the revised D model achieved 69.2% agreement with the one-way geometric baseline across 530 seed-controlled runs and produced a more balanced prediction distribution across X, Y, and Z, reducing the earlier Y-axis collapse observed in the previous conference version. Internal validation of the optional D classifier achieved 76.85% validation accuracy and 0.7709 macro-F1 on 540 pseudo-labelled samples. To examine generalization under a stricter setting, an expanded ABC-derived dataset was also constructed using 1000 CAD models and 10000 seed-controlled samples with a CAD-model-level split. On the unseen test split, the expanded E classifier achieved 64.87% test accuracy and 0.6493 macro-F1. The results show that the main contribution is not standalone prediction, but a reproducible inspection workflow that combines measurable geometric evidence with interpretable localization for smart engineering and robotic CAD analysis.**

Keywords - CAD analysis; point cloud; symmetry quantification; geometric validation; asymmetry localization; smart manufacturing

الخلاصة ـ يُعدّ تحليل التماثل أمرًا مهمًا في التصميم بمساعدة الحاسوب للأنظمة الروبوتية، إذ تُصمَّم كثير من القطع لتكون شبه متوازنة مع احتوائها في الوقت نفسه على عدم تماثل وظيفي مثل الثقوب والحوامل وأسطح التثبيت ومسارات الكابلات .تقدّم هذه الورقة إطارًا قائمًا على الهندسة الرياضية للقياس القابل للتفسير للتماثل وتحديد الروبوتية .تعتمد الطريقة على أخذ عينات من CAD مواضع عدم التماثل في قطع لتكوين سحابات نقاط مُطبَّعة، وتقييم اتساق الانعكاس على المحاور CAD نماذج وحساب درجات عدم تماثل مراعية للمقياس، واستخراج ،Zو Yو X الهندسية واصفات ثابتة مُختصرة، وتحديد المناطق ذات الانحراف العالي باستخدام الخرائط الحرارية وصناديق الإحاطة لأسوأ المناطق .ويُستخدم مُصنِّف خفيف كوحدة اختيارية لاقتراح المحور فقط، بينما يبقى التفسير النهائي مستندًا إلى التحقق الهندسي الحتمي. روبوتية، ومجموعة مرجعية موسّعة تضم CAD 53 أُجريت التجارب على سبع قطع التابع لوكالة ناسا .وفي التقييم المرجعي RASSOR نموذجًا، ودراسة حالة لروبوت المُنقّح توافقًا بنسبة 69.2 %مع الأساس الهندسي D الموسّع المُحدَّث، حقق النموذج أحادي الاتجاه عبر 530 تشغيلًا مضبوط البذور، وأنتج توزيعًا أكثر توازنًا للتنبؤات عبر الذي لوحظ في النسخة السابقة .وبلغت دقة Y المحاور الثلاثة، مما قلّل انهيار المحور تساوي macro-F1 نسبة 76.85 %مع قيمة D التحقق الداخلي للمُصنِّف الاختياري على 540 عينة موسومة آليًا .ولاختبار التعميم في إعداد أكثر صرامة، أُنشئت 0.7709 و10000 عينة CAD تضم 1000 نموذج ABC مجموعة بيانات موسّعة مشتقة من وعلى قسم الاختبار غير .CAD مضبوطة البذور مع تقسيم على مستوى نموذج تساوي macro-F1 دقة 64.87 %وقيمة E المرئي، حقق المُصنِّف الموسّع وتُظهر النتائج أن الإسهام الرئيس ليس التنبؤ المستقل، بل سير عمل تفتيشي .0.6493 قابل للتكرار يجمع بين الأدلة الهندسية القابلة للقياس والتحديد المكاني القابل للتفسير الروبوتي CAD في الهندسة الذكية وتحليل.

سحابة النقاط، قياس التماثل، التحقق ،CAD الكلمات المفتاحية – تحليل الهندسي، تحديد مواضع عدم التماثل، التصنيع الذكي

I. INTRODUCTION

Symmetry is a useful design principle in mechanical engineering, robotics, and computer-aided design (CAD). It reduces design complexity, supports part reuse, and can simplify inspection. In practice, however, robotic components are rarely perfectly symmetric [1], [2]. A part may be globally balanced while still containing one-sided features such as fastener holes, brackets, cable-routing paths, mounting offsets, and clearances. These features are often intentional rather than defective [3]. Therefore, a practical CAD inspection tool should not only classify a model as symmetric or asymmetric; it should measure how strongly the model agrees with a reflected version of itself and show where the largest deviations occur.

This paper presents a geometry-grounded framework for explainable symmetry quantification and asymmetry localization in robotic CAD parts. The framework converts a CAD mesh into a normalized point cloud, evaluates reflection consistency along the X, Y, and Z axes, computes normalized asymmetry metrics, extracts compact invariant descriptors, and visualizes localized deviations using heatmaps and a worst-region bounding box. A lightweight classifier is included only as an optional axis-suggestion module. Its output is treated as a hypothesis, not as final evidence. The final interpretation is based on deterministic reflection scores and localized deviation patterns.

The work fits the scope of intelligent engineering systems and smart manufacturing because it links geometric theory with a practical inspection workflow. In a digital design or quality-control setting, the method can help engineers compare candidate symmetry axes, quantify deviations, and localize functional asymmetries before downstream manufacturing or reporting. The contribution is intentionally positioned as an explainable decision-support workflow, not as a claim of a fully general black-box symmetry detector. This positioning is important because CAD inspection often needs traceable evidence. If a system only returns a label, an engineer still has to inspect the part manually to understand whether the deviation is caused by a true defect, a modeling artifact, or an intended functional feature. The proposed framework keeps the numerical score and the spatial explanation together, which makes the result easier to audit and discuss.

A second motivation is reproducibility. Surface sampling is stochastic, and small CAD features can be sensitive to point density and seed selection [4]. For that reason, the framework records the sampling seed, sample size, scoring settings, selected axes, asymmetry statistics, and exported artifacts. The goal is not only to obtain one result for one uploaded model, but to make the analysis repeatable across single-run inspection, batch evaluation, and ablation studies.

The main contributions are: (i) a reproducible geometry-grounded workflow for axis-aligned symmetry analysis of CAD-derived point clouds; (ii) deterministic reflection scoring using one-way nearest-neighbour and Chamfer-style consistency measures; (iii) normalized asymmetry quantification using mean, median, trimmed mean, and error percentiles; (iv) explainable asymmetry localization using deviation heatmaps and top-error worst-region bounding boxes; (v) compact invariant descriptors based on PCA ratios, radial statistics, and bounding-box ratios; (vi) an updated evaluation showing that the revised optional classifier reduces earlier axis-collapse behaviour, while deterministic geometric validation remains the primary evidence source.

II. Related Work

Symmetry detection has been studied in geometry processing, computer vision, robotics, point-cloud analysis, and CAD inspection. Classical geometric methods usually estimate a plane or axis by measuring the consistency between a shape and its reflected or registered form. Iterative closest-point registration and related nearest-neighbour matching ideas remain important foundations for comparing 3D shapes because they provide distance-based evidence rather than only a semantic label [2], [4]. Point-cloud toolkits and 3D processing libraries further made such geometric workflows practical for engineering data, including sampled CAD meshes and scanned components [5]. These methods are attractive in inspection settings because the result can be connected to measurable quantities such as reflection error, local deviation, and correspondence distance.

Learning-based point-cloud methods have also influenced 3D shape analysis. PointNet showed that neural networks can process unordered point sets through shared pointwise features and global aggregation [4]. ModelNet40 and related benchmarks have supported many studies on 3D classification and shape representation [5], [6]. The ABC dataset provides a large-scale source of CAD models for geometric learning and is useful for expanding CAD-oriented evaluation beyond a small local collection [7]. Broader surveys on deep learning for 3D point clouds show that classification, segmentation, detection, and registration remain active research areas, but they also emphasize challenges caused by irregular sampling, data sparsity, noise, and domain shifts [8]. More specific symmetry-related work includes learning-based symmetry detection for occluded point clouds [9], [10], symmetry-plane fitting and point-set registration [11], [12], and benchmark tracks such as SHREC 2023 for detecting symmetries in 3D point clouds [13], [14].

Industrial CAD inspection has different requirements from general object classification. A predicted label is not sufficient unless it can be linked to measurable geometric evidence. Recent surveys on geometric deep learning for CAD and industrial point-cloud analysis highlight the need for interpretable and application-oriented 3D analysis tools [15], [16]. In manufacturing and digital engineering contexts, smart manufacturing is commonly associated with the integration of design data, sensing, computing, simulation, and predictive engineering [17]. Digital-twin research also emphasizes traceable digital representations that can support design, monitoring, and decision-making in industrial systems [18], [19]. Although the present work does not implement a full digital twin, it follows the same practical direction by turning CAD geometry into repeatable measurements and visual evidence that can support inspection-oriented decisions.

Explainability is also important. Explainable AI research argues that users need outputs that can be understood, trusted, and acted upon in context [20], [21]. Recent surveys specifically address explainability for methods operating on point-cloud data [22], [23]. In CAD symmetry inspection, explainability does not need to rely only on abstract feature attribution. It can be expressed directly through reflection scores, per-point errors, heatmaps, worst-region bounding boxes, and robust statistics. This form of explanation is useful because an engineer can inspect whether the high-error region corresponds to a functional feature, an unintended modeling issue, or a sampling artifact.

The gap addressed in this paper is the need for a simple and reproducible workflow that combines axis-aligned engineering interpretation, deterministic reflection scoring, normalized asymmetry measurement, invariant descriptors, and visual localization of deviations. The proposed method is designed for practical robotic CAD inspection rather than for purely predictive benchmarking. In contrast to methods that estimate arbitrary planes, the framework intentionally focuses on X/Y/Z axes because these axes are directly meaningful in many engineering coordinate systems and are easier to communicate in inspection reports. This restriction is a limitation for arbitrary orientations, but it improves clarity for the targeted use case.

The framework also differs from a standard classification pipeline in how results are used. In a pure classification system, the predicted class is the final output. In this work, the predicted axis is only one input to the analysis. The user can compare it with the one-way geometric baseline, the Chamfer-style baseline, and the PCA sanity check. If these outputs disagree, the framework exposes the scores and heatmap instead of hiding the disagreement. This design is more suitable for engineering reporting, where uncertainty and evidence are often more useful than a single confident label.

III. Methodology

A. Workflow Overview

Fig. 1 summarizes the proposed workflow. A CAD model is sampled into a point cloud, normalized, optionally passed through an axis-suggestion module, and then evaluated using deterministic reflection scoring. The output includes quantitative metrics, invariant descriptors, and localized visual evidence.

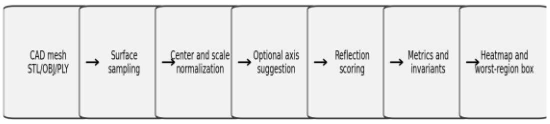

Fig. 1. Proposed geometry-grounded CAD symmetry analysis workflow. The optional learned module suggests a candidate axis, while final interpretation is based on deterministic reflection scoring and localized deviation evidence.

B. Point Sampling and Normalization

Given a mesh, N points are sampled from the surface to form a point cloud $P = \{p_i\}_{i=1}^{N}$. The points are centered and normalized by the maximum radial distance:

$$\tilde{p}_i = \frac{p_i - \mu}{s}, \quad \mu = \frac{1}{N}\sum_{i=1}^{N} p_i, \quad s = \max_i \| p_i - \mu \|_2.$$

This normalization reduces sensitivity to translation and inconsistent CAD units. It also allows asymmetry scores to be compared across models of different sizes. The normalization does not remove shape differences; it only ensures that the reflection-based distance is not dominated by the absolute scale of the imported CAD file.

C. Reflection Scoring

For each candidate axis $a \in \{X, Y, Z\}$, a reflection operator $R_a(\cdot)$ mirrors the normalized point cloud across the corresponding coordinate plane. The one-way nearest-neighbor score is:

$$S_a = \frac{1}{N}\sum_{i=1}^{N} \min_j \| R_a(\tilde{p}_i) - \tilde{p}_j \|_2.$$

The deterministic baseline axis is selected as:

$$a^* = \arg\min_{a\in\{X,Y,Z\}} S_a.$$

A bidirectional Chamfer-style score is also computed:

$$C_a = \frac{1}{2}\left(\frac{1}{N}\sum_{i=1}^{N} \min_j \| R_a(\tilde{p}_i) - \tilde{p}_j \|_2 + \frac{1}{N}\sum_{j=1}^{N} \min_i \| \tilde{p}_j - R_a(\tilde{p}_i) \|_2\right).$$

Lower scores indicate stronger reflection consistency. The one-way score is used as the primary baseline because it is simple, efficient, and directly reflects how well the reflected sample can be explained by the original point set. The Chamfer-style score is used as a supporting check because it considers both directions of correspondence. In the evaluated settings, the one-way and Chamfer-style baselines often selected the same axis, but both are retained to make the analysis more transparent.

D. Asymmetry Quantification and Localization

For a selected axis $\bar{a}$, the per-point reflection deviation is:

$$e_i = \min_j \| R_{\bar{a}}(\tilde{p}_i) - \tilde{p}_j \|_2.$$

The mean deviation $\bar{e}$ is normalized by the bounding-box diagonal d:

$$\text{Asymmetry}(\%) = \frac{\bar{e}}{d} \times 100.$$

The implementation also reports the median, trimmed mean, maximum error, and the $p50$, $p90$, and $p95$ percentiles. These additional summaries are necessary because CAD components may contain small but important localized features. A single mean value can hide whether the mismatch is distributed over the whole part or concentrated around one bracket or hole. To localize asymmetry, the top $k\%$ highest-error points are enclosed in an axis-aligned 3D bounding box and displayed with a deviation heatmap. The bounding box is not intended to replace engineering judgement; it narrows attention to the region that contributes most strongly to the measured reflection mismatch.

E. Invariant Descriptors

A compact descriptor vector is computed using PCA eigenvalue ratios λ_2/λ_1 and λ_3/λ_1, radial mean, radial standard deviation, radial maximum, and bounding-box ratios L_y/L_x and L_z/L_x. These descriptors provide a lightweight shape signature for reporting and comparison.

IV. System Design and Architecture

A. Implementation

The implementation is a local Python and Streamlit application. It supports STL, OBJ, and PLY files, surface sampling, seed control, optional axis suggestion, deterministic scoring, invariant extraction, batch evaluation, ablation settings, and exportable JSON, CSV, and PDF reports. The updated application uses D_best_valAccuracy_model.pth for optional axis suggestion when the model is available. The application also records reproducibility metadata such as sample size, seed, worst-region percentage, trim ratio, and runtime. Batch evaluation is included because single CAD examples can be misleading. By running several seeds per file, the user can observe whether the selected axis and asymmetry score are stable under stochastic sampling. The ablation controls allow the user to vary sampling density and worst-region percentage, which is useful when preparing figures and tables for research reporting.

Table I summarizes the main outputs. The classifier output is intentionally listed as a supporting hypothesis only, while the geometric baseline axes and deviation metrics are treated as inspection evidence. This separation makes the system safer to interpret when the classifier and the geometric baseline agree, the learned module can speed up the workflow; when they disagree, the system still provides reflection scores and heatmaps that explain the disagreement.

TABLE I. MAIN OUTPUTS PRODUCED BY THE FRAMEWORK

Output	Meaning	Inspection value
Optional model axis	Classifier-suggested X/Y/Z axis	Fast hypothesis, not final evidence
One-way baseline axis	Lowest reflected nearest-neighbour score	Primary deterministic evidence
Chamfer-style axis	Lowest bidirectional reflection score	Cross-check for scoring consistency
Asymmetry percentage	Mean error normalized by bounding-box diagonal	Scale-aware deviation measurement
Robust errors	Median and trimmed-mean deviations	Reduce outlier sensitivity
Heatmap	Per-point reflection deviation	Visual explanation of asymmetry location
Worst-region box	Top-error region enclosed in 3D	Localizes the most relevant deviation area
Invariants	PCA, radial, and bounding-box descriptors	Compact shape signature

B. Datasets and Settings

Three evaluation settings were used. First, seven robotic CAD parts from a TurtleBot3 Manipulation source were evaluated using ten stochastic surface-sampling seeds, $N = 2048$, and worst-region $k = 5\%$. This subset represents targeted robotic parts where near-symmetry and functional asymmetry commonly appear together. Second, an extended collection of 53 CAD models was evaluated to study broader behavior and axis-distribution patterns. The updated D-model evaluation used ten seeds per model, producing 530 runs, matching the run count of the earlier extended-benchmark protocol. Third, a NASA RASSOR 3D asset was used as a case study to examine the effect of sampling density. The NASA case is not treated as a dataset-level benchmark; it is used to visually and numerically inspect whether increasing point density changes the overall asymmetry interpretation.

The optional classifier was first trained on 540 pseudo-labelled samples using 432 training samples and 108 validation samples. The selected D experiment used balanced sampling and weighted cross-entropy, no axis augmentation, $N = 2048$, batch size 16, learning rate 0.001, and 50 epochs. These results are used to describe the supporting classifier, not to replace the geometric baseline. The pseudo-labels were derived from reflection-based geometric scoring; therefore, the learning task should be understood as learning to approximate a geometric teacher signal rather than learning from manually certified labels. This is practical for a prototype, but it also motivates the conservative interpretation used throughout the paper.

A fourth evaluation was added to examine the optional classifier under a stricter and larger CAD setting. An expanded dataset was constructed from the ABC CAD dataset by selecting 1000 valid STL CAD models. Each model was evaluated using ten seed-controlled surface-sampling runs at $N = 2048$, producing 10000 pseudo-labeled samples. The dataset was split at the CAD-model level rather than at the seed level: 700 models were used for training, 150 models for validation, and 150 models for testing. This avoids seed-level leakage, because all ten samples from the same CAD model remain in only one split. The expanded experiment is therefore treated as a conservative test of the optional classifier on unseen CAD geometry, not as a replacement for deterministic geometric validation.

The robotic CAD parts were obtained from the TurtleBot3 Manipulation source [24], the expanded collection was derived from the ABC CAD dataset [7], and the sampling-density case study used the NASA RASSOR 3D asset [25].

C. Important Comparison Note

The earlier conference version reported 530 extended benchmark runs using ten seeds per model. The updated D evaluation reported here uses the same 53-model collection, the same main geometric settings, and the same ten-seed protocol, producing 530 updated runs. This makes the before–after comparison directly matched in both model collection and seed count. The comparison is still interpreted conservatively because the updated classifier was trained under a revised setting and the pseudo-labelling process is geometry-derived rather than manually certified. However, the key observation is clear: the earlier classifier predicted the Y-axis in all 530 runs, while the updated D model produced X, Y, and Z predictions across the same model collection and seed count.

V. Implementation and Results

A. Robotic CAD Subset

On the seven-part robotic subset, the earlier evaluation produced 70 runs. The optional model agreed with the one-way geometric baseline in 61.4% of runs, and the mean asymmetry ratio on the model-suggested axis was 2.093% with standard deviation 0.846%. Several linkage components showed stable agreement, while gripper palm components showed persistent mismatch. This result supports the need for geometric validation rather than relying only on a learned axis suggestion.

B. Updated Extended Benchmark Comparison

Table II presents the key before–after comparison. The earlier classifier predicted Y for every extended-benchmark run, producing 43.0% agreement with the one-way baseline. Under the matched ten-seed updated evaluation, the D classifier produced a more balanced distribution across X, Y, and Z and achieved 69.2% agreement. The mismatch count decreased from 302 to 163 runs, and the mean asymmetry on the model axis decreased from 1.875% to 1.186%.

TABLE II. BEFORE-AFTER COMPARISON ON THE EXTENDED CAD BENCHMARK

Metric	Earlier classifier	Updated D classifier
Runs/Models	530/53	530/53
Seeds	10	10
Agreement (%)	43.0	69.2
Mismatch runs	302	163
Mean Asym. (%)	1.875	1.186
Std Asym. (%)	1.458	0.444
X/Y/Z predictions	0 / 530 / 0	217 / 183 / 130

The updated result does not mean that the learned component is fully reliable as a standalone symmetry detector. It means that the revised classifier reduced the previous axis-collapse behaviour and became more useful as a supporting hypothesis. The final decision remains based on geometric reflection scores and local deviation evidence. This is the main reason the updated result is useful even though the classifier is imperfect: the model no longer dominates the pipeline, but it can provide a more reasonable starting point for the deterministic analysis.

The mismatch pattern is also informative. For baseline-X cases, 93 out of 99 runs were predicted as X, while baseline-Y and baseline-Z cases still showed more cross-axis confusion. This indicates that the revised model did not simply learn to spread predictions randomly across classes. It learned a more diverse pattern, but the Y/Z boundary remains challenging for some CAD shapes. This observation is consistent with the nature of mechanical components, where several axes may appear plausible depending on whether global shape, local functional details, or reflection distance is emphasized.

Table III gives a more detailed view of the updated run-level axis distribution. The baseline selected Y most often, followed by Z and X. The updated model predicted X most often, followed by Y and Z. The crosstab shows that most baseline-X cases were predicted correctly, while baseline-Y and baseline-Z still contained mismatches. This is a realistic result and indicates improvement without overstating generalization.

TABLE III. UPDATED D-MODEL RUN-LEVEL AXIS DISTRIBUTION AND AGREEMENT WITH THE ONE-WAY GEOMETRIC BASELINE

One-way baseline axis	Predicted X	Predicted Y	Predicted Z
X	93	6	0
Y	72	150	6
Z	52	27	124

Across the 530 updated runs, the one-way and Chamfer-style geometric baselines produced the same overall mean asymmetry of 1.148% with coefficient of variation 0.363. The PCA axis produced a higher mean asymmetry of 2.351% with coefficient of variation 0.726. This supports the use of reflection-based geometric scoring over a simple PCA-axis heuristic. PCA is still useful as a quick sanity check because it summarizes the dominant spread of the point cloud, but it should not be treated as a symmetry criterion. A long or elongated part may have a strong PCA direction even when the most consistent reflection axis is different. The reflection-based baselines are more directly connected to the inspection question because they compare the part with its mirrored version.

C. *Optional Classifier Validation and Expanded Dataset Test*

Table IV reports the validation results of the selected D classifier. The model achieved 76.85% validation accuracy and 0.7709 macro-F1 at epoch 32. The class-level results show strong recall for X, stronger precision for Y and Z, and a more balanced overall behaviour than the earlier collapsed model.

An additional balanced augmented experiment with a symmetry-consistency term reached a lower best macro-F1 of 0.5924 under the tested settings. For this reason, the D model was selected for the updated application. This outcome suggests that more complex augmentation is not automatically beneficial unless it is carefully matched to the labelling strategy and CAD data distribution. The negative result is retained as a useful ablation observation rather than removed from the discussion.

TABLE IV. VALIDATION PERFORMANCE OF THE SELECTED OPTIONAL D CLASSIFIER

Class	Precision	Recall	F1-score	Support
X	0.57	0.96	0.71	27
Y	0.89	0.69	0.78	45
Z	0.96	0.72	0.83	36
Accuracy	0.77	0.77	0.77	108
Macro average	0.80	0.79	0.77	108
Weighted average	0.83	0.77	0.78	108

To further test the optional classifier under a stricter and more diverse setting, an expanded E experiment was conducted using 1000 ABC-derived CAD models and 10000 seed-controlled samples. Unlike the D validation setting, the expanded experiment used a CAD-model-level split, meaning that models in the test set were not seen during training. The expanded dataset contained 7000 training samples from 700 CAD models, 1500 validation samples from 150 CAD models, and 1500 test samples from 150 CAD models. The best validation result occurred at epoch 51 with 62.20% validation accuracy and 0.6182 validation macro-F1. On the unseen test split, the model achieved 64.87% test accuracy and 0.6493 macro-F1.

Table V summarizes this comparison between the smaller D validation experiment and the expanded E test experiment.

TABLE V. COMPARISON BETWEEN THE SMALLER D-VALIDATION EXPERIMENT AND THE EXPANDED E-TEST EXPERIMENT

Aspect	D classifier	E classifier
Data scale	540 samples	10000 samples / 1000 CAD models
Split/reporting setting	Validation on prepared pseudo-labelled data	Unseen test set with CAD-model-level split
Accuracy	76.85%	64.87%
Macro-F1	0.7709	0.6493

Table VI shows the class-level test results for the expanded E experiment. The F1-scores for X, Y, and Z are close to each other, which indicates that the model did not collapse into a single-axis prediction pattern. The result is lower than the smaller D validation result, but it is more realistic because the test set contains unseen CAD models rather than additional seed samples from the same model split.

TABLE VI. TEST PERFORMANCE OF THE EXPANDED E CLASSIFIER ON 150 UNSEEN CAD MODELS AND 1500 TEST SAMPLES

Class	Precision	Recall	F1-score	Support
X	0.5990	0.6901	0.6413	526
Y	0.6761	0.6195	0.6466	502
Z	0.6889	0.6335	0.6600	472
Accuracy	0.6487	0.6487	0.6487	1500
Macro average	0.6547	0.6477	0.6493	1500
Weighted average	0.6531	0.6487	0.6490	1500

For the expanded E test split, the confusion counts were 363/82/81 for true X, 137/311/54 for true Y, and 106/67/299 for true Z across the predicted X/Y/Z columns. These values show moderate cross-axis confusion, but they also show that the model continues to predict all three axes rather than collapsing to a single output class. This supports the central design choice of the paper: the learning module can provide a useful starting hypothesis, but deterministic geometric validation and localized deviation evidence remain the final basis for interpretation.

Fig. 2 shows selected training diagnostics for the updated D classifier.

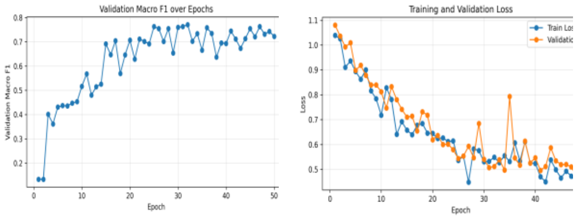

Fig. 2. Selected training diagnostics for the updated D classifier: validation macro-F1 (left) and training/validation loss (right). The curves show improvement during training, but the classifier is still used only as a supporting axis suggestion.

D. Explainable Localization

Fig. 3 shows a representative mismatch case where the optional model and geometric baseline selected different axes. The heatmap and bounding box make the disagreement inspectable rather than hidden. This is important because a wrong axis suggestion should not end the analysis; it should trigger a comparison with deterministic geometric evidence. In this type of case, the visual output helps distinguish a model-bias problem from a genuine geometric ambiguity. If the high-error region is concentrated around a small functional feature, the engineer may decide that the global part remains acceptable. If the error is widespread, the part may require closer review.

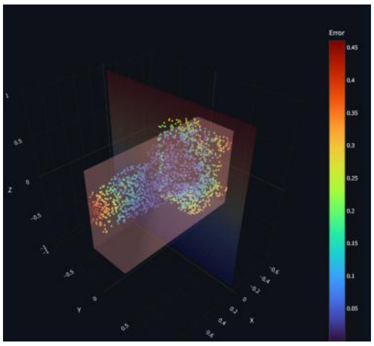

Fig. 3. Representative mismatch case from the earlier evaluation. The heatmap highlights local reflection deviations, while the bounding box encloses the top-error region.

E. NASA RASSOR Sampling-Density Case Study

The NASA RASSOR case study was used to examine sampling-density behaviour. Increasing the number of sampled points from 2048 to 4096 produced smoother spatial error patterns while preserving the same broad interpretation. Table VII and Fig. 4 summarize the result. The numerical changes are modest rather than dramatic: the mean, median, and trimmed-mean asymmetry values decrease slightly at the higher sampling density. This suggests that increasing the sampling density improves visual smoothness and local coverage, but it does not fundamentally change the interpretation of where asymmetry is concentrated.

TABLE VII. NASA RASSOR ROBUST ASYMMETRY SUMMARIES AT WORST-REGION $\kappa = 5\%$

N	Mean Asym. (%)	Median Asym. (%)	Trimmed Mean Asym. (%)	Runtime (s)
2048	5.7383	3.8816	5.0709	8.9328
4096	5.4072	3.5004	4.6660	8.6479

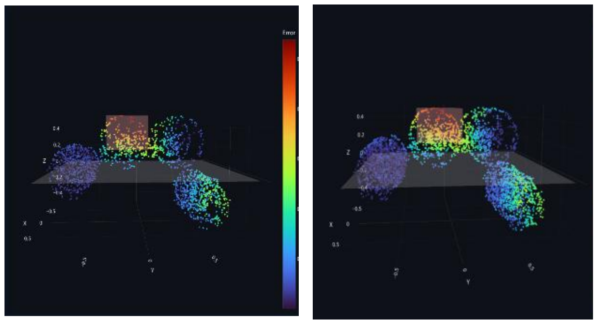

Fig. 4. NASA RASSOR deviation heatmaps for N = 2048 (left) and N = 4096 (right). Higher sampling density produces a smoother heatmap while preserving the overall asymmetry pattern.

F. Discussion

The results support four observations. First, deterministic reflection scoring is a more reliable basis for inspection than a classifier alone. The optional classifier improved from the earlier collapsed behaviour, but it still disagrees with the geometric baseline in some cases. This is expected because pseudo-labelled CAD symmetry is ambiguous for parts with localized functional features. A bracket or mounting hole may be important for function but may also shift the apparent best axis. Second, localized heatmaps and worst-region boxes make the analysis explainable. Instead of reporting only an agreement score or a predicted axis, the framework shows where reflection mismatch occurs. This makes the result more useful in an engineering setting because the user can decide whether the localized deviation is acceptable, expected, or suspicious. Third, robust error summaries such as median, trimmed mean, and percentiles are useful because CAD parts may contain small, localized features that strongly affect maximum error. Fourth, the expanded E experiment shows that classifier performance decreases under a stricter CAD-model-level test split, but remains balanced across X, Y, and Z. This is a useful result because it gives a more conservative estimate of generalization than the smaller validation-only experiment.

The updated extended benchmark result clarifies the role of the classifier. The earlier version showed a severe Y-axis collapse. The updated D model produced X, Y, and Z predictions across the same 53-model collection and improved agreement with the one-way baseline. The expanded E experiment further shows that, when evaluated on unseen CAD models from a larger 1000-model dataset, the classifier achieves moderate test performance without collapsing to one axis. However, both results support the same conclusion: the learning component is useful as a starting hypothesis, but not reliable enough to replace deterministic geometric validation. The strongest part of the framework is therefore the integration of the learned suggestion with reflection scoring, robust asymmetry statistics, and spatial explanation.

The before–after comparison is encouraging but intentionally interpreted conservatively. The updated D model improved agreement and prediction diversity on the same 53-model collection using the same ten-seed run count as the earlier extended evaluation. This strengthens the comparison because the change is no longer explained by using fewer stochastic runs. At the same time, the expanded E experiment shows why a larger unseen-model split is necessary: performance is lower under a stricter test condition, which is expected when the model must generalize to CAD geometries do not present in training. The better-supported conclusion is that the optional classifier improved and is no longer collapsed, while the reliability of the full framework still comes from deterministic geometric validation and localized evidence.

G. Practical Implications

The proposed workflow can support smart engineering and robotic CAD inspection in several practical ways. First, it produces scale-aware asymmetry measurements that can be compared across parts and across repeated runs. This is useful during early design review because the user can decide whether a part is globally near symmetric or whether a localized feature produces a measurable deviation. Second, the heatmap and worst-region bounding box provide visual evidence that helps engineers interpret whether deviations correspond to expected functional features. For example, a mounting hole, bracket, or cable-routing structure may increase local error without indicating a defective part. Third, the exported JSON, CSV, and PDF outputs make the analysis easier to document, repeat, and discuss with supervisors or design reviewers.

The framework is not intended to replace professional CAD inspection or manufacturing quality-control systems. Its practical value is more limited and specific: it provides a lightweight decision-support layer for symmetry-oriented review of robotic mechanical parts. In a design workflow, an engineer can upload a CAD model, inspect candidate axes, compare one-way and Chamfer-style reflection scores, view the most concentrated deviation region, and export a short report. This reduces manual effort, but it still leaves the final engineering judgement to the user. Such a conservative role is appropriate because some asymmetry is intentional and should not automatically be treated as an error.

The method also aligns with data-driven smart manufacturing in a modest but useful way. It converts CAD geometry into structured inspection data: selected axes, asymmetry percentages, robust error summaries, invariant descriptors, runtime, and seed-controlled metadata. These outputs can later be aggregated across part families, design iterations, or inspection batches. In that sense, the framework can serve as a bridge between individual CAD analysis and larger digital engineering records. The current prototype is not a complete industrial platform, but its output structure supports future integration with design repositories, manufacturing dashboards, or digital-twin workflows.

A further implication is transparency. Because the optional classifier is not treated as final evidence, the system remains interpretable even when the classifier is wrong. A mismatch between the model-suggested axis and the geometric baseline becomes a useful diagnostic signal rather than a hidden failure. This is especially important for student research, small engineering teams, and early prototypes, where the available training data may be limited. By preserving deterministic scores and visual localization, the workflow remains useful even before the learning component reaches high generalization performance.

H. Threats to Validity

Internal validity. Nearest-neighbour deviation depends on sampling density and random surface sampling. Multi-seed evaluation reduces this risk, but it does not eliminate it. Thin structures and sharp edges may still cause correspondence sensitivity. Another internal threat is implementation dependence: different mesh sampling libraries or different nearest-neighbour settings could slightly change the reported numbers. The framework addresses this by exporting seeds, sample sizes, and run-level CSV files, but exact reproduction still requires using the same software settings.

External validity. The robotic subset contains seven parts and the main extended benchmark contains 53 CAD models. The expanded ABC-derived experiment improves the evidence base by adding 1000 CAD models and a CAD-model-level test split, but it still does not prove universal generalization across all mechanical CAD families. The ABC-derived models increase shape diversity, yet future validation should include different robot families, manufacturing components, scanned parts, manually reviewed labels, and CAD models with deliberately rotated symmetry planes.

Construct validity. The asymmetry percentage is normalized by the bounding-box diagonal. This enables comparison across differently scaled models, but elongated shapes may reduce the reported percentage even when local deviations are meaningful. For this reason, the framework reports both global percentages and localized heatmap evidence.

Learning-component validity. The optional classifier was trained using pseudo-labels rather than manually verified symmetry labels. Pseudo-labels are practical for scaling the dataset, but they may contain ambiguity because CAD parts can have more than one plausible engineering axis depending on whether the analysis prioritizes global shape, local functional features, or reflected nearest-neighbour distance. The expanded E experiment reduces the risk of seed-level leakage by using a CAD-model-level split, but it does not remove the limitation that the labels are geometry-derived rather than manually certified. Therefore, classifier performance should be interpreted as the ability to approximate the selected geometric baseline, not as proof of human-level symmetry understanding. This is why the classifier remains an optional axis-suggestion module while deterministic reflection scoring remains the main inspection evidence.

VI. Conclusion

This paper presented a geometry-grounded framework for explainable symmetry quantification and asymmetry localization in robotic CAD parts. The framework combines normalized point-cloud sampling, deterministic reflection scoring, robust asymmetry metrics, invariant descriptors, and localized heatmap visualization. The updated D classifier improved internal validation performance and reduced earlier axis-collapse behaviour on the extended benchmark evaluation, but it remains a supporting component rather than the final decision source. The expanded ABC-derived experiment further strengthened this interpretation by using 1000 CAD models, 10000 seed-controlled samples, and a CAD-model-level train/validation/test split. Its 64.87% test accuracy and 0.6493 macro-F1 indicate moderate but balanced generalization on unseen CAD models, which is lower than the smaller D validation result but more conservative and realistic. The main contribution is therefore an interpretable and reproducible inspection workflow that makes symmetry measurable and localizes functional asymmetry in CAD models. This makes the framework useful for smart engineering contexts where users need both numerical evidence and a visual explanation before making a design or inspection decision.

Data and code availability information is omitted from the anonymous manuscript during double-blind review and will be supplied after acceptance according to the journal policy. The author declares no conflict of interest.

VII. Future Work

The current framework is limited to axis-aligned X/Y/Z reflection symmetry. Parts with arbitrary symmetry planes require future extension. The method also relies on nearest-neighbour matching rather than full registration, which may be sensitive to sampling and local geometry. The optional classifier improved under the updated D setting and was also tested on a larger ABC-derived dataset with a CAD-model-level split, but broader validation with manually reviewed labels, more balanced engineering categories, external CAD sources, and scanned physical parts is still needed. Future work should extend the method to continuous symmetry-plane estimation, stronger pseudo-label filtering, richer point-cloud architectures, and integration with CAD or manufacturing quality-control systems.

References

[1] C. R. Qi, H. Su, K. Mo, and L. J. Guibas, "PointNet: Deep learning on point sets for 3D classification and segmentation," in Proc. IEEE Conf. Computer Vision and Pattern Recognition (CVPR), Honolulu, HI, USA, 2017, pp. 652–660. doi: 10.1109/CVPR.2017.16.

[2] N. J. Mitra, M. Pauly, M. Wand, and D. Ceylan, "Symmetry in 3D geometry: Extraction and applications," Computer Graphics Forum, vol. 32, no. 6, pp. 1–23, Sep. 2013. doi: 10.1111/cgf.12010.

[3] R. B. Rusu and S. Cousins, "3D is here: Point Cloud Library (PCL)," in Proc. IEEE Int. Conf. Robotics and Automation (ICRA), Shanghai, China, 2011, pp. 1–4. doi: 10.1109/ICRA.2011.5980567.

[4] P. J. Besl and N. D. McKay, "A method for registration of 3-D shapes," IEEE Transactions on Pattern Analysis and Machine Intelligence, vol. 14, no. 2, pp. 239–256, Feb. 1992. doi: 10.1109/34.121791.

[5] Z. Wu, S. Song, A. Khosla, F. Yu, L. Zhang, X. Tang, and J. Xiao, "3D ShapeNets: A deep representation for volumetric shapes," in Proc. IEEE Conf. Computer Vision and Pattern Recognition (CVPR), Boston, MA, USA, 2015, pp. 1912–1920. doi: 10.1109/CVPR.2015.7298801.

[6] Q.-C. Xu, T.-J. Mu, and Y.-L. Yang, "A survey of deep learning-based 3D shape generation," Computational Visual Media, vol. 9, no. 3, pp. 407–442, Sep. 2023. doi: 10.1007/s41095-022-0321-5.

[7] S. Koch, A. Matveev, Z. Jiang, F. Williams, A. Artemov, E. Burnaev, M. Alexa, D. Zorin, and D. Panozzo, "ABC: A big CAD model dataset for geometric deep learning," in Proc. IEEE/CVF Conf. Computer Vision and Pattern Recognition (CVPR), Long Beach, CA, USA, 2019, pp. 9601–9611. doi: 10.1109/CVPR.2019.00983.

[8] Y. Guo, H. Wang, Q. Hu, H. Liu, L. Liu, and M. Bennamoun, "Deep learning for 3D point clouds: A survey," IEEE Transactions on Pattern Analysis and Machine Intelligence, vol. 43, no. 12, pp. 4338–4364, Dec. 2021. doi: 10.1109/TPAMI.2020.3005434.

[9] Z. Wu, H. Jiang, and S. He, "Symmetry detection of occluded point cloud using deep learning," arXiv preprint arXiv:2003.06520, 2020. doi: 10.48550/arXiv.2003.06520.

[10] L. Gao, L.-X. Zhang, H.-Y. Meng, Y.-H. Ren, Y.-K. Lai, and L. Kobbelt, "PRS-Net: Planar reflective symmetry detection net for 3D models," IEEE Transactions on Visualization and Computer Graphics, vol. 27, no. 6, pp. 3007–3018, Jun. 2021. doi: 10.1109/TVCG.2020.3003823.

[11] L. Hu and L. Kneip, "Globally optimal point set registration by joint symmetry plane fitting," Journal of Mathematical Imaging and Vision, vol. 63, no. 5, pp. 623–640, Jun. 2021. doi: 10.1007/s10851-021-01015-1.

[12] R. Nagar, "Robust extrinsic symmetry estimation in 3D point clouds," The Visual Computer, vol. 41, no. 1, pp. 115–128, Jan. 2025. doi: 10.1007/s00371-024-03313-6.

[13] I. Sipiran, C. Romanengo, B. Falcidieno, S. Biasotti, G. Arvanitis, C. Chen, V. Fotis, J. He, X. Lv, K. Moustakas, S. Peng, I. Romanelis, W. Sun, C. Vlachos, Z. Wu, and Q. Xie, "SHREC 2023: Detection of symmetries on 3D point clouds representing simple shapes," in Proc. Eurographics Workshop on 3D Object Retrieval (3DOR), Lille, France, 2023, pp. 1–8. doi: 10.2312/3dor.20231148.

[14] I. Sipiran, G. Santelices, L. Oyarzún, A. Ranieri, C. Romanengo, S. Biasotti, and B. Falcidieno, "Symmetria: A synthetic dataset for learning in point clouds," arXiv preprint arXiv:2510.23414, 2025. doi: 10.48550/arXiv.2510.23414.

[15] N. Heidari and A. Iosifidis, "Geometric deep learning for computer-aided design: A survey," arXiv preprint arXiv:2402.17695, 2024. doi: 10.48550/arXiv.2402.17695.

[16] Y. Liu, C. Zhang, X. Dong, and J. Ning, "Point cloud-based deep learning in industrial production: A survey," ACM Computing Surveys, vol. 57, no. 7, pp. 1–36, Jul. 2025. doi: 10.1145/3715851.

[17] A. Kusiak, "Smart manufacturing," International Journal of Production Research, vol. 56, no. 1–2, pp. 508–517, Jan. 2018. doi: 10.1080/00207543.2017.1351644.

[18] F. Tao, H. Zhang, A. Liu, and A. Y. C. Nee, "Digital twin in industry: State-of-the-art," IEEE Transactions on Industrial Informatics, vol. 15, no. 4, pp. 2405–2415, Apr. 2019. doi: 10.1109/TII.2018.2873186.

[19] D. Alfaro-Viquez, M. Zamora-Hernandez, M. Fernandez-Vega, J. Garcia-Rodriguez, and J. Azorin-Lopez, "A comprehensive review of AI-based digital twin applications in manufacturing: Integration across operator, product, and process dimensions," Electronics, vol. 14, no. 4, p. 646, Feb. 2025. doi: 10.3390/electronics14040646.

[20] A. B. Arrieta, N. Díaz-Rodríguez, J. Del Ser, A. Bennetot, S. Tabik, A. Barbado, S. Garcia, S. Gil-Lopez, D. Molina, R. Benjamins, R. Chatila, and F. Herrera, "Explainable artificial intelligence (XAI): Concepts, taxonomies, opportunities and challenges toward responsible AI," Information Fusion, vol. 58, pp. 82–115, Jun. 2020. doi: 10.1016/j.inffus.2019.12.012.

[21] D. Gunning and D. Aha, "DARPA's explainable artificial intelligence (XAI) program," AI Magazine, vol. 40, no. 2, pp. 44–58, Jun. 2019. doi: 10.1609/aimag.v40i2.2850.

[22] R. N. Mulawade, C. Garth, and A. Wiebel, "Explainable artificial intelligence (XAI) for methods working on point cloud data: A survey," IEEE Access, vol. 12, pp. 146830–146851, 2024. doi: 10.1109/ACCESS.2024.3472872.

[23] M. E. Atik, Z. Duran, and D. Z. Seker, "Explainable artificial intelligence for machine learning-based photogrammetric point cloud classification," IEEE Journal of Selected Topics in Applied Earth Observations and Remote Sensing, vol. 17, pp. 5834–5846, 2024. doi: 10.1109/JSTARS.2024.3370159.

[24] ROBOTIS, "TurtleBot3 manipulation: CAD models and robot description files," GitHub repository, 2026. [Online]. Available: https://github.com/ROBOTIS-GIT/turtlebot3_manipulation

[25] NASA, "RASSOR: Regolith Advanced Surface Systems Operations Robot 3D model," NASA 3D Resources, 2026. [Online]. Available: https://science.nasa.gov/3d-resources/regolith-advanced-surface-systems-operations-robot-rassor/

Journal of Big Data & Smart City
Middle East College

AI Based Adaptive Behavioral Monitoring for Handicap Persons Using Smart Glove

Noor Aldeen Mohamed Zaidan
Department of Computing and Electronics Engineering
Middle East College
Muscat, Sultanate of Oman
24F26158@mec.edu.om

Dr. Muhammad Nauman Bashir
Department of Computing and Electronics Engineering
Middle East College
Muscat, Sultanate of Oman
mbashir@mec.edu.om

Arsalan Asif
Department of Computing and Electronics Engineering
Middle East College
Muscat, Sultanate of Oman
arsalan_as96@yahoo.com

Received: 5th May 2026; Revised: 12th June 2026;

Accepted: 12th July 2026

***Abstract*— In this project, the design and complete implementation of a smart glove system based on artificial intelligence (AI) and adaptive behavioral monitoring for supporting people with physical disabilities is presented. It fills in critical gaps in the field of assistive technologies, especially in the Middle East and North Africa (MENA) region, where affordable, multi-user, and culturally relevant solutions are lacking. The prototype developed consists of four flex sensors, an ADS1115 16-bit ADC (I2C, 0x48), an MPU-6050 inertial measurement unit (I2C, 0x68), and a MAX30102 pulse oximeter and heart rate sensor (I2C, 0x57) mounted on a Raspberry Pi Zero 2W. The Pi receives raw data from the sensors and sends it over http post to a locally installed PHP/MySQL-based backend server which is also running a copy of WAMP. The split architecture is edge computing with all intelligence residing on the server, including adaptive gesture detection, health anomaly detection, baseline computation and bilingual email alerting. One of the important innovations of MediGlove is its completely adaptive threshold system. The system automatically learns the resting hand pose of each patient's hand by taking the first ten readings and uses those to calculate the per-finger thresholds for bent and straight poses (bent = avg_resting + 8 degrees, straight = avg_resting + 4 degrees). The health baselines start with medically accurate clinical defaults (AHA, Cleveland Clinic) per decade age/gender, then use rolling average and 2-sigma outlier removal. All thresholds are adjusted in relation to 3 care modes (Normal, Active, Sleep). The switchability of multi-patient operation, the adaptive health monitoring of shifting HR ranges (63-103 BPM to 56-96 BPM), the automatic availability of bilingual email alerts, and the gesture recognition in all four fingers were all confirmed through live testing on two patients with different profiles.**

Keywords*— *Smart glove, Assistive technology, Artificial intelligence, Adaptive monitoring, Gesture recognition, Health monitoring, Edge computing, Physical disabilities, Wearable sensors.

الخلاصة **- يُعدّ تكامل التكنولوجيا مع الصناعة من أبرز سمات العصر الحالي، وتُعدّ في هذا المشروع، تم تقديم التصميم والتنفيذ الكامل لنظام قفاز ذكي قائم على الذكاء الاصطناعي (AI) والمراقبة السلوكية التكيفية، بهدف دعم الأشخاص ذوي الإعاقات الجسدية. ويسد النظام فجوات مهمة في مجال التقنيات المساعدة، ولا سيما في منطقة الشرق الأوسط وشمال أفريقيا(MENA) ، حيث تفتقر الحلول المتاحة إلى القدرة على تحمل التكلفة، ودعم تعدد المستخدمين، والملاءمة مع السياقات الثقافية المحلية.**

يتكون النموذج الأولي المطوَّر من أربع مستشعرات للانحناء(Flex Sensors) ، ومحوّل تناظري إلى رقمي ADS1115 بدقة 16 بتI2C) ، العنوان (0x48)، ووحدة قياس بالقصور الذاتيI2C) MPU-6050 ، العنوان 0(x68)، ومستشعر MAX30102لقياس نسبة الأكسجين في الدم ومعدل ضربات القلبI2C) ، العنوان 0(x57)، وجميعها مثبتة على حاسوب Raspberry Pi Zero 2W. يستقبل الحاسوب Raspberry Pi البيانات الخام من المستشعرات ويرسلها باستخدام طلبات HTTP POSTإلى خادم خلفي محلي قائم علىPHP/MySQL ، يعمل أيضًا ضمن بيئة WAMP. تعتمد البنية المقسمة على مفهوم الحوسبة الطرفية (Edge Computing)، مع وجود جميع وظائف الذكاء والتحليل على الخادم، بما في ذلك الكشف التكيفي عن الإيماءات، واكتشاف الحالات الصحية غير الطبيعية، وحساب خطوط الأساس الصحية، وإرسال تنبيهات عبر البريد الإلكتروني باللغتين العربية والإنجليزية.

تتمثل إحدى أهم ابتكارات نظام Medi Glove في اعتماده الكامل على نظام عتبات تكيفية. حيث يتعلم النظام تلقائيًا وضعية اليد أثناء الراحة لكل مريض من خلال أخذ القراءات العشر الأولى، ثم يستخدم هذه القراءات لحساب العتبات الخاصة بكل إصبع للكشف عن وضعيتي الانحناء والاستقامة؛ إذ تُحسب عتبة الانحناء بإضافة 8 درجات إلى متوسط وضعية الراحة، بينما تُحسب عتبة الاستقامة بإضافة 4 درجات إلى متوسط وضعية الراحة. تبدأ الخطوط الأساسية للمؤشرات الصحية بقيم سريرية افتراضية دقيقة طبيًا، مستندة إلى بيانات من جمعية القلب الأمريكية (AHA) وCleveland Clinic، ومصنفة وفق الفئة العمرية والعمر والجنس، ثم يتم تحديثها باستخدام المتوسط المتحرك مع استبعاد القيم الشاذة التي تتجاوز انحرافين معياريين .(2-Sigma) كما يتم ضبط جميع العتبات وفقًا لثلاثة أوضاع للرعاية، وهي: الوضع الطبيعي(Normal) ، والوضع النشط(Active) ، ووضع النوم.(Sleep)

وقد تم تأكيد إمكانية التبديل بين المستخدمين في نظام متعدد المرضى، والتكيف مع التغير في نطاقات معدل ضربات القلب (من 63–103 نبضة في الدقيقة إلى 56–96 نبضة في الدقيقة)، والتوافر التلقائي للتنبيهات عبر البريد الإلكتروني باللغتين، بالإضافة إلى التعرف على الإيماءات باستخدام الأصابع الأربعة، من خلال الاختبارات الحية التي أُجريت على مريضين ذوي خصائص مختلفة.

الكلمات المفتاحية – القفاز الذكي، التقنيات المساعدة، الذكاء الاصطناعي، المراقبة التكيفية، التعرف على الإيماءات، المراقبة الصحية، الحوسبة الطرفية.

I. INTRODUCTION

The population of individuals with disabilities is growing every day and with it there is a rising demand for inclusive technologies. This has created an urgent need for assistive solutions to these problems. According to the World Health Organization (2023), over 1.3 billion people experience disabilities [1] that hinder their lives, creating a demand for solutions to overcome these challenges and perform daily tasks.

With current solutions that are available to these problems include the neo effect smart glove which offers rehabilitation using sensors and virtual reality [2], [3], and rehabilitation which provides motorized therapy for stroke recovery [2], [3], [4]. (as seen in figure 1-2, 1-3 below) Research shows

Journal of Big Data & Smart City, Vol. 6, Issue 2, July 2026

that gesture recognition using flex sensors and machine learning is feasible [5], [6], [7]

Current solutions that are available to these problems include the neo effect smart glove which offers rehabilitation using sensors and virtual reality [2], [3], and rehabilitation which provides motorized therapy for stroke recovery [2], [3], [4]). Research shows that gesture recognition using flex sensors and machine learning is feasible [5], [6], [7].

From these examples, common shortcomings can be identified:

1. High cost of device and therapy-grade hardware.
2. Focus on single users or one specific impairment type and makes it single usage (e.g., stroke rehab).
3. Lack of behavioural logging and caregiver dashboard for continuous home monitoring.
4. Reliance on cloud/internet or external apps, increasing cost and reducing privacy. Limited multi-user capability (different users needing separate devices or complex recalibration).

For this current project their organizations for disabled which include:

1. Oman Association for the Disabled: This non-profit organization, with its main branch in Al Azaiba, Muscat, and numerous branches across the country, provides support, education, recreational activities, and equipment (like wheelchairs) to people with disabilities.

2. Al Wafa Centres for the Rehabilitation of People with Disabilities: Operated under the Ministry of Social Development (MoSD), these centres (also known as Al Wafa Social Centres) offer various services, including educational, cultural, and mental healthcare, and vocational training. They have workshops in various specializations like paper recycling, food processing, and handicrafts to enable economic empowerment and integration into the labour market.

II. Related Work

A. *Flex Sensor-Based Hand Gesture Recognition Using Machine Learning*

The research conducted by the authors represented a cornerstone study in sensor-based gesture recognition, providing essential validation for the core technological approach adopted in the current project. The work they did on hand gesture recognition with flex sensors and machine learning algorithms sets an important benchmark in terms of the accuracy achieved, with results claiming >85% accuracy for static hand gesture classification. The quantitative validation is of special interest because it shows that flex sensors, which are inexpensive sensors whose electrical resistance is proportional to the bending curvature, can produce discriminative enough patterns of data for reliable classification if processed through appropriate machine learning pipelines. The study's methodology, which presumably is analogue to digital conversion of the sensor signals, feature extraction from the time-series data, and systematic training of models on a curated set of data, provides a foundation of ideas that must be considered in any real-world application. The context for the abstract, however, seems to indicate that the research was more about the validation of the sensor-ML combination, and much of it still appears to have been at the laboratory level. There is a huge gap in transition between the laboratory environment where the proof of concept is performed (i.e., sensors are fixed in place, no interference of the environment, participants cooperate with the experiment) and the environment in which assistive devices function in a reliable manner (i.e., the environment is variable, there is no cooperation from the participants). Moreover, there is no reference to multi-user adaptability or to any type of personalization system, which indicates that the system was designed as a single, generalized model rather than a dynamic adaptive system that can respond to hand anatomy and/or movement patterns, or disability-specific constraints. The current project builds on the validated technical approach and significantly extends it by introducing a multi-user calibration approach, incorporating motion context from complementary inertial measurement units, and creating a comprehensive system architecture—and its web-based configuration interfaces and caregiver notification mechanisms—that are not addressed by the authors.

B. *Obstacles for Using Assistive Technology in Centers of Special Needs in the UAE .*

The survey study conducted by the authors was indispensable in providing a context for their study of the challenges associated with the use of assistive technologies in the United Arab Emirates (UAE) [8], [9]. Their research approach was a systematic process of data collection from stakeholders in assistive technology ecosystems, which revealed the following major barriers to AT: cost, cultural and linguistic adaptation, and user training and device maintenance. The results of this study are important because they shed light on a fact that is not always taken into account when developing technologies: the most advanced assistive technologies are not very effective if they are not accessible because of economic, cultural, or logistical constraints. The barriers they report are cost-related and have direct and significant impact on the design process, with many assistive products in the region not being affordable to many potential users, especially in the absence of insurance and government support systems. It is an economic fact that a component design philosophy focused on cost is essential, that incremental capability growth is achieved through modular design and that manufacturing methods that reduce production costs are mandatory. In addition to the economic considerations, the identification of cultural and linguistic adaptation gaps highlights the need to create assistive technologies that are relevant to the local context of users as opposed to those that are imported from the west. Assistive devices should also be designed to support regional languages, especially the interface in Arabic, take into account local social norms on disability and taking care of it, and fit the regional realities of technology, including different internet connections. In addition, the operational difficulties they describe, especially in the area of user training and maintenance, have implications for how complex the system can be, how long the learning curve, and what kind of user interface to design, meaning that the more complex the system the higher the learning curve, and therefore the less successful in adoption the system will be, even if it is technically possible. Although the authors work is good at the diagnosis of the systemic barriers, they do not show progression to solution prototyping and implementation in their abstract, which is a typical missing step in social science research that can be handled by technical projects. The project then takes a practical tack at the identified challenges and proposes specific engineering solutions, such as using widely available commodity parts, designing for off-line operation and using a culturally appropriate gesture mapping and bilingual interface where suitable.

.

C. *Hand Gesture Recognition Using Artificial Intelligence and IMU-Based Wearable Device*

The researchers developed a multi-modal smart glove which is designed to address the comprehensive needs of paralyzed patients. Their research methodology takes a more general approach which uses both sensing modalities: physiological monitoring via DHT11 (temperature), MAX30100 (oximetry/pulse), and an ECG sensor; gesture-based communication using an MPU6050 accelerometer; and emotional state detection via a camera module processed with OpenCV. Data taken in using a raspberry pi which transmits it to a cloud and allows it to be displayed on a dedicated web dashboard. [10], [11] This study provides proof of concept for the combination of remote health telemetry and alternative communication channels with a single wearable platform. The study takes isolation and continues monitoring main challenges that were faced by the vulnerable population. The research has a problem of being stuck in a position of clinical ambition and practical wearability This highlights a critical gap between engineering comprehensiveness and user-centric design. Furthermore, the system's complexity inherently leads to high cost, directly exacerbating the economic accessibility barriers and there is another inconsistency being in the gesture recognition system which might not be generalizable in a wide spectrum of different paralysis , finally the research shows a notable gap in lacking clinical trials or longitudinal user studies to assess impact on the patients and system reliability outside the lab.

D. *Smart Glove with Gesture-Based Communication and Monitoring Paralyzed Patient*

The researchers developed a multi-modal smart glove which is designed to address the comprehensive needs of paralyzed patients. Their research methodology takes a more general approach which uses both sensing modalities: physiological monitoring via DHT11 (temperature), MAX30100 (oximetry/pulse), and an ECG sensor; gesture-based communication using an MPU6050 accelerometer; and emotional state detection via a camera module processed with OpenCV. Data taken in using a raspberry pi which transmits it to a cloud and allows it to be displayed on a dedicated web dashboard. [10], [11] This study provides proof of concept for the combination of remote health telemetry and alternative communication channels with a single wearable platform. The study takes isolation and continues monitoring main challenges that were faced by the vulnerable population. The research has a problem of being stuck in a position of clinical ambition and practical wearability This highlights a critical gap between engineering comprehensiveness and user-centric design. Furthermore, the system's complexity inherently leads to high cost, directly exacerbating the economic accessibility barriers and there is another inconsistency being in the gesture recognition system which might not be generalizable in a wide spectrum of different paralysis , finally the research shows a notable gap in lacking clinical trials or longitudinal user studies to assess impact on the patients and system reliability outside the lab.

E. *Enhanced Health Monitoring Using IoT-Embedded Smart Glove and Machine Learning*

The researchers implemented IOT architecture for remote health monitoring [12], [13] this is done through development of a E-health smart glove it followed the establishment of a embedded system pipeline with sensing vital signs (temperature, pressure and heartrate) with a integrated systems on a radio uno microcontroller with classification of data in a MATLAB environment using K-nearest neighbor (KNN) algorithm [14], this study shows an educational model for IOT in healthcare. The main inconsistency of this research is that it depends on MATLAB which runs on an external computer for its core machine learning classification which the main goal of a wearable embedded IoT device since it makes the user have to be near their desktop This design choice shows the project's framing. In addition, the noted 75.82% average classification efficiency does not give us confidence for health applications and shows the limitations in the sensor data quality, and the appropriateness of the basic KNN model applied to such a temporal multi-parametric dataset. This research also shows a main contradiction by emphasizing the personalization of health monitoring however the model was trained on a generic classification model and a limited data set. Suggested improvements for this study mainly lie in moving the machine learning model directly into the microcontroller and the classification engine should be upgraded to be able to handle time-series data and incorporation of a simpler user interface and allowing the manual triggering of measurements.

TABLE I. SUMMARY OF PAPERS REVIEWED ON" AI BASED ADAPTIVE BEHAVIORAL MONITORING FOR HANDICAP PERSONS USING SMART GLOVE."

Title / Author / Year	Core Idea	Key Gap	Suggested Improvement
Hand gesture recognition using flex sensor and machine learning algorithms. [5]	Uses flex sensors with machine learning algorithms (Random Forest, SVM) for static hand gesture classification in controlled environments. Analysis shows high accuracy rates (85%+).	Laboratory setting only, single-user focus, no integration with other sensors (IMU, health), no real-world communication application addressed.	Extend to multi-user system, integrate with IMU and health sensors, apply to real-world assistive communication .
Obstacles for using assistive technology in centers of special needs in the UAE. [8]	Survey-based analysis identifying barriers to assistive technology adoption: high cost, lack of cultural relevance, limited training	Identifies problems but provides no technical solutions. Focuses on adoption barriers rather than device design improvements.	Design low-cost, culturally relevant device with simple calibration suitable for Omani/GCC care contexts.

	in MENA region.		
Efficient Hand Gesture Recognition	Uses IMU (accelerometer, gyroscope) with 1-D CNN for gesture recognition. Analysis shows 97.88% accuracy with optimized model for wearable devices. [15], [16], [17]	No vehicle control, location Relies only on IMU, missing finger flexion details. Focuses on algorithmic efficiency rather than multi-user adaptability or communication applications.	Add GPS tracking, access control, and Implement hybrid sensing (IMU + flex sensors), add multi-user adaptive layer, focus on gesture-to-message communication.
Smart Glove with Gesture Based Communication and Monitoring of Paralyzed Patient. [10]	Multi-sensor glove (temperature, oximeter, ECG, camera, MPU6050) for paralyzed patients. Cloud-based monitoring and gesture communication.	Overly complex with many sensors, cloud-dependent, designed only for paralyzed patients in clinical settings.	Simplify to core sensors (flex, IMU, heart rate), prioritize offline capability, broaden user base beyond paralysis.
Enhanced Health Monitoring Using IoT-Embedded Smart Glove and Machine Learning. [12]	IoT-based smart glove with multiple sensors for health monitoring. Uses K-NN classifier in MATLAB for health prediction with cloud connectivity.	Focuses on health monitoring rather than communication, requires continuous internet, complex system architecture.	Adopt communication-first approach, use local processing instead of cloud, maintain offline functionality.

III. METHODOLOGY

The waterfall methodology [18] was chosen to complete this paper. Since this technique follows a sequential and systematic process where the progress flows through clearly defined stages following an academic timeline which is fixed, unlike the agile method it does not require constant user feedback cycles and unlike the spiral and v-models, it is less time consuming which could be used especially that the scope is fixed.

Basically, the processes are executed one after the other in the model. It is a linear approach where the project flows downwards through set phases, on completion of the previous phase, the next phase will begin, which leads towards project completion with clear documentation at each stage.

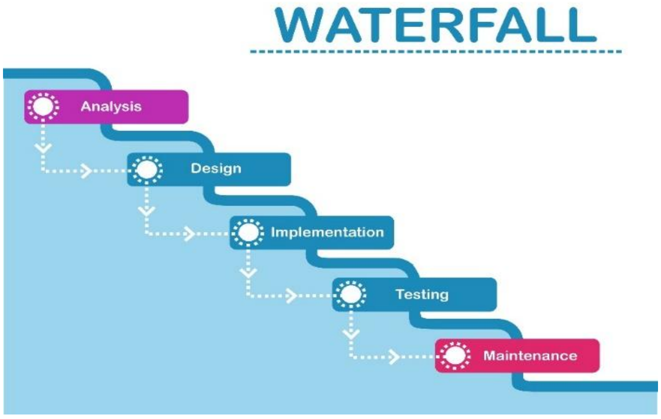

Fig. 1. Project Methodology

IV. SYSTEM DESIGN AND ARCHITECTURE

The MediGlove system is organized across four functional layers. Figure 2 shows the complete implementation block diagram. The sub-sections below explain each layer in detail.

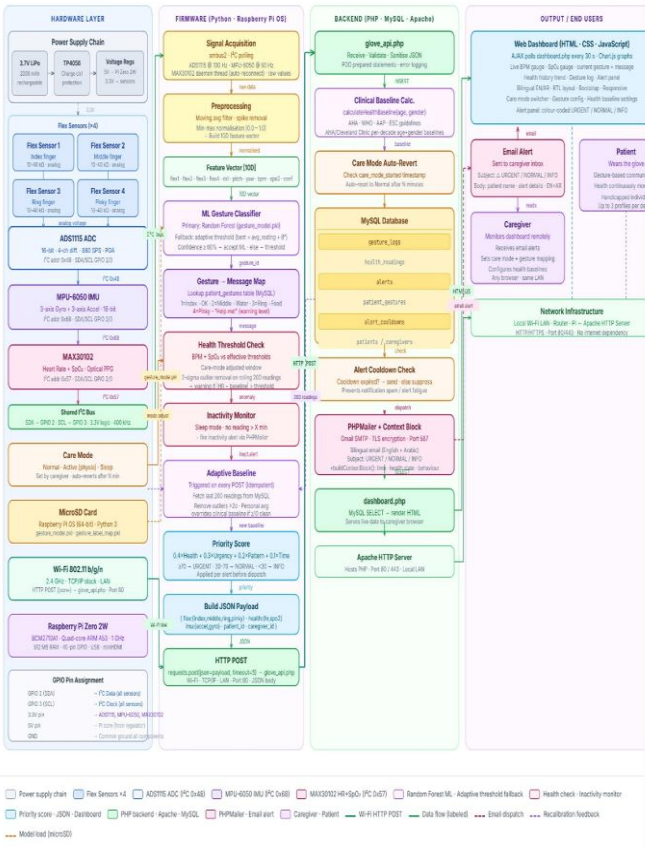

Fig. 2. MediGlove Complete System Block Diagram (Implementation Version)

Layer 1 — Hardware Layer

The hardware are all the physical parts that are attached to the glove. The power chain consists of a 3.7V LiPo battery, a TP4056 charge controller, two voltage regulators, one to supply a stable 5V rail to the Raspberry Pi Zero 2W [19] and another to supply a stable 3.3V rail to all sensors. The four Spectra Symbol flex sensors are wired to the ADS1115 16-bit ADC [20] (I2C address 0x48)-channel 0 to channel 3, corresponding to the index, middle, ring and Pinky fingers. The MPU-6050 IMU [21] (I2C address 0x68) supplies three-axis accelerometer and gyroscope data to use for hand orientation context. The pulse oximeter (I2C address 0x57) from the MAX30102 [22] reads the heart rate and SpO2 continuously. SDA/SCL bus is shared with three I2C devices over GPIO2 and GPIO3 of the raspberry pi.

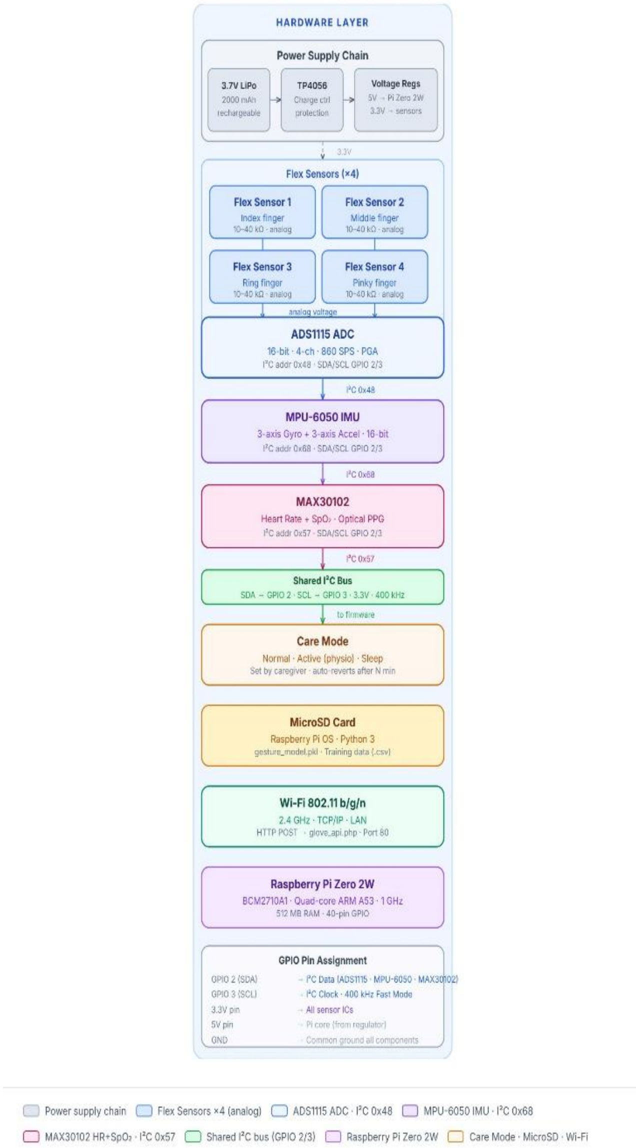

Fig. 3. Hardware Layer — Sensors, ADC, Power Chain

Layer 2 —Firmware Layer (Python on Raspberry Pi OS)

The firmware layer is the python script smart_glove_pi.py on raspberry pi os 64-bit bookworm. It runs concurrently three tasks performed using the Python threading module: it reads every 2 seconds the flex channels and various registers of the ADS1115 and MPU-6050 sensors and then HTTP POSTs the raw values to the server, a dedicated health thread keeps reading every second the MAX30102 sensor and updates a shared dictionary protected by a threading lock, and a dedicated config refresh thread polls get_config.php every 5 minutes to update the current patient assignment without needing to restart the Pi. Most importantly, there is no intelligence here — the firmware only needs to be reliable in its ability to grab the sensors and send a structured JSON.

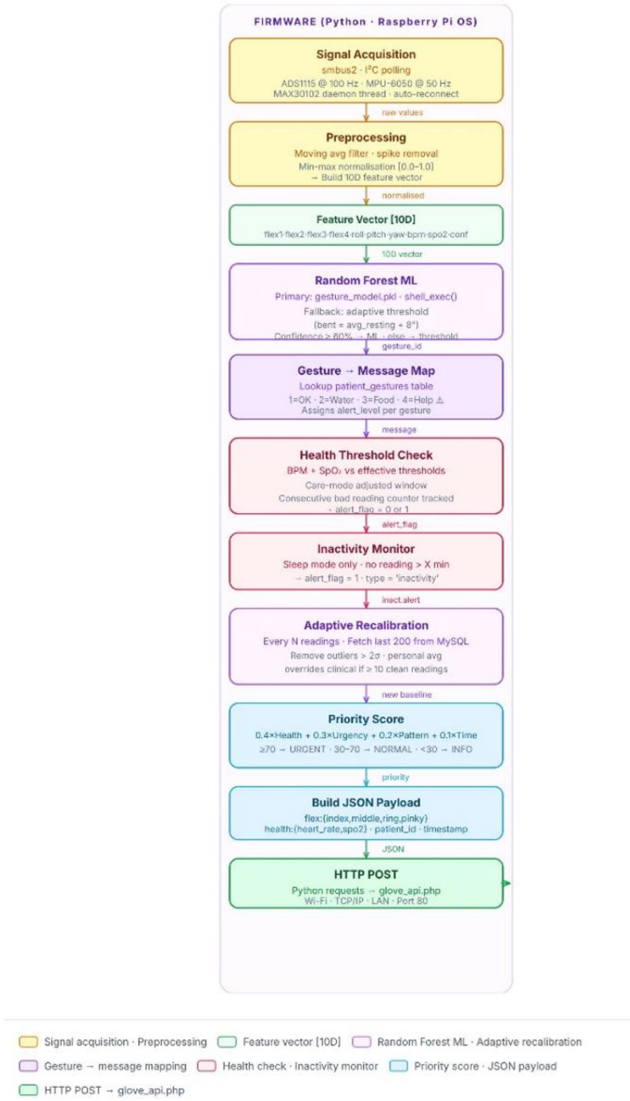

Fig. 4. Firmware Layer — Python Threading, I2C Reads, HTTP POST

Layer 3 — Backend Intelligence Layer (PHP / MySQL / Apache)

The backend layer is where all adaptive intelligence runs. The Apache server (WAMP on Windows, with httpd.conf modified to permit LAN connections) receives JSON POST requests from the Pi at the glove_api.php endpoint. On every POST, the backend executes: automatic database table creation via CREATE TABLE IF NOT EXISTS; patient and caregiver data retrieval; health reading storage; adaptive HR baseline computation (rolling 200-reading window with 2-sigma outlier removal); adaptive flex threshold computation (resting averages plus fixed buffers after ten calibration readings); gesture detection using per-patient thresholds; health anomaly checking against care-mode-adjusted ranges; alert cooldown enforcement; priority score computation; and bilingual PHPMailer email dispatch. The MySQL database stores eight tables: patients, caregivers, health_readings, flex_resting_readings, gesture_logs, alerts, alert_cooldowns, and patient_gestures.

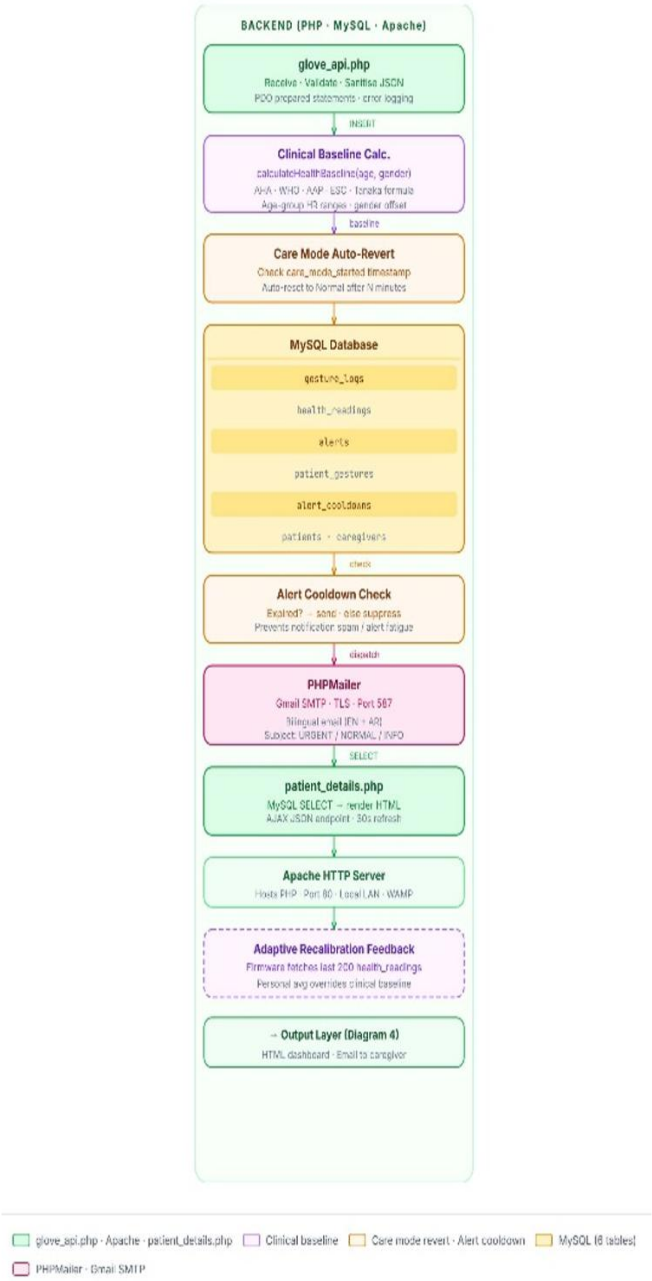

Fig. 5. Backend Intelligence Layer — PHP/MySQL Adaptive Processing

Layer 4 — Output Layer (Dashboard & Alerts)

The output layer delivers actionable information to the caregiver through two channels. The Apache-served web dashboard (dashboard.php) renders live health gauges, a gesture history log, and patient management controls including the Assign to Glove button that activates dynamic patient switching. The PHPMailer email system dispatches bilingual HTML emails to the caregiver's registered address, categorized by priority: URGENT emails for health anomalies, NORMAL emails for recognized gesture messages, and INFO emails for behavioural pattern reports. Both channels are accessible from any device on the local LAN without any internet dependency.

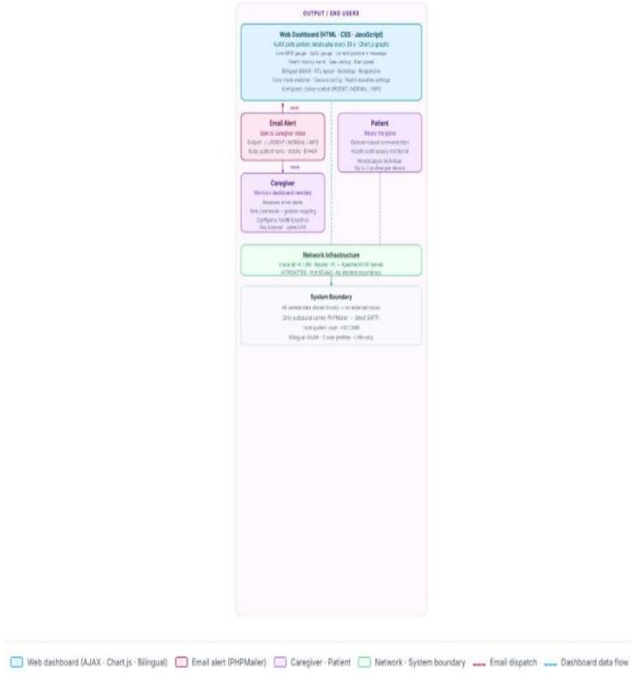

Fig. 6. Output Layer — Caregiver Dashboard and Email Alert Channels

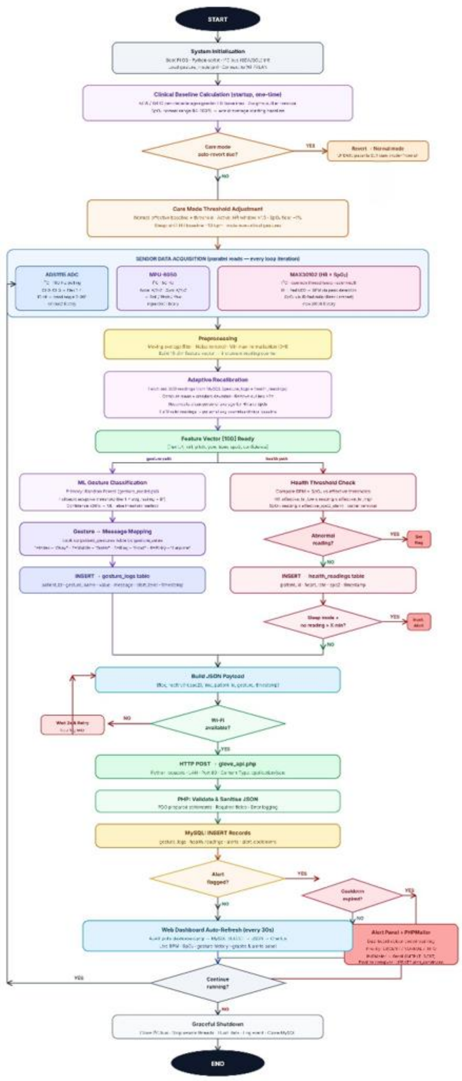

Fig. 7. System Flowchart

The figure above shows the complete system flowchart for MediGlove. The sub-sections below annotate each phase of the flow in detail.

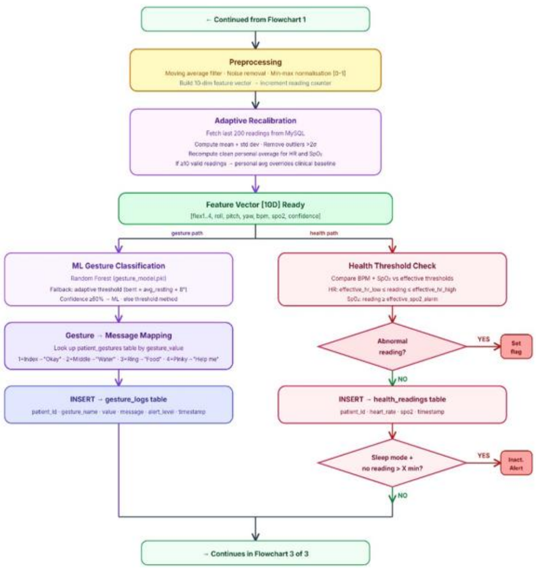

Fig. 8. Phase 1 — System Startup and Sensor Acquisition

A. *Phase 1 — Startup and Sensor Acquisition*

On boot, the Raspberry Pi OS starts automatically via systemd and launches smart_glove_pi.py. The script initialises the smbus2 I2C bus, wakes the MPU-6050 by writing 0 to its power management register (0x6B), and starts the MAX30102 health reader thread. A clinical baseline is then calculated using AHA [23] and Cleveland Clinic [24] per-decade age and gender HR ranges, providing medically appropriate starting thresholds before any personal data has been collected. The system checks whether a care mode auto-revert is due and if so updates the patient record to Normal mode. Care mode threshold adjustment is then applied — Normal mode uses the personal baseline plus or minus the standard threshold, Active mode expands the HR window by a factor of 1.5, and Sleep mode shifts the HR baseline down by 10 BPM and mutes non-critical gesture alerts. The system then begins sensor acquisition: the ADS1115 ADC reads all four flex sensor channels via I2C at 100Hz, converting 16-bit raw values to bend angles between 0 and 90 degrees; the MPU-6050 is read at 50Hz providing accelerometer and gyroscope data converted to roll, pitch, and yaw; and the MAX30102 runs continuously in a dedicated daemon thread with automatic reconnection on I2C error, providing heart rate and SpO2 via IR and red LED photoplethysmography.

B. *Phase 2 — Processing and Classification*

Raw sensor values are passed through a preprocessing stage that applies a moving average filter for noise removal and min-max normalisation to produce a standardised 10-dimensional feature vector comprising the four flex angles, roll, pitch, yaw, BPM, SpO2, and a confidence score. Adaptive recalibration is performed by fetching the last 200 readings from MySQL, computing the mean and standard deviation, removing outliers beyond two standard deviations, and recomputing a clean personal average once ten or more valid readings have accumulated, this personal average overrides the clinical baseline for both HR and SpO2. The feature vector is then split into two parallel paths. On the gesture path, the Random Forest classifier [25] (gesture_model.pkl) classifies the four flex angles into one of four gesture classes; predictions with confidence below 60% fall back to the adaptive threshold method where a finger is considered bent if its angle exceeds the patient's average resting angle by 8 degrees. The recognised gesture is mapped to a caregiver message via the patient_gestures table and inserted into gesture_logs. On the health path, BPM and SpO2 are compared against the effective care-mode-adjusted thresholds — an abnormal reading sets an alert flag — and the values are inserted into health_readings. If sleep mode is active and no reading has been received beyond the inactivity threshold, an inactivity alert flag is set.

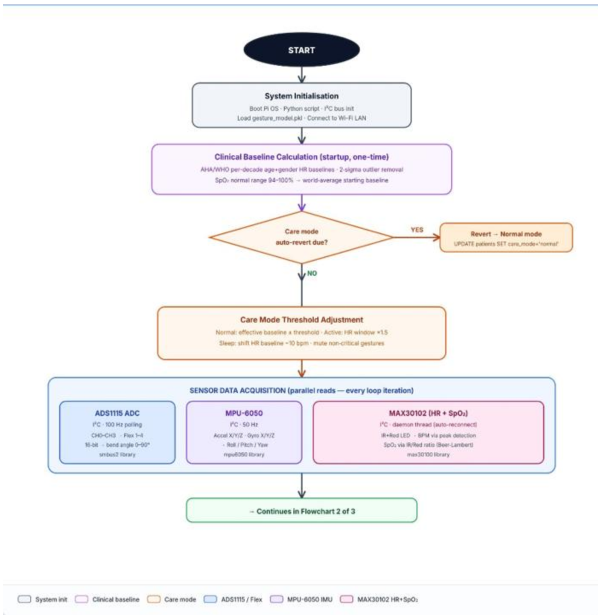

Fig. 9. Phase 2 — Processing and Classification

C. *Phase 3 — Transmission, Alert Dispatch and Loop Control*

The processed data is packaged into a nested JSON payload containing the flex readings, health values, IMU data, patient ID, gesture result, and timestamp. Before transmission, the system checks Wi-Fi availability if the LAN is unreachable, the firmware waits two seconds and retries, logging locally only. Once connected, the payload is transmitted via HTTP POST to glove_api.php using the Python requests library on port 80 with a five-second timeout. The PHP backend validates and sanitises the incoming JSON using PDO prepared statements before inserting records into the gesture_logs, health_readings, alerts, and alert_cooldowns tables. If an alert flag was raised, the system checks whether the cooldown period has expired if it has, the alert panel is updated and PHPMailer dispatches a bilingual HTML email to the caregiver via Gmail SMTP on TLS port 587 with the appropriate URGENT, NORMAL, or INFO priority label; if the cooldown has not expired, the alert is suppressed to prevent notification spam. The web dashboard auto-refreshes every 30 seconds via AJAX polling of dashboard.php, querying MySQL and rendering live BPM, SpO2, gesture history, and charts via Chart.js. The system then checks whether it should continue running if yes, it loops back to sensor acquisition in Phase 1; if no, it performs a graceful shutdown by closing the I2C bus, stopping all sensor threads, flushing remaining data, and closing the MySQL connection before ending.

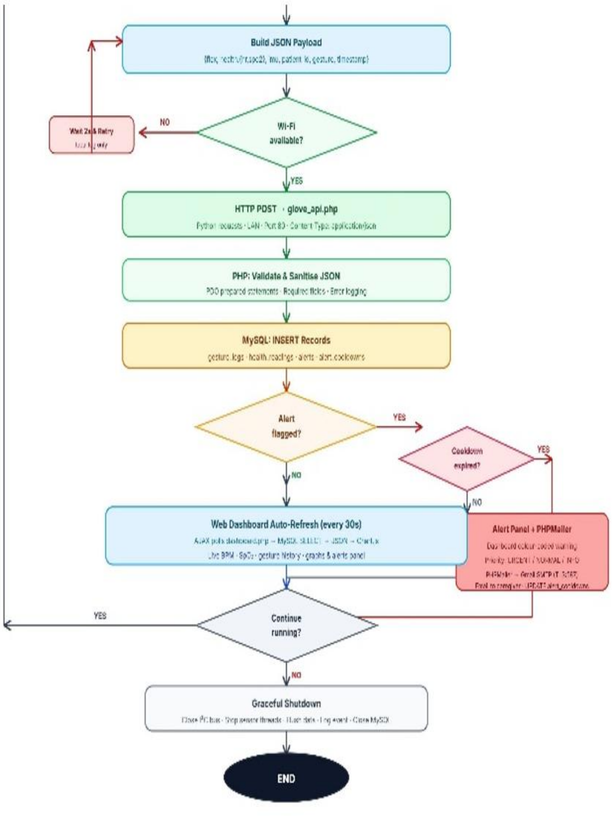

Fig. 10. Phase 3 — Transmission, Alert Dispatch and Loop Control

V. Implementation and Results

This chapter presents the MediGlove implementation results, test case outcomes, and system validation. Live testing was conducted on 31 May 2026 and 2 June 2026 using a Raspberry Pi Zero 2W connected to a WAMP server via a Windows mobile hotspot at 192.168.137.1. Two patient profiles were tested: Patient 7 (elderly female, Arabic name) and Patient 8 (fidaa). No circuit simulation was used; all validation was conducted through live hardware testing and server log analysis.

A. *Schematic Diagram and Pin Diagram*

This figure shows the MediGlove circuit schematic. A shared 3.3V power rail and a common GND rail run horizontally across the top of the diagram, supplying all three sensor ICs. The Raspberry Pi Zero 2W sits on the left, with GPIO 2 (SDA, pin 3) and GPIO 3 (SCL, pin 5) forming the shared I2C bus running vertically through the schematic at 400kHz. The ADS1115 16-bit ADC (I2C address 0x48) connects its VDD, GND, SDA, and SCL pins to the shared rails and bus, with its four AIN0–AIN3 input channels each connected to the midpoint of a voltage divider formed by the flex sensor and a fixed 10kΩ resistor between 3.3V and GND. The MPU-6050 IMU (I2C address 0x68, set by AD0 pulled to GND) and the MAX30102 pulse oximeter (I2C address 0x57) each connect their VCC/VIN, GND, SDA, and SCL pins to the same shared rails and bus. The firmware smart_glove_pi.py running on the Pi transmits all processed data via HTTP POST to the WAMP server.

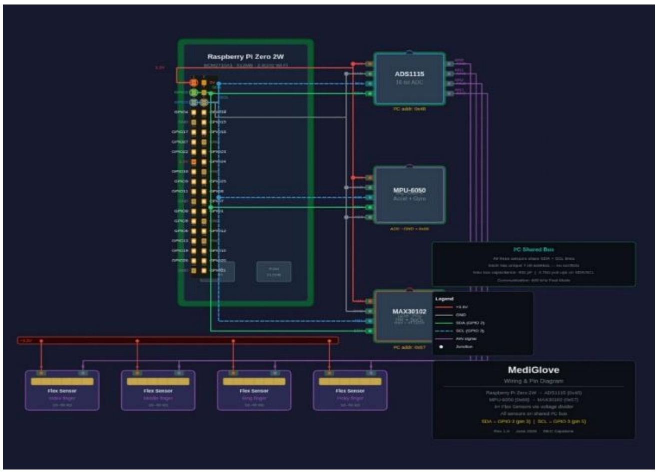

Fig.11. Mediglove pin diagram

The figure also shows the MediGlove wiring and pin diagram. The Raspberry Pi Zero 2W 40-pin GPIO header is shown on the left with all active pins highlighted. Pin 1 (3.3V) supplies the ADS1115 VDD, MPU-6050 VCC, and MAX30102 VIN through a shared red power wire. Pin 6 (GND) connects to a common ground rail shared by all three ICs and all four flex sensor voltage dividers. Pin 3 (GPIO 2, SDA) and Pin 5 (GPIO 3, SCL) form the shared I2C bus connecting to the SDA and SCL pins of the ADS1115 (0x48), MPU-6050 (0x68), and MAX30102 (0x57) in parallel. The ADS1115 AIN0 through AIN3 channels connect to the four flex sensors index, middle, ring, and pinky fingers respectively each wired as a voltage divider with a 10kΩ fixed resistor. The MPU-6050 AD0 pin is pulled to GND to set its I2C address to 0x68. The MAX30102 operates with its Red and IR LEDs providing PPG-based heart rate and SpO2 measurement via 18-bit ADC.

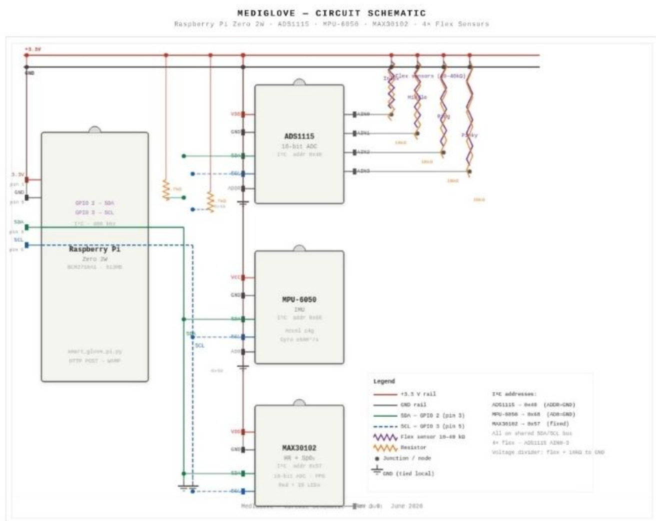

Fig. 12. MediGlove Circuit Diagram

Moreover, the circuit shows the MediGlove circuit schematic. A shared 3.3V power rail and a common GND rail run horizontally across the top of the diagram, supplying all three sensor ICs. The Raspberry Pi Zero 2W sits on the left, with GPIO 2 (SDA, pin 3) and GPIO 3 (SCL, pin 5) forming the shared I2C bus running vertically through the schematic at 400kHz. The ADS1115 16-bit ADC (I2C address 0x48) connects its VDD, GND, SDA, and SCL pins to the shared rails and bus, with its four AIN0–AIN3 input channels each connected to the midpoint of a voltage divider formed by the flex sensor and a fixed 10kΩ resistor between 3.3V and GND. The MPU-6050 IMU (I2C address 0x68, set by AD0 pulled to GND) and the MAX30102 pulse oximeter (I2C address 0x57) each connect their VCC/VIN, GND, SDA, and SCL pins to the same shared rails and bus. The firmware smart_glove_pi.py running on the Pi transmits all processed data via HTTP POST to the WAMP server.

B. *Live System Screenshots*

The following images show the MediGlove system during live operation. The screenshots provided are inserted from the actual deployment session.

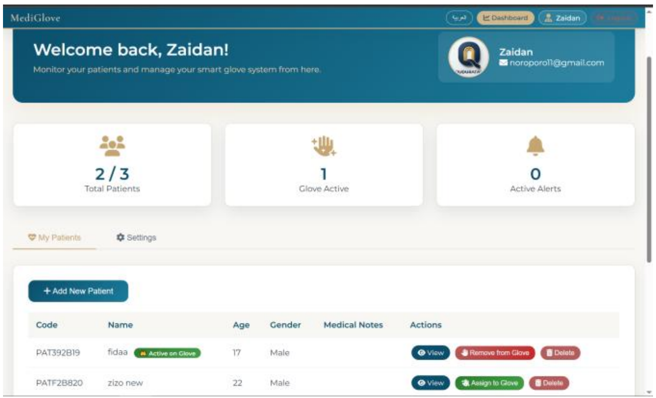

Fig. 13. Add New Patient Page

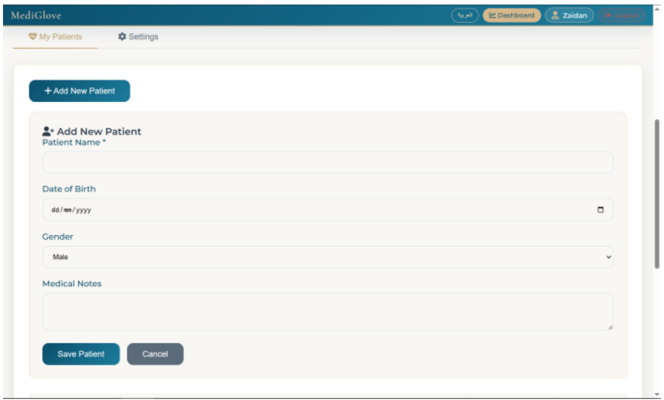

Fig. 14. Displays the add new patient form where the caregiver enters the patient's name, date of birth, gender, and any relevant clinical notes before registering them in the system.

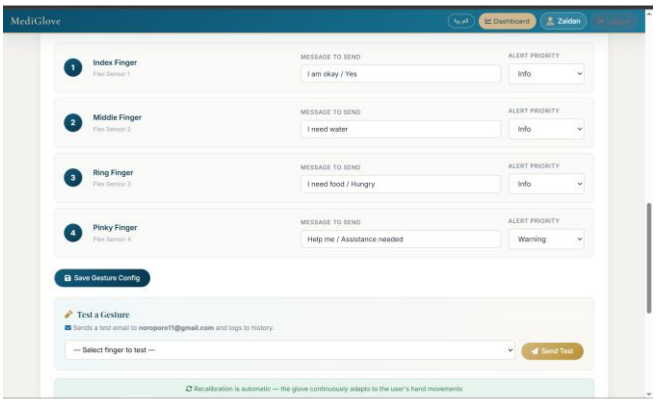

Fig. 15. shows the gesture message configuration page where each finger is assigned a custom message and alert level. A live test button allows the caregiver to trigger a test notification to verify the configuration before deployment.

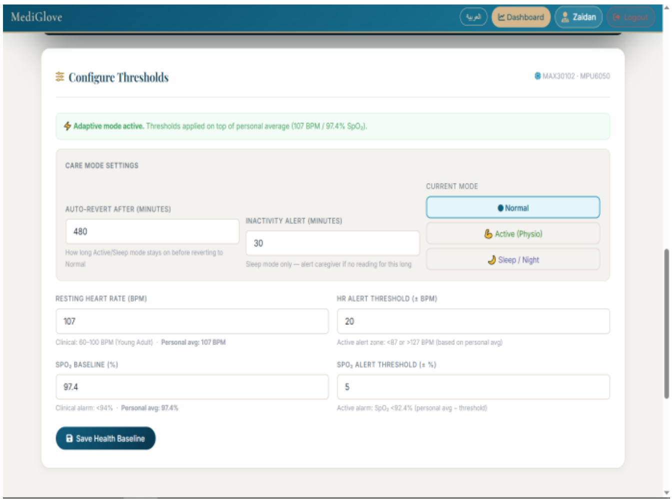

Fig. 16. this image shows the health threshold configuration panel where caregivers can manually override the adaptive HR and SpO2 alert thresholds with patient-specific clinical values if required.

Fig. 17. showcases the live health monitoring panel displaying the current HR and SpO2 readings alongside the patient's adaptive baseline range as it converged during the session.

Fig. 18. Shows the health history page with a chart of HR and SpO2 readings over the session timeline and a tabular summary showing date, time, individual readings, and status classification.

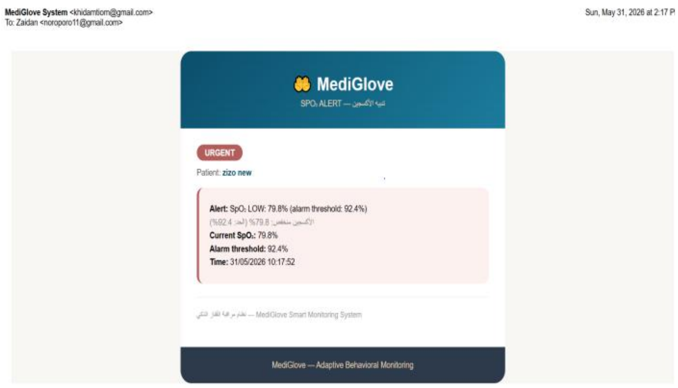

Fig. 19. shows an URGENT level email triggered when the patient's SpO2 reading fell outside the adaptive safe range, with the subject line and header clearly marked as urgent to prompt immediate caregiver response.

Fig. 20. shows a NORMAL level health alert email triggered by an elevated heart rate reading, containing the deviation from the patient's personal baseline in both absolute BPM and percentage terms within the context block.

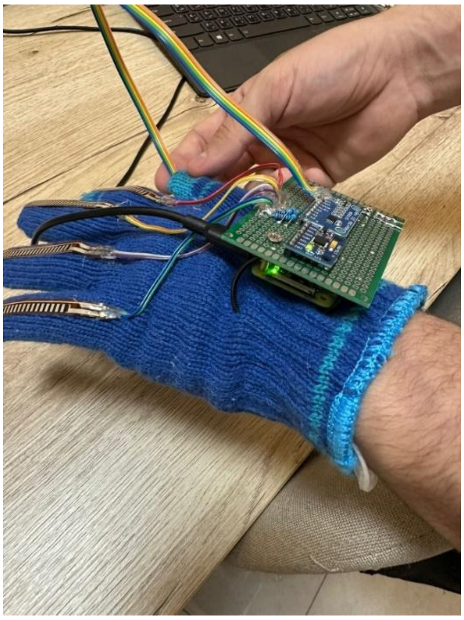

Fig. 21. shows the MediGlove prototype worn on the hand during the live testing session, demonstrating the ergonomic fit of the glove and the placement of the flex sensors across the four instrumented fingers.

Fig. 22. shows the bilingual email format with both English and Arabic text present throughout the main body and the context block, confirming the PHPMailer implementation of the dual-language alert system

C. *System Validation*

System validation was performed step by step as proposed in methodology to ensure that the system fulfils project objectives and user requirements.

TABLE II. System Validation

Objective	Validation Method	Outcome	Status
To design a Raspberry Pi-based glove with health monitoring and flex sensors for gesture recognition	Physical prototype assembled and operational	All sensors reading; data transmitted every 2s via json= POST	Met
To develop a web application to capture user preferences and behaviours and integrate with a database	Dashboard accessed in browser during live testing	Patient assignment, care mode, gesture logs all functional	Met
To collect user data through sensors, store,	Two patients with different resting	Thresholds differ per patient; personal_adaptive after 10 readings	Met
To train the model to customise the glove for multi-user adaptability	Multiple readings collected across 30-minute sessions	HR range evolved: 63-103 -> 56-96 BPM personal adaptive	Met

VI. CONCLUSION

This project successfully designed and implemented MediGlove, an AI-based adaptive behavioral monitoring smart glove for individuals with physical disabilities. The system achieves its primary aim of facilitating gesture-based communication and enabling caregiver health monitoring through a fully functional prototype validated in live testing across two patients with contrasting physiological profiles.

The key technical contribution of MediGlove is its fully server-side adaptive intelligence architecture. The system automatically learns each patient's resting hand position from the first ten readings and computes personalized per-finger gesture thresholds without any manual calibration. Health baselines evolve from medically accurate age-and-gender-specific clinical defaults to individualized personal averages as readings accumulate, implementing genuinely adaptive monitoring requiring zero user intervention.

All four project objectives were met and confirmed through live testing. The adaptive HR baseline was observed converging from clinical default 63-103 BPM to personal range 56-96 BPM within a single session. Bilingual English/Arabic email alerts were delivered correctly for all gesture and health anomaly events. The system operated reliably on a local LAN at 145 OMR total hardware cost without any internet dependency.

The edge-computing architecture proved to be a sound design decision: the Raspberry Pi Zero 2W's limited resources are dedicated entirely to reliable sensor reading and HTTP transmission, while all adaptive intelligence runs unencumbered on the PHP server. Compared to existing solutions, MediGlove demonstrates significant advantages in cost, adaptability, multi-user support, bilingual cultural relevance, and local operation — directly addressing the gaps identified in the literature review and the barriers documented by some of the authors.

VII. Future Work

To make this invention operates at optimal level future work will focus on improving the functionality, reliability, and clinical applicability of MediGlove. A fifth flex sensor will be added to monitor thumb movement and support a wider range of complex gestures. Motion artifact rejection will also be enhanced by using MPU-6050 accelerometer data to suppress unreliable MAX30102 readings during periods of significant movement. Gesture recognition will be improved through a confirmation window requiring consistent readings across multiple samples, while an exponential moving average will allow health baselines to adapt more effectively to genuine changes in the user's condition.

Further developments will include additional alert channels such as WhatsApp Business API or Firebase Cloud Messaging, a mobile-optimized caregiver dashboard, and structured clinical trials involving patients at Al Wafa Rehabilitation Centres in Oman. Furthermore, the system will also be enhanced with improved battery efficiency, Bluetooth fallback communication for areas without Wi-Fi connectivity, and over-the-air firmware updates to support reliable long-term deployment and maintenance of the smart glove.

References

[1] World Health Organization, "Disability and health," Fact Sheet, Mar. 2023. [Online]. Available: https://www.who.int/news-room/fact-sheets/detail/disability-and-health.

[2] S. Shin, H.-J. Lee, W. H. Chang, S. H. Ko, Y.-I. Shin, and Y.-H. Kim, "A smart glove digital system promotes restoration of upper limb motor function and enhances cortical hemodynamic changes in subacute stroke patients with mild to moderate weakness: A randomized controlled trial," *Journal of Clinical Medicine*, vol. 11, no. 24, p. 7343, 2022. doi: 10.3390/jcm11247343.

[3] M.-G. Kang, S. J. Yun, S. Y. Lee, B.-M. Oh, H. H. Lee, S.-U. Lee, and H. G. Seo, "Effects of upper-extremity rehabilitation using smart glove in patients with subacute stroke: Results of a prematurely terminated multicenter randomized controlled trial," *Frontiers in Neurology*, vol. 11, art. 580393, 2020. doi: 10.3389/fneur.2020.580393.

[4] XiangAi, "XiangAi rehabilitation robot gloves for stroke patients," 2025. [Online]. Available: https://xiang-ai.com/.

[5] A. K. Panda, R. Chakravarty, and S. Moulik, "Hand gesture recognition using flex sensor and machine learning algorithms," in *Proc. 2020 IEEE-EMBS Conf. Biomedical Engineering and Sciences (IECBES)*, Langkawi Island, Malaysia, 2021, pp. 1-6. doi: 10.1109/IECBES48179.2021.9398789.

[6] R. Tchantchane, H. Zhou, S. Zhang, and G. Alici, "A review of hand gesture recognition systems based on noninvasive wearable sensors," *Advanced Intelligent Systems*, vol. 5, no. 10, art. 2300207, 2023. doi: 10.1002/aisy.202300207.

[7] M. Caeiro-Rodríguez, I. Otero-González, F. A. Mikic-Fonte, and M. Llamas-Nistal, "A systematic review of commercial smart gloves: Current status and applications," *Sensors*, vol. 21, no. 8, p. 2667, 2021. doi: 10.3390/s21082667.

[8] M. Fteiha, M. Al-Rashaida, D. Elsori, A. Khalil, and G. Al Bustami, "Obstacles for using assistive technology in centres of special needs in the UAE," *Disability and Rehabilitation: Assistive Technology*, vol. 19, no. 8, pp. 2934-2944, 2024. doi: 10.1080/17483107.2024.2323698.

[9] World Health Organization and UNICEF, "Global Report on Assistive Technology," Geneva, Switzerland, 2022. [Online]. Available: https://www.who.int/publications-detail-redirect/9789240049178.

[10] H. M. Kalpana, A. B. Kulkarni, M. Tiwari, O. R. Chitmalwar, and R. S. TR, "Smart glove with gesture based communication and monitoring of paralyzed patient," in *Proc. 2023 Int. Conf. Smart Systems for Applications in Electrical Sciences (ICSSES)*, Tumakuru, India, 2023, pp. 1-6. doi: 10.1109/ICSSES58299.2023.10199446.

[11] P. S. Miranda, A. K. Acharya, S. F. Dante, S. Rai, S. J. Ail, V. Arun Dsouza, S. Bhat, and S. Adarsh Rag, "GSM-based smart glove for gesture recognition and health monitoring in paralysis patients," in *Proc. 2025 Int. Conf. Biomedical Engineering and Sustainable Healthcare (ICBMESH)*, Manipal, India, 2025. doi: 10.1109/ICBMESH66209.2025.11182196.

[12] G. Yang, J. Deng, G. Pang, H. Zhang, J. Li, B. Deng, Z. Pang, J. Xu, M. Jiang, P. Liljeberg, H. Xie, and H. Yang, "An IoT-enabled stroke rehabilitation system based on smart wearable armband and machine learning," *IEEE Journal of Translational Engineering in Health and Medicine*, vol. 6, art. 2100510, 2018. doi: 10.1109/JTEHM.2018.2822681.

[13] M. H. B. Ucar, A. Adjevi, F. Aktaş, and S. Solak, "Utilizing IoMT-based smart gloves for continuous vital sign monitoring to safeguard athlete health and optimize training protocols," *Sensors*, vol. 24, no. 20, p. 6500, 2024. doi: 10.3390/s24206500.

[14] T. M. Cover and P. E. Hart, "Nearest neighbor pattern classification," *IEEE Transactions on Information Theory*, vol. 13, no. 1, pp. 21-27, 1967. doi: 10.1109/TIT.1967.1053964.

[15] A. Dahiya, D. Wadhwa, R. Katti, and L. G. Occhipinti, "Efficient hand gesture recognition using artificial intelligence and IMU based wearable device," *IEEE Sensors Letters*, vol. 8, no. 12, art. 601560, 2024. doi: 10.1109/LSENS.2024.3501586.

[16] M. Kim, J. Cho, S. Lee, and Y. Jung, "IMU sensor-based hand gesture recognition for human-machine interfaces," *Sensors*, vol. 19, no. 18, p. 3827, 2019. doi: 10.3390/s19183827.

[17] L. Fan, Z. Zhang, B. Zhu, D. Zuo, X. Yu, and Y. Wang, "Smart-data-glove-based gesture recognition for amphibious communication," *Micromachines*, vol. 14, no. 11, p. 2050, 2023. doi: 10.3390/mi14112050.

[18] W. W. Royce, "Managing the development of large software systems," in *Proc. IEEE WESCON*, Los Angeles, CA, USA, Aug. 1970, pp. 1-9.

[19] Raspberry Pi Ltd, "Raspberry Pi Zero 2 W product brief," Apr. 2024. [Online]. Available: https://pip.raspberrypi.com/documents/RP-008359-DS-raspberry-pi-zero-2-w-product-brief.pdf.

[20] Texas Instruments, *ADS111x Ultra-Small, Low-Power, I2C-Compatible, 860-SPS, 16-Bit ADCs With Internal Reference, Oscillator, and Programmable Comparator*, Datasheet SBAS444, Texas Instruments, Dallas, TX, USA. [Online]. Available: https://www.ti.com/lit/ds/symlink/ads1115.pdf.

[21] InvenSense Inc., *MPU-6000 and MPU-6050 Product Specification*, Rev. 3.4, Doc. No. PS-MPU-6000A-00, Aug. 19, 2013.

[22] Analog Devices (Maxim Integrated), *MAX30102: High-Sensitivity Pulse Oximeter and Heart-Rate Sensor for Wearable Health*, Data Sheet, Rev. 1, Nov. 8, 2018.

[23] American Heart Association, "Target heart rates chart," 2024. [Online]. Available: https://www.heart.org/en/healthy-living/fitness/fitness-basics/target-heart-rates.

[24] Cleveland Clinic, "Heart rate: Normal rates and what to know," 2026. [Online]. Available: https://my.clevelandclinic.org/health/diagnostics/heart-rate.

[25] L. Breiman, "Random forests," *Machine Learning*, vol. 45, no. 1, pp. 5-32, 2001. doi: 10.1023/A:1010933404324.

Journal of Big Data & Smart City

كلية الشرق الأوسط
Middle East College

Automatic Sleep Stage Classification and Sleep Quality Assessment Using EEG Signals and Convolutional Neural Networks

Khalid Al Jassasi
Department of Computing and Electronics Engineering
Middle East College
Muscat, Sultanate of Oman
23F24848@mec.edu.om

Mr. Jayasankar Srilla
Department of Computing and Electronics Engineering
Middle East College
Muscat, Sultanate of Oman
jayasankar@mec.edu.om

Received: 12th May 2026; Revised: 15th June 2026;

Accepted: 14th July 2026

***Abstract* — Sleep is very important in physical well-being, cognitive ability, and emotional stability. The uncritical classification of sleep phases as well as objective measurement of sleep quality are critical in diagnosing sleep disorders and sleep health. The traditional sleep staging is conducted manually with the help of polysomnography records, and it is time-consuming, expensive and prone to inter-scorer discrepancy. Such constraints have inspired the creation of automated systems of sleep analysis involving electroencephalographic (EEG) and artificial intelligence methodologies. This research introduces an automatic sleep stage classification and sleep quality evaluation system based on EEG signals and the Convolutional Neural Networks (CNNs) using datasets. Clinically annotated sleep EEG datasets are publicly available, and they are used so that the quality of recordings, standard labelling, and reproducible results can be guaranteed. The EEGs are pre-treated to eliminate noise and artifact, divided into normal 30-second epochs and converted to frequency representations to extract spectral and temporal features. The inputs are these representations to a CNN model which is trained to distinguish between sleep stages Wake, N1, N2, N3, and REM. After classifying sleep stages, objective sleep quality measures are calculated based on the inferred sleep architecture such as total sleep time, sleep efficiency, duration distribution of sleep stages, proportion of deep sleep and sleep fragmentation measures. The efficiency of the suggested system is measured in terms of typical classification measure of accuracy, precision, recall, F1-score, and confusion matrix analysis and is contrasted with the methods that are known to be used in the research. The development of the suggested system is supposed to minimize the use of manual sleep scoring, enhance the consistency and efficiency of sleep analysis procedures, and create a basis on scalable sleep monitoring solutions.**

Keywords — EEG, Sleep Staging, CNN, Deep Learning, PSD, Sleep Quality, Signal Processing, Sleep Monitoring

النوم مهم جدًا للصحة البدنية والقدرة المعرفية والاستقرار العاطفي. يعد التصنيف غير النقدي لمراحل النوم بالإضافة إلى القياس الموضوعي لجودة النوم أمرًا بالغ الأهمية في تشخيص اضطرابات النوم وصحة النوم. يتم إجراء تصنيف النوم التقليدي يدويًا بمساعدة سجلات تخطيط النوم، وهو يستغرق وقتًا طويلاً ومكلفًا وعرضة للتناقض بين المسجلين. وقد ألهمت هذه القيود إنشاء أنظمة آلية لتحليل النوم تتضمن منهجيات تخطيط كهربية الدماغ (EEG) والذكاء الاصطناعي. يقدم هذا البحث تصنيفًا تلقائيًا لمرحلة النوم ونظامًا لتقييم جودة النوم يعتمد على إشارات تخطيط كهربية الدماغ والشبكات العصبية التلافيفية (CNNs) باستخدام مجموعات البيانات. مجموعات بيانات تخطيط كهربية الدماغ أثناء النوم المشروحة سريريًا متاحة للجمهور، ويتم استخدامها بحيث يمكن ضمان جودة التسجيلات ووضع العلامات القياسية والنتائج القابلة للتكرار. يتم معالجة تخطيط كهربية الدماغ مسبقًا لإزالة الضوضاء والتحف، وتقسيمه إلى عصور عادية مدتها 30 ثانية وتحويله إلى تمثيلات ترددية لاستخراج الميزات الطيفية والزمنية. المدخلات هي هذه التمثيلات لنموذج CNN الذي تم تدريبه على التمييز بين مراحل النوم Wake وN1 وN2 وN3 وREM. بعد تصنيف مراحل النوم، يتم حساب مقاييس جودة النوم الموضوعية بناءً على بنية النوم المستنتجة مثل إجمالي وقت النوم، وكفاءة النوم، وتوزيع مدة مراحل النوم، ونسبة النوم العميق، ومقاييس تجزئة النوم. يتم قياس كفاءة النظام المقترح من حيث مقياس التصنيف النموذجي للدقة والضبط والتذكر ودرجة F1 وتحليل مصفوفة الارتباك ويتم مقارنتها بالطرق المعروفة المستخدمة في البحث. ومن المفترض أن يؤدي تطوير النظام المقترح إلى تقليل استخدام تسجيل النوم اليدوي، وتعزيز اتساق وكفاءة إجراءات تحليل النوم، وإنشاء أساس لحلول مراقبة النوم القابلة للتطوير.

الكلمات المفتاحية— تخطيط كهربية الدماغ، تحديد مراحل النوم، *CNN*، التعلم العميق، *PSD*، جودة النوم، معالجة الإشارات، مراقبة النوم

I. Introduction

Sleep is a basic biological condition, which is vital in ensuring physical wellness, cognitive functions, moodiness, and good health. The recent way of living, the level of stress, and the overuse of digital technologies have led to mass sleep disorders in populations. Consequently, sleep-related disorders and subpar sleep quality have become major issues of global public health. The ability to measure sleep stages and sleep quality accurately can be important in the diagnosis of sleep disorders, in assessing the effectiveness of treatment or in determining the interaction between sleep and long-term health outcomes. Conventionally, sleep analysis has been based on manual interpretation of physiological signals which is time consuming and can be affected by human variations. In recent years, there has been an increase in the number of people interested in creating automated systems capable of processing sleep data efficiently and objectively with the help of the latest achievements in signal processing and artificial intelligence.

Sleep represents about a third of the total human life and is fundamentally important in a variety of physiological and neurological activities. Thus, it has been demonstrated that lack of sleep or low sleep quality correlates with poor cognitive abilities, mood, cardiovascular, metabolic, and higher risks of death [1]. Therefore, the knowledge of the sleep structure and the correct evaluation of the quality of sleep play a significant role in clinical practice and the field

Journal of Big Data & Smart City, Vol. 6, Issue 2, July 2026

of biomedical studies. Sleep architecture is the cyclic organization of human sleep that is divided into several stages that are repeated during the night. The American Academy of Sleep Medicine (AASM) describes five stages of sleep as the Wake, Non-Rapid Eye Movement (NREM) stages N1, N2, and N3, and Rapid Eye Movement (REM) sleep [2]. The stages of sleep are distinguished by the peculiarities of the brain activity which could be detected with the help of EEG signals. Electroencephalography (EEG) is a non-invasive test involving a test that measures and records electrical brain activity using electrodes that are placed on the head. EEG is the most important signal to be used in classifying sleep stages because of its great temporal resolution as well as the fact that it is able to record various neural oscillations related to various sleep stages. Indicatively, deep sleep (N3) is characterized by slow delta waves whereas the REM sleep has the low-amplitude mixed-frequency activity resembling those in the state of wakefulness [3].

Overnight polysomnography (PSG) that records EEG and other physiological parameters, including electrooculography and electromyography, is traditionally used in clinical settings to identify sleep stages. PSG recordings are manually scored by sleep specialists who visually examined EEG data in regard to 30-second epochs. Manual sleep staging is tedious, expensive, and prone to inter-scorer inconsistency even though PSG is viewed as the gold standard of sleep evaluation; especially during transitional stages of sleep like N1 and N2 [4]. The constraints have led to a lot of studies on automated sleep stage classification techniques. The recent progress in artificial intelligence, especially deep learning allowed creating models that are able to learn complex patterns on EEG data by default. CNNs have proven to be quite effective in the classification of sleep stages by training on discriminative features of frequency-domain representations of EEG signals [5].

II. Related Work

A. Automatic Sleep Stage Classification Using Fine-Grained CNN Segments

Cui et al. [5] proposed an automatic sleep-stage classification method that combines a convolutional neural network with fine-grained multiscale-entropy segments extracted from single-channel EEG. Each 30-second epoch is analysed at multiple temporal scales before being passed to the CNN, allowing the network to capture both short-duration transients and longer sleep-stage patterns. Evaluated on a public sleep-EEG dataset, the fine-grained CNN outperformed classifiers trained on hand-crafted features alone, particularly for N2 and N3. The study confirms the general effectiveness of CNN architectures for automated staging and supports the dataset-driven evaluation approach adopted in the present work. However, the fine-grained segmentation adds computational overhead, and, like most classification-only studies, the paper does not derive any downstream sleep-quality measures from the predicted hypnogram. The current research retains the core CNN-based classification strategy but replaces multiscale-entropy segments with PSD band-power features, which are computationally lighter and more directly interpretable in clinical terms, and extends the pipeline with an explicit sleep-quality assessment stage.

B. Automatic Sleep Stage Scoring from Raw Single-Channel EEG

Supratak et al. [6] introduced DeepSleepNet, a two-stage deep network that combines convolutional layers for representation learning from raw, single-channel EEG with bidirectional long short-term memory (LSTM) layers to model stage-transition rules across epochs. Trained and evaluated on public PSG datasets, DeepSleepNet achieved strong overall accuracy without requiring hand-crafted features, establishing an influential end-to-end baseline for the field. The model's reliance on raw time-domain input, however, increases training cost and reduces the interpretability of the learned features relative to spectral representations, and no sleep-quality metrics are reported. The present study builds on the same end-to-end philosophy but substitutes raw-signal input with PSD band-power features to retain interpretability and reduce computational cost, while adding explicit sleep-quality computation absent from DeepSleepNet.

C. Temporal Deep Learning for Multimodal Sleep Stage Classification

Chambon et al. [7] proposed one of the first fully end-to-end deep architectures for temporal sleep-stage classification, learning spatial filters directly from multivariate, multimodal polysomnography signals (EEG, EOG and EMG) without computing spectrograms or hand-crafted features. Their network outperformed conventional decision-tree and CNN baselines across several public datasets and demonstrated that spatial-filtering layers can substitute for manual channel selection. The approach depends on multichannel PSG, which is not always available in simplified or wearable monitoring setups, and the paper does not address sleep-quality reporting. The current work targets a lighter, single-channel EEG configuration more consistent with scalable monitoring, using PSD features in place of learned spatial filters, and complements the classification stage with sleep-quality metrics.

D. Convolutional Neural Networks on Raw EEG for Sleep Staging

Sors et al. [8] trained a deep convolutional network directly on raw single-channel EEG for five-class sleep-stage scoring, reporting classification performance close to human inter-scorer agreement on a large PSG cohort. Their results reinforced the viability of CNNs for automated staging from a single channel, matching the streamlined-hardware philosophy underlying the present system. Because the network consumes raw time-series data, however, it offers limited insight into which spectral characteristics drive each classification decision, and, as with the other CNN studies discussed here, sleep-quality assessment is outside its scope. The present research keeps the single-channel, CNN-based design but replaces raw-signal input with PSD-derived band-power features to improve interpretability and extends the pipeline to report clinically meaningful sleep-quality indices.

E. Transformer-Based Sleep Staging for Clinical Practice

Zhang et al. [9] proposed SwinSleep, a deep learning framework that adapts a one-dimensional Swin Transformer for overnight sleep staging directly from PSG features, aiming explicitly at clinical deployment. Evaluated across multiple cohorts, SwinSleep outperformed several CNN and RNN baselines and additionally predicted standard sleep-architecture metrics from the scored hypnogram, illustrating the growing trend toward combining stage classification with downstream sleep-quality reporting. The transformer backbone, however, is markedly more parameter-heavy than convolutional alternatives, increasing training and inference cost, which limits its suitability for lightweight or resource-constrained monitoring. The present system pursues the same goal of pairing classification with sleep-quality reporting but adopts a considerably lighter one-dimensional CNN operating on PSD features, prioritising computational efficiency and interpretability over transformer-scale capacity.

F. Recurrent Neural Networks for Single-Channel Sleep Staging

Michielli et al. [10] proposed a cascaded LSTM recurrent network for automated sleep-stage classification from single-channel EEG, using a two-stage architecture in which an initial classifier's outputs are refined by a second LSTM stage that models inter-epoch temporal dependencies. The cascaded design improved discrimination of transitional stages relative to a single-stage baseline, evaluated on a public PSG dataset. The sequential two-stage architecture, however, increases model complexity and training time relative to a single feed-forward CNN, and the study reports only classification metrics without deriving sleep-quality indices. The current work favours a single-stage one-dimensional CNN over PSD features for computational simplicity, while incorporating sleep-quality computation that the cascaded-LSTM study omits.

G. Review of Automated EEG-Based Sleep Stage Classification

Zhang et al. [11] conducted a systematic review of automated EEG-based sleep-stage classification methods, comparing feature-based and deep learning approaches and specifically examining how staging accuracy differs between healthy individuals and patients with sleep apnea. The review highlights persistent challenges in cross-population generalisation and stresses that staging accuracy alone is an incomplete measure of a system's clinical value. This review substantiates the motivation for the current study's dataset-driven evaluation and its inclusion of sleep-quality metrics as a complement to classification accuracy, while, as a review, it offers no new implementation or experimental results of its own that could be directly benchmarked against the proposed pipeline.

H. Recent Advances in Generalisable and Efficient Sleep Staging (2021–2024)

Beyond individual architectures, several recent studies have targeted generalisation, efficiency and interpretability in automated sleep staging. Perslev et al. [12] introduced U-Sleep, a fully convolutional U-Net-style network capable of resilient, high-frequency staging across a wide range of PSG channel configurations and cohorts. Guillot and Thorey [13] proposed RobustSleepNet, which uses an attention-based channel-fusion mechanism to transfer across arbitrary PSG montages without retraining. Vallat and Walker [14] developed YASA, an open-source, feature-based staging tool validated on tens of thousands of hours of recordings and widely adopted for its accessibility outside specialised deep-learning environments. Phan et al. [15] proposed SleepTransformer, a fully attention-based architecture that additionally quantifies prediction uncertainty at the epoch level, and Eldele et al. [16] conducted a comprehensive evaluation of self-supervised pre-training for label-efficient sleep staging, showing that competitive performance can be reached with only a small fraction of labelled data. Most recently, Lee et al. [17] proposed SleePyCo, combining a multiscale feature pyramid with supervised contrastive learning to improve discrimination of the N1 and REM stages across four public datasets. Collectively, these studies illustrate a shift toward generalisable, data-efficient and interpretable staging systems, a direction the present PSD-based CNN pipeline follows by favouring a compact, physiologically interpretable feature representation over large multichannel or transformer-scale models, while retaining an explicit, clinically oriented sleep-quality assessment stage that few of these systems provide.

TABLE I. SUMMARY OF LITERATURE REVIEWED ON AUTOMATIC SLEEP STAGE CLASSIFICATION AND SLEEP QUALITY ASSESSMENT

Title / Author / Year	Core Idea	Key Gap	Suggested Improvement
Fine-Grained CNN Segments [5]	CNN with multiscale-entropy segments outperforms hand-crafted-feature classifiers.	High computational overhead from multiscale segmentation; no sleep-quality output.	Use lighter PSD band-power features; add sleep-quality assessment pipeline.
DeepSleepNet [6]	CNN + bi-LSTM learns features directly from raw single-channel EEG.	High computational cost of raw-signal processing; low feature interpretability.	Replace raw input with interpretable PSD features; add sleep-quality metrics.
Multimodal Temporal CNN [7]	End-to-end spatial-filter learning across multichannel PSG.	Requires multichannel PSG; no sleep-quality reporting.	Adopt single-channel PSD features; add sleep-quality computation.
Raw Single-Channel CNN [8]	CNN on raw EEG approaches human inter-scorer agreement.	Limited interpretability of raw-signal features; no sleep-quality output.	Use PSD-derived features for interpretability; add sleep-quality metrics.
SwinSleep [9]	Swin Transformer combines staging with sleep-architecture reporting.	High parameter count and computational cost.	Use lightweight CNN on PSD features; retain sleep-quality reporting.
Cascaded LSTM [10]	Two-stage LSTM refines transitional-stage classification.	Higher model complexity and training time; no sleep-quality output.	Use single-stage CNN for simplicity; add sleep-quality computation.
Review of Automated Sleep Staging [11]	Surveys feature-based and deep learning methods; notes generalisation gaps across populations.	No new implementation or experimental benchmark.	Use dataset-driven evaluation with explicit sleep-quality assessment.
Recent Generalisable /Efficient Staging Systems [12]-[17]	U-Net, attention-based transfer, feature-based, transformer and contrastive-learning approaches targeting generalisation, efficiency and label efficiency.	Predominantly multichannel or large-model designs; sleep-quality reporting largely absent.	Favour a compact PSD + CNN model with explicit sleep-quality assessment.

III. Methodology

The research follows the applied, data-centric research approach common to EEG signal-processing and deep-learning studies, in which the pipeline is developed through staged experimentation, evaluation, and feedback rather than a fixed software lifecycle [18]. The stages are: dataset acquisition and exploration, EEG pre-processing, epoch segmentation, PSD-based feature extraction, CNN-based classification, sleep-quality assessment, and performance evaluation, as summarised in Fig. 1.

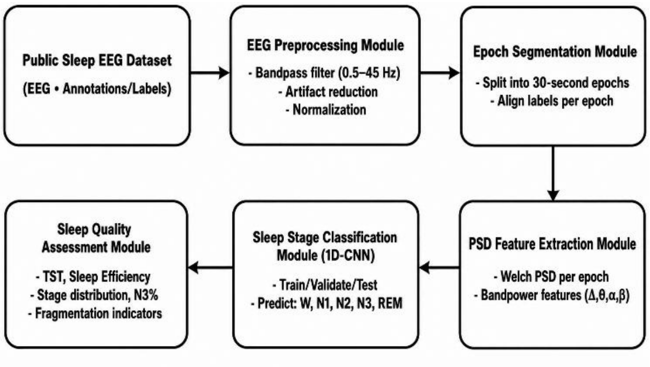

Fig. 1. *System block diagram of the proposed EEG sleep-staging pipeline*

A. Dataset Acquisition and Exploration

EEG data is obtained from publicly available, clinically annotated sleep-EEG datasets rather than real-time acquisition, following common practice in sleep research [19]. Public datasets provide reproducibility, standardised labelling, and sufficient volume to train deep-learning models without the ethical and logistical overhead of collecting human EEG data [19]. Candidate datasets were compared on data quality, annotation standard, subject diversity, and prevalence in the literature [20], and the Sleep-EDF Database Expanded from PhysioNet was selected [21]. Exploratory analysis examined recording duration and subject count, channel configuration and sampling rate, stage-distribution class imbalance, and missing or corrupted data; as expected, N2 dominates total sleep time relative to transitional stages such as N1 [20], a factor that subsequently informs training and evaluation.

B. EEG Pre-processing

Raw EEG is susceptible to noise from eye movement, muscle activity, electrode motion, and environmental interference [22]. Each recording is bandpass-filtered to 0.5–45 Hz to remove baseline drift and high-frequency noise [3], processed with artefact-mitigation to suppress transient disturbances while preserving physiologically meaningful activity [22], and normalised to reduce inter-subject variability and stabilise training [18]. The pre-processed signal is obtained as

$$xp(n) = N\{F[x(n)]\}$$

where F denotes bandpass filtering and N denotes normalisation.

C. Epoch Segmentation

The pre-processed signal is segmented into non-overlapping 30-second epochs consistent with AASM guidelines [2]. If fs is the sampling frequency, each epoch contains $L = 30 \cdot fs$ samples, and epoch Ek is associated with the sleep-stage label from the dataset annotation. This converts a long continuous recording into discrete, labelled samples suitable for supervised learning [3].

D. PSD-Based Feature Extraction

Because sleep stages correlate strongly with EEG spectral content, each 30-second epoch is represented by its Power Spectral Density (PSD), estimated with Welch's method for its favourable variance properties [23], [24]:

$$Pk(f) = Welch(Ek)$$

Band-power features are then obtained by integrating Pk(f) over the standard delta, theta, alpha, and beta EEG bands [2], [3], giving a compact, physiologically interpretable feature vector $Fk = [BPk,\delta, BPk,\theta, BPk,\alpha, BPk,\beta]$ for each epoch [20].

E. Sleep Stage Classification Model

The PSD feature vectors are treated as 1-D sequences across frequency bins and classified with a one-dimensional CNN, chosen for its ability to learn local, frequency-localised patterns and inter-band interactions relevant to sleep staging [5], [6]:

$$\hat{y}k = C(Fk; \theta)$$

where C is the CNN model with learned parameters θ, and $\hat{y}k \in \{Wake, N1, N2, N3, REM\}$. Data is split into training, validation, and test sets for unbiased evaluation [18]; the network is trained with categorical cross-entropy loss and an adaptive optimiser, and dropout regularisation is used to limit overfitting while keeping model complexity feasible and reproducible [5].

F. Sleep Quality Assessment

From the predicted stage sequence $\hat{Y} = \{\hat{y}1, \ldots, \hat{y}K\}$ across a full recording, clinically defined sleep-quality metrics are computed [2], [3]:

$$TST = \Sigma k\, If(\hat{y}k \neq wake) \times 30\ s$$

$$SE = (TST / Total\ Recording\ Time) \times 100\%$$

$$N3\% = (\Sigma k\, If(\hat{y}k = N3) / K) \times 100\%$$

where If is an indicator function. These metrics — total sleep time (TST), sleep efficiency (SE), and deep-sleep proportion (N3%) — summarise sleep architecture in clinically meaningful terms [1].

G. Performance Evaluation

Model performance is assessed with standard multi-class metrics — accuracy, precision, recall, F1-score, Cohen's Kappa, and confusion-matrix analysis [25] — chosen to reveal both overall behaviour and per-class performance, which is important given the under-representation of stages such as N1.

IV. System Design and Architecture

This section translates the methodological pipeline of Section III into an implementable system, describing the execution flow, requirements, and test strategy used to validate the design.

A. System Flow

Fig. 2 shows the execution flow of the implemented system. Processing begins by loading and verifying the chosen EEG dataset; incomplete or corrupted files trigger corrective handling before continuing. Verified signals are filtered and normalized, resampled if the sampling rate does not match the target and segmented into 30-second epochs aligned with their stage labels. PSD features are then extracted for each epoch and assembled into training, validation, and test splits. During training, the CNN is fit on the training set and validated, with model or feature adjustments applied if performance is unacceptable, particularly for the harder classes such as N1. During inference, the trained model predicts stage labels for unseen epochs, from which sleep-quality metrics are computed and classification performance is evaluated and reported.

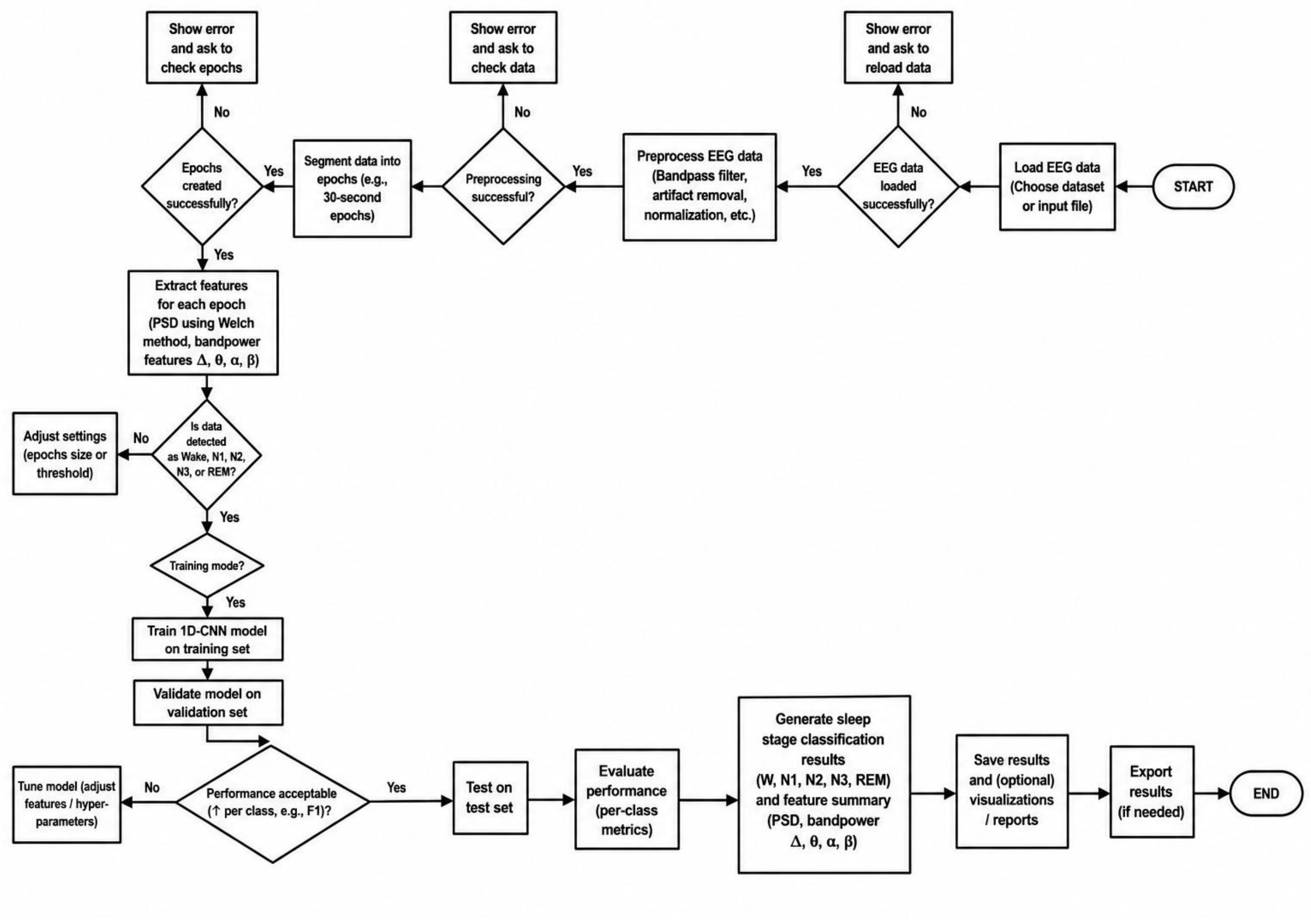

Fig. 2. *System flow chart describing the execution logic from dataset loading to results reporting.*

B. Hardware and Software Requirements

As a dataset-based software system, hardware requirements are modest: a standard PC or laptop with an Intel Core i5-class processor (or better), 8 GB RAM (16 GB recommended for training), and 20–30 GB of free storage for datasets, models, and results. The software stack is entirely open-source and cross-platform (Windows, Linux, or macOS), built on Python 3.8+ with NumPy and SciPy for numerical processing, MNE-Python for EEG handling, scikit-learn for data splitting and evaluation, TensorFlow or PyTorch for the CNN, and Matplotlib/Seaborn for visualization, developed within Jupyter Notebook or a standard IDE. Data requirements are limited to publicly available sleep-EEG recordings with known sampling frequency and expert-annotated stage labels, such as those provided by PhysioNet [19].

C. System Test Plan

Test points were defined at the input and output of every functional unit; dataset input, pre-processing, epoch segmentation, PSD extraction, classification, sleep-quality assessment, and performance evaluation to verify correct operation and data integrity throughout the pipeline. Table II summarizes the resulting test cases and outcomes.

TABLE II. SUMMARY OF SYSTEM TEST CASES

Test	Subject	Action / Expected Result	Implemented Result	Status
T1	EEG Dataset Input	Load Sleep-EDF recordings and annotations	Dataset loaded successfully	Pass
T2	EEG pre-processing	Apply 0.5–45 Hz bandpass filter	Filter applied successfully	Pass

T3	EEG pre-processing	Normalise EEG amplitude	Normalised signal generated	Pass
T4	Epoch Segmentation	Segment into 30-second epochs	1002 epochs generated	Pass
T5	PSD Feature Extraction	Compute Welch PSD / band-power features	Features extracted successfully	Pass
T6	Sleep Stage Classification	Predict W, N1, N2, N3, REM with trained CNN	All classes predicted	Pass
T7	Performance Evaluation	Compute accuracy, Kappa, confusion matrix, F1	70.06% / 0.687 obtained	Pass
T8	Sleep Quality Assessment	Derive TST, efficiency, stage distribution	Metrics generated successfully	Pass

All test cases passed within the expected operating ranges, confirming that each functional unit meets its design requirement before assessment of overall system performance in Section V.

V. Implementation and Results

The complete pipeline was implemented and validated on the Sleep-EDF Database Expanded from PhysioNet [19], [21], covering data loading, pre-processing, epoch segmentation, PSD-based feature extraction, CNN-based stage prediction, sleep-quality computation, and performance evaluation. The processed recording yielded 1002 valid 30-second epochs used for training, validation, and testing.

A. Classification Performance

The system achieved an overall classification accuracy of 70.06% and a Cohen's Kappa of 0.687, indicating moderate-to-substantial agreement between predicted and true sleep stages. Table III summarises the overall performance indicators, and Table IV reports precision, recall, and F1-score for each sleep stage.

Table III. Measurement of Overall System Performance

Parameter	Value	Description
Total Epochs	1002	30-second EEG epochs processed
Accuracy	70.06%	Overall classification accuracy
Cohen's Kappa	0.687	Agreement beyond chance
Weighted F1-Score	0.691	Class-size-weighted F1
Macro F1-Score	0.562	Unweighted mean F1 across classes

Table IV. Per-Class Classification Performance

Sleep Stage	Precision	Recall	F1-Score
Wake	0.951	0.443	0.605
N1	0.000	0.000	0.000
N2	0.619	0.866	0.722
N3	0.795	0.884	0.837
REM	0.746	0.573	0.648

N3 achieved the strongest F1-score (0.837), showing reliable detection of deep sleep, followed by N2 (0.722). N1 performed poorest, consistent with its nature as a brief, transitional stage that is difficult to separate from adjacent stages in EEG literature. Fig. 3 shows the corresponding normalised confusion matrix: most misclassifications occur between neighbouring stages, particularly N1↔N2 and REM↔N2, reflecting the similarity of their spectral characteristics.

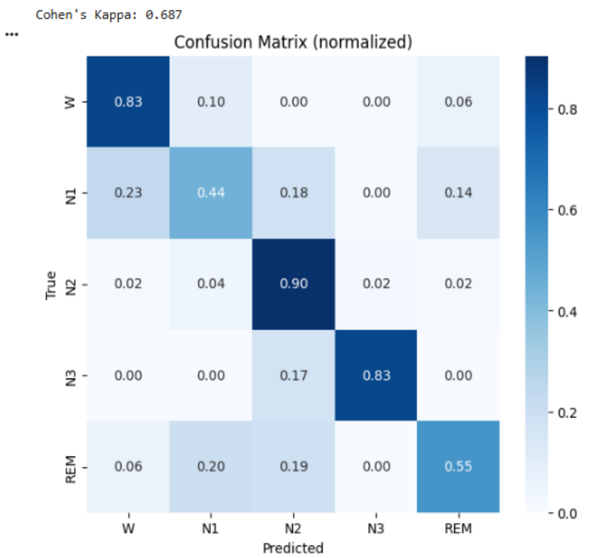

Fig. 3. *Normalised confusion matrix for the five-class sleep-stage prediction.*

B. Hypnogram and Temporal Behaviour

Fig. 4 compares the true and predicted hypnograms alongside rolling classification accuracy and per-class F1-scores. The predicted stage sequence follows the same overall trend as the ground truth, indicating that the model captures the temporal structure of sleep architecture even where individual epochs are misclassified.

Fig. 4. *True vs. predicted hypnograms, rolling accuracy, and per-class F1-scores.*

C. Results Dashboard

An interactive dashboard (Fig. 5) was built to present sleep-analysis outputs, including overall accuracy (80.8% on the displayed session), Kappa score, per-class F1-scores, confusion matrix, and a qualitative sleep-quality rating

("Good"), making the results accessible to non-technical users.

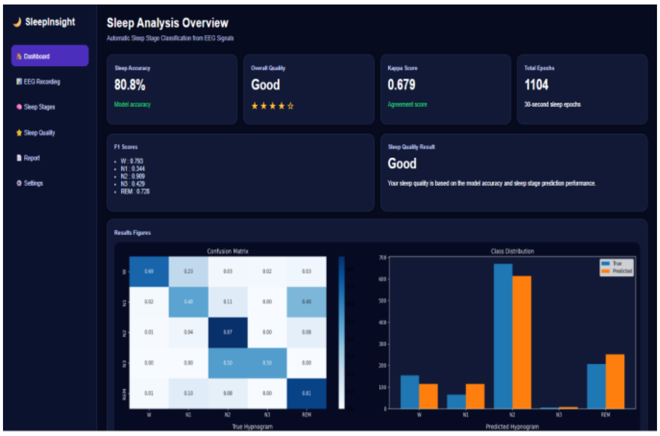

Fig. 5. *Sleep-analysis results dashboard summarising accuracy, Kappa, F1-scores, and sleep quality.*

D. System Validation

The system was validated both objectively and subjectively against the goals defined in Section I. Objective validation used standard classification metrics, 70.06% accuracy and a Kappa of 0.687, together with the confusion matrix and per-class F1-scores, confirming strong performance on N2, N3, and REM. Subjective validation involved visual inspection of the generated hypnograms and dashboard outputs, which were consistent with expected sleep architecture. Together, these results confirm that the system meets its design objectives for EEG-based sleep-stage classification and sleep-quality assessment.

VI. Conclusion

This research work designed and implemented a dataset-driven system that classifies EEG signals into five sleep stages which are Wake, N1, N2, N3, and REM using PSD-based features and a CNN and derives clinically meaningful sleep-quality metrics from the predicted architecture. The system achieved an overall accuracy of 70.06% and a Cohen's Kappa of 0.687, with strong performance on N2 and N3 and weaker performance on the transitional N1 stage, consistent with the wider sleep-staging literature. Class-wise F1-scores, confusion-matrix analysis, and hypnogram comparison confirm that the model captures the temporal structure of sleep, and the derived sleep-quality indicators align with clinical expectations. Each functional module pre-processing, feature extraction, classification, and sleep-quality assessment was independently tested and integrated into a reproducible pipeline, with an interactive dashboard providing an accessible view of the results. Compared with related work, the proposed system offers a favourable balance of interpretability, computational efficiency, and integrated sleep-quality assessment, while classification of the N1 stage and reliance on a single dataset remain the main limitations.

VII. Future Work

Several directions are proposed to extend this work. Dataset compatibility should be broadened beyond Sleep-EDF to improve generalization across recording protocols and populations. More sophisticated artefact-removal techniques could improve pre-processing quality, particularly for muscle and eye-movement artefacts. Sequence models such as LSTMs or temporal CNNs could be explored to improve classification of transitional stages, especially N1, by exploiting inter-epoch context. Feature selection or dimensionality reduction may reduce computation while preserving accuracy. The dashboard could be extended with longitudinal reporting across multiple nights and automated alerts for abnormal sleep patterns. Finally, extending the system to real-time EEG acquisition and online classification would enable continuous monitoring in clinical or home settings, moving the system from retrospective analysis toward practical, deployable sleep monitoring.

References

[1] M. Walker, Why We Sleep: Unlocking the Power of Sleep and Dreams. New York, NY, USA: Scribner, 2017.

[2] R. B. Berry et al., The AASM Manual for the Scoring of Sleep and Associated Events: Rules, Terminology and Technical Specifications, Version 3. Darien, IL, USA: American Academy of Sleep Medicine, 2023.

[3] C. Iber, S. Ancoli-Israel, A. L. Chesson Jr., and S. F. Quan, The AASM Manual for the Scoring of Sleep and Associated Events: Rules, Terminology and Technical Specifications. Westchester, IL, USA: AASM, 2007.

[4] L. Fiorillo et al., "Automated sleep scoring: A review of the latest approaches," Sleep Med. Rev., vol. 48, art. no. 101204, 2019, doi: 10.1016/j.smrv.2019.07.007.

[5] Z. Cui, X. Zheng, X. Shao, and L. Cui, "Automatic sleep stage classification based on convolutional neural network and fine-grained segments," Complexity, vol. 2018, art. no. 9248410, 2018, doi: 10.1155/2018/9248410.

[6] A. Supratak, H. Dong, C. Wu, and Y. Guo, "DeepSleepNet: A model for automatic sleep stage scoring based on raw single-channel EEG," IEEE Trans. Neural Syst. Rehabil. Eng., vol. 25, no. 11, pp. 1998–2008, 2017, doi: 10.1109/TNSRE.2017.2721116.

[7] S. Chambon, M. N. Galtier, P. J. Arnal, G. Wainrib, and A. Gramfort, "A deep learning architecture for temporal sleep stage classification using multivariate and multimodal time series," IEEE Trans. Neural Syst. Rehabil. Eng., vol. 26, no. 4, pp. 758–769, 2018, doi: 10.1109/TNSRE.2018.2813138.

[8] A. Sors, S. Bonnet, S. Mirek, L. Vercueil, and J.-F. Payen, "A convolutional neural network for sleep stage scoring from raw single-channel EEG," Biomed. Signal Process. Control, vol. 42, pp. 107–114, 2018, doi: 10.1016/j.bspc.2017.12.001.

[9] D. Zhang, Y. She, J. Sun, X. Yang, X. Zeng, and W. Qin, "SwinSleep: A deep learning framework advancing overnight sleep staging toward clinical practice," IEEE Trans. Instrum. Meas., vol. 73, pp. 1–14, 2024, doi: 10.1109/TIM.2024.3470049.

[10] N. Michielli, U. R. Acharya, and F. Molinari, "Cascaded LSTM recurrent neural network for automated sleep stage classification using single-channel EEG signals," Comput. Biol. Med., vol. 106, pp. 71–81, 2019, doi: 10.1016/j.compbiomed.2019.01.013.

[11] X. Zhang, X. Zhang, Q. Huang, Y. Lv, and F. Chen, "A review of automated sleep stage based on EEG signals," Biocybern. Biomed. Eng., vol. 44, no. 3, pp. 651–673, 2024, doi: 10.1016/j.bbe.2024.06.004.

[12] M. Perslev, S. Darkner, L. Kempfner, M. Nikolic, P. J. Jennum, and C. Igel, "U-Sleep: Resilient high-frequency sleep staging," npj Digit. Med., vol. 4, art. no. 72, 2021, doi: 10.1038/s41746-021-00440-5.

[13] A. Guillot and V. Thorey, "RobustSleepNet: Transfer learning for automated sleep staging at scale," IEEE Trans. Neural Syst. Rehabil. Eng., vol. 29, pp. 1441–1451, 2021, doi: 10.1109/TNSRE.2021.3098968.

[14] R. Vallat and M. P. Walker, “An open-source, high-performance tool for automated sleep staging,” eLife, vol. 10, art. no. e70092, 2021, doi: 10.7554/eLife.70092.

[15] H. Phan, K. Mikkelsen, O. Y. Chén, P. Koch, A. Mertins, and M. De Vos, “SleepTransformer: Automatic sleep staging with interpretability and uncertainty quantification,” IEEE Trans. Biomed. Eng., vol. 69, no. 8, pp. 2456–2467, 2022, doi: 10.1109/TBME.2022.3147187.

[16] E. Eldele, M. Ragab, Z. Chen, M. Wu, C.-K. Kwoh, and X. Li, “Self-supervised learning for label-efficient sleep stage classification: A comprehensive evaluation,” IEEE Trans. Neural Syst. Rehabil. Eng., vol. 31, pp. 1333–1342, 2023, doi: 10.1109/TNSRE.2023.3245285.

[17] S. Lee, Y. Yu, S. Back, H. Seo, and K. Lee, “SleePyCo: Automatic sleep scoring with feature pyramid and contrastive learning,” Expert Syst. Appl., vol. 240, art. no. 122551, 2024, doi: 10.1016/j.eswa.2023.122551.

[18] I. Goodfellow, Y. Bengio, and A. Courville, Deep Learning. Cambridge, MA, USA: MIT Press, 2016.

[19] A. L. Goldberger et al., “PhysioBank, PhysioToolkit, and PhysioNet: Components of a new research resource for complex physiologic signals,” Circulation, vol. 101, no. 23, pp. e215–e220, 2000, doi: 10.1161/01.CIR.101.23.e215.

[20] M. Gaiduk, Á. Serrano Alarcón, R. Seepold, and N. M. Madrid, “Current status and prospects of automatic sleep stages scoring: Review,” Biomed. Eng. Lett., vol. 13, no. 3, pp. 247–272, 2023, doi: 10.1007/s13534-023-00299-3.

[21] B. Kemp, A. H. Zwinderman, B. Tuk, H. A. C. Kamphuisen, and J. J. L. Oberye, “Analysis of a sleep-dependent neuronal feedback loop: The slow-wave microcontinuity of the EEG,” IEEE Trans. Biomed. Eng., vol. 47, no. 9, pp. 1185–1194, 2000, doi: 10.1109/10.867928.

[22] H. Phan and K. Mikkelsen, “Automatic sleep staging of EEG signals: Recent development, challenges, and future directions,” Physiol. Meas., vol. 43, no. 4, art. no. 04TR01, 2022, doi: 10.1088/1361-6579/ac6049.

[23] P. D. Welch, “The use of fast Fourier transform for the estimation of power spectra: A method based on time averaging over short, modified periodograms,” IEEE Trans. Audio Electroacoust., vol. 15, no. 2, pp. 70–73, 1967, doi: 10.1109/TAU.1967.1161901.

[24] A. V. Oppenheim and R. W. Schafer, Discrete-Time Signal Processing, 3rd ed. Upper Saddle River, NJ, USA: Prentice Hall, 2010.

[25] E. Eldele et al., “An attention-based deep learning approach for sleep stage classification with single-channel EEG,” IEEE Trans. Neural Syst. Rehabil. Eng., vol. 29, pp. 809–818, 2021, doi: 10.1109/TNSRE.2021.3076234.

Journal of Big Data & Smart City
كلية الشرق الأوسط Middle East College

AI-Based Smart Child Life Detection and Rescue System in Vehicles

Alkawthar Moosa Al Ruqaishi
Department of Computing and Electronics Engineering
Middle East College
Muscat, Sultanate of Oman
21f21920@mec.edu.om

Ajitha Sajan
Department of Computing and Electronics Engineering
Middle East College
Muscat, Sultanate of Oman
ajitha@mec.edu.om

Received: 20th May 2026; Revised: 22nd June 2026;

Accepted: 18th July 2026

***Abstract* — Cases of leaving children unattended in parked cars are on the rise, exposing them to life-threatening cardiac conditions without actual supervision worldwide, especially due to rising temperatures. This project aims to develop and design a child detection and rescue system based on artificial intelligence, which can effectively detect a child or person in a parked car, giving it high reliability. The logic behind the proposed solution is to integrate computer vision methods with sensor integration, where the YOLOv8 deep learning model with OpenCV (cv2) for camera capture and image processing. will be implemented on a Raspberry Pi to process images captured by a camera inside the car in real-time. Visual detection is supported by multiple sensors, including an air quality sensor to indicate changes in air composition associated with human presence, a human presence motion sensor (PIR) to detect movement, and a DHT11 sensor to monitor temperature and humidity conditions inside the vehicle. The system also follows the V-model development process to verify the integration of hardware and software at each step. After verifying the presence of a human user, a multi-level warning system will be activated, including an audible alarm, flashing warning lights, and a mobile notification system supported by Internet of Things technology. The proposed system will help enhance individual safety by providing reliable real-time monitoring and smart alerts, which will reduce the likelihood of children dying in parked vehicles and assist in the smart use of safety devices in cars.**

Keywords — Artificial Intelligence, YOLOv8, Child Presence Detection, Sensor Fusion, Raspberry Pi, Internet of Things, Vehicular Heatstroke

الخلاصة - **تتزايد حالات ترك الأطفال دون رقابة داخل المركبات المتوقفة، مما يعرّضهم لمخاطر صحية تهدد الحياة في ظل غياب إشراف فعلي، وخاصة مع ارتفاع درجات الحرارة .يهدف هذا المشروع إلى تصميم وتطوير نظام ذكي للكشف عن الأطفال وإنقاذهم يعتمد على الذكاء الاصطناعي، وقادر على اكتشاف وجود طفل أو شخص داخل مركبة متوقفة بموثوقية عالية .وتقوم فكرة الحل المقترح على دمج تقنيات الرؤية الحاسوبية مع تكامل المستشعرات، حيث يُطبَّق نموذج التعلم العميق YOLOv8 مع مكتبة OpenCV لالتقاط الصور ومعالجتها على متحكم Raspberry Pi لتحليل الصور الملتقطة داخل المركبة في الزمن الحقيقي .ويُدعم الكشف البصري بمجموعة من المستشعرات تشمل مستشعر جودة الهواء للدلالة على التغيرات في تركيب الهواء المرتبطة بوجود الإنسان، ومستشعر الحركة والوجود البشري (PIR) لرصد الحركة، ومستشعر DHT11 لمراقبة درجة الحرارة والرطوبة داخل المركبة .كما يتبع النظام منهجية النموذج V للتحقق من تكامل العتاد والبرمجيات في كل مرحلة .وبعد التأكد من وجود شخص داخل المركبة، يُفعَّل نظام إنذار متعدد المستويات يشمل إنذارًا صوتيًا، وأضواء تحذيرية وامضة، ونظام إشعارات عبر الهاتف المحمول مدعومًا بتقنيات إنترنت الأشياء .ومن المتوقع أن يسهم النظام المقترح في تعزيز السلامة الفردية من خلال توفير مراقبة موثوقة في الزمن الحقيقي وتنبيهات ذكية، بما يقلل من احتمالية وفاة الأطفال داخل المركبات المتوقفة ويدعم الاستخدام الذكي لأجهزة السلامة في السيارات.**

الكلمات المفتاحية — الذكاء الاصطناعي، YOLOv8، الكشف عن وجود الأطفال، دمج بيانات المستشعرات، Raspberry Pi، إنترنت الأشياء، ضربة الشمس داخل المركبات.

I. Introduction

The rising cases of child deaths because of heatstroke in closed vehicles have become a serious international concern owing to the drastic increase in the cabin temperature over a brief duration of time. Research indicates that the temperature in a parked car can rise over 20 C in the first ten minutes, which makes cars dangerous to children who are accidentally left without any supervision [1], [2]. Vehicular safety systems, including motion-based, temperature, and air-quality-based detection systems, offer partial solutions, but, nonetheless, they cannot still reliably detect the presence of human life, which leads to false alarms and unreliability [3], [4]. The latest innovations in the fields of artificial intelligence (AI), embedded systems, and deep learning algorithms have made a great contribution to the ability of intelligent systems to recognize the presence of people through visual recognition and multi-sensor validation [5], [6].

Hence, it is necessary to find a stable and intelligent system that can properly recognize the existence of a child in a vehicle parked and takes immediate action to avoid deaths. The possible advantage of the suggested system is that it will enhance safety within vehicles through the application of advanced technologies that will be able to detect life signs with the maximum accuracy to minimize false alarms and enhance the response time in the case of an emergency. The project is selected because of the severe necessity of the dependable detection solutions and the possibility to implement the recent development in AI and embedded systems to the real-life safety applications.

The problem of children being left unattended in parked cars has been of great concern to researchers and safety organizations as there is high potential for heat-related deaths.

With the temperature in the cabin of vehicles increasing dramatically in a matter of minutes, there is an impending threat of intelligent systems that identify human presence thus helping to take the necessary rescue measures in good time. As a result, a few researchers have worked on the development of smart car safety systems based on different sensing and detection methods.

Earlier work explored carbon-dioxide-based sensing to detect children in closed vehicles [4]. Even though their system showed the possibility of using respiration-based detection, it fell prey to environmental perturbation, airflow changes, and lag time. On the same note, IoT-based child safety monitoring systems that used temperature sensors and motion sensors [3] failed to differentiate between living and non-living objects reliably, which led to false alarms. These constraints point out the difficulties of single-sensor and rule-based detection methods.

The most recent developments in the field of artificial intelligence and computer vision have brought more valid approaches to the problem of human presence detection. YOLOv8 (You Only Look Once) has demonstrated good performance in real-time human detection performance in detecting humans in real-time and under different lighting and environmental conditions [7], [8]. Although promising in accuracy, vision-based systems might not be robust enough in that even with their accuracy, the systems can still be influenced by factors like camera views, cabin shadows and visual similarities between objects and thus bring down the reliability of the detection.

To solve these problems, the most recent studies focus on the fusion of computer vision and sensor fusion to enhance system stability and minimize false positives [9], [10]. In a continuation of these results, the proposed project integrates AI-based visual recognition with a YOLOv8 model running on a Raspberry Pi with several auxiliary sensors Furthermore, an Arduino microcontroller is utilized as an auxiliary device to acquire the data from the sensors and send it to the Raspberry Pi, thus enhancing system modularity and efficiency . These include an air quality sensor to detect changes in cabin air composition caused by human respiration, a human presence sensor in a human form with the capability to recognize human presence without necessarily movement being detected making it more dependable as compared to the traditional human presence motion sensor (PIR) in closed vehicle settings, and a DHT11 temperature and humidity sensor to monitor the conditions in the cabin. It is a multi-layer verification method that improves the accuracy of detection and consumes low power that is applicable in embedded edge computing systems.

The proposed system is designed as an artificial intelligence-based embedded system capable of continuously surveilling the inside of a parked car after engine has been turned off. The central processing unit is a Raspberry Pi, connected to a camera module to take pictures of the cabin and analyze them with a human detector trained on a base of YOLOv8 object detection model with OpenCV (cv2). When a person or a child is detected, the system triggers several verification sensors, including a human presence sensor which works on radar technology to identify the presence of a human being inside the vehicle even when the child is asleep without making any noticeable movement, an air quality sensor to monitor the change in cabin air composition linked with people presence and a DHT11 temperature and humidity sensor to measure the environmental conditions. Multi-channel alert system follows multi-sensor validation when the presence of human beings is confirmed, i.e. audible alarms, flashing warning lights and internet-of-things enabled mobile notifications. This multi-tiered verification system offers many advantages over single-sensor systems in that it greatly improves the detection rate and reduces instances of false alarms. Furthermore, an intermediate device (Arduino microcontroller) is used for the acquisition of sensor data. Arduino is connected to all the environmental sensors, and it processes and sends the sensor data to the Raspberry Pi via serial communication. This will make the system more modular and decrease the processing load of the Raspberry Pi.

The project aim is as follows. This project seeks to establish and deploy a smart child life detecting and rescuing system via an artificial intelligence system that can autonomously detect the presence of a child in a parked car through a computer vision and sensor fusion and then activate an alert system to stop instances of child death. The specific objectives of the work are: (i) Integrate an air quality sensor, human presence sensor (PIR), and DHT11 temperature and humidity sensor to support visual detection and reduce false alarms. (ii) Install a real time alarm system which will give audible alarms, visual signals and IoT enable mobile signals when the human presence is detected. (iii) To detect human presence inside the vehicle using a PIR Human Presence Sensor and trigger an alert whenever human presence is detected. (iv) To monitor temperature and humidity levels inside the vehicle using a DHT11 sensor and display the readings on the monitoring dashboard. (v) To monitor air quality inside the vehicle using an MQ135 gas sensor and provide environmental condition information through the dashboard. (vi) To develop a real-time dashboard for displaying camera feed, sensor readings, notifications, image capture, and video recording functions.

II. Related Work

Surveillance of children in closed cars has been a popular topic of research as the cases of injuries related to heatstroke in cars continue to rise. Multiple research papers have come up with solutions based on sensors, Internet of things (IoT), and smart detection algorithms. The literature review analyzes the available methods, strategies, constraints, and technologies that have helped in formulating the child rescue systems within vehicles. The review covers five scholarly works in journals and international conferences dealing with human detection, embedded safety systems and sensor fusion applications. The aim is to comprehend the current research condition and find out gaps that can justify the proposed approach to this project.

There are three broad directions of previous studies (i) systems based on physical and environmental sensors, including temperature, humidity, and air quality sensors, (ii) systems based on IoT and microcontrollers, remote alerting, and (iii) systems deployed based on computer vision and AI-based classifiers, child recognizing in vehicles. Although sensor-based methodology is a good method at identifying the environmental risks, it cannot verify the existence of a living child and often causes false alarms. In the meantime, computer vision techniques have been demonstrated to be very accurate with humans but can only be ineffective in low light or when partly obscured. The latest developments in deep learning and especially the YOLO (You Only Look Once) algorithm have been successful in providing high precision, low computational cost, and real-time detection to be used on embedded applications like Raspberry Pi. [5], [11], [12].

A. *Visual-Based Children and Pet Rescue from Suffocation and Hyperthermia in Enclosed Vehicles*

This paper introduces an intelligent rescue system based on a vision that is developed to identify children and pets abandoned in parked cars. The suggested system is based on lightweight deep learning object detector models, such as different versions of YOLO and NanoDet, and optimized to run on embedded systems in real-time. To create the special in-cabin dataset, the authors took videos under practical conditions of the vehicle, such as changes in lighting, the camera angle, and seating arrangements, and partial obstructions. The augmentation of data was done with the help of brightness adjustment, rotation, and simulation of an occlusion to improve the robustness of the trained models. The system architecture will include the in-vehicle camera which is linked to an embedded processor that will handle the continuous monitoring and send an alert in case of detection. [13]. It was experimentally determined that the optimized YOLO-based models had high detection accuracy, precision and recall rates and these demonstrated reliable real-time performance in the confined vehicle cabins. The findings proved that visual detection would be able to identify children and pets in normal light conditions and moderate occlusion. The built deployment was practical, and acceptable inference latency and power usage, so the strategy is applicable to in-vehicle safety. Although these were encouraging findings, the authors have also pointed out some of the limitations of a vision-only process. The performance of the system was poor in case of extreme occlusion, low light and shadow cases. Also, non-living things like bags, dolls or child seat were sometimes misclassified as children, which resulted in false alarms by the visual models. These constraints minimize the reliability of the system in the real life where the environmental conditions cannot be controlled. To overcome these challenges, the authors suggested that more sensing modalities need to be incorporated to ensure that life presence is verified as well as false positives are minimized. The current project is embracing this suggestion directly by integrating YOLO/CNN-based visual detection with environmental sensors, including a human presence sensor (PIR), an air quality sensor for breathing-related changes, and a temperature–humidity sensor. Such a multi-sensor fusion approach enhances the reliability of the detection process, and only under the response of a human presence is ensured.

B. *WiCPD – Wireless Child Presence Detection System for Smart Cars*

The paper presents a child presence detection system based on Wi-Fi Channel State Information (CSI) and is wireless in nature. The system records micro-motions and respiration patterns due to breathing of a child. CSI signals are converted to spectrogram-related features and processed by machine learning classifiers to differentiate between human presence and inanimate object. The solution does not use cameras, as it takes into consideration the issue of privacy. [14]. This system has been able to achieve over 95 percent detection rates in controlled car settings where not only moving but also sleeping children were also detected. These findings indicate that wireless sensing will be able to record vital signs without the need to have line-of-sight or visual information. CSI-based sensing is very sensitive to environmental noise, multipath reflections as well as variations in cabin materials. In the real-life situation where ventilation airflow or signal interference occurs, performance is likely to deteriorate significantly. The technique does not also possess the capability of visualizing the object detected. The authors propose to use CSI sensing with vision-based AI or environmental sensors such as air quality and temperature–humidity sensors. to enhance robustness and minimize the noise-related false detections. Follow-up work by the same group has since improved robustness of WiFi-based detection under unfavourable cabin conditions [15], [16].

C. *BSENSE – In-Vehicle Child Detection and Vital-Sign Monitoring Using a Single mmWave Radar and Synthetic Reflectors*

This article provides the BSENSE which is an in-vehicle child and vital-sign monitor system that is powered by a single mmWave radar and synthetic reflectors. The system uses the Frequency-Modulated Continuous Wave (FMCW) radar technology to acquire micro-Doppler signatures created due to breathing of human beings. Strategically located synthetic reflectors are also used in the vehicle cabin to enhance the reflectiveness of radar and its coverage to the various seating areas. Improved signal-processing methods are used to isolate breathing signals in a noisy radar signal enabling the system to understand that a living child is present even when the body is partly or fully covered, e.g. under blankets or under seats. The strategy is based on radar sensing to eliminate privacy issues with camera-based systems. [17]. Experimental analysis showed that its accuracy of detection was over 95 percent in determining the presence of a child and estimating respiration rates in different scenarios of occlusion. The system was found to be consistent in various seating arrangements and lighting conditions which proved that radar-based sensing is resistant to visual obstructions. The error in the breathing rate estimation was also acceptable, meaning that radar sensing of vital signs was possible in a closed vehicular setup. Although the BSENSE system is strong in the ability to detect vital signs, it does not have the capability of identity discrimination. The radar can detect the existence of living object but cannot be sure of the object is a child, an adult, or a pet. As well, the system performance may be influenced by the vehicle vibration and positioning of the radar. Depending on artificial reflectors brings complexity to its installation that can be a barrier to its application in commercial vehicles on a large scale. The authors propose the combination of AI detection in a visual way or environmental sensors with radar sensing to increase identity verification and decrease misclassification. It is also suggested to improve the algorithms of vibration compensation and strategizing radar location. Such improvements would allow a more robust and thorough child detection system that can be used in practice. Radar-based sensing is suitable in terms of vital-sign detection, whereas it is less applicable on low-cost embedded systems because of its complexity and high cost.

D. *Vehicle Occupant Detection Based on mmWave Radar*

This paper suggests a car occupant sensor based on MIMO FMCW mmWave radar to produce high-resolution range azimuth heatmap of the car interior. These heatmaps are used by deep learning models to identify occupants using spatial and motion characteristics. The system is made to work without cameras, and it deals with privacy issues and allows it to work in lowlight or even in non-light conditions. The radar scan is constantly performed on the cabin to identify the presence of occupants and identify adults and children. [18].

The proposed system had a high classification accuracy in controlled experimental conditions, which were able to recognize occupants and differentiate between adults and children. The radar-based solution proved to have a high degree of resistance to lighting conditions, and the sitting posture, and this may emphasize the capability of the radar-based solution as an effective camera-free detection method. Deep learning-based classification was feasible on the generated heatmaps which have adequate spatial data. The system was mainly tested in controlled laboratory- and test-vehicle-based conditions, which restricted its applicability to real-life conditions. It was noted that performance deteriorated with the introduction of vehicle vibrations, dynamic background motion and the use of different materials in the cabin. Besides, the radar is able to detect the presence of an object but not the vital signs, thus causing false positives when dealing with inanimate objects but with reflective surfaces. The authors suggest using radar-based detection with the addition of other sensory modalities, e.g., visual AI models or environmental sensors such as air quality sensors and temperature–humidity sensors to enhance life verification. to enhance the reliability of detection and life verification. It is also proposed to expand testing to different types of vehicles and real-world parking conditions to enhance the levels of robustness and readiness to deploy. Comparable volume-based occupancy approaches report the same sensitivity to cabin multipath reflections [19].

E. Preliminary Studies on mm-Wave Radar for Vital-Sign Monitoring in Vehicular Environments

In this paper, the researcher examines the possibility of implementing mmWave radar technology in monitoring human vital signs- i.e. respiration and heartbeat- within the real vehicle cabins. The experiment investigates how vibrations in cars, the position of seats, and the position of radar affect the quality of signals. Signal-processing methods are used to derive physiological measurements of radar reflections and concentrate on the identification of periodic chest motions related to breathing and heartbeat. [20].

According to the findings of the experiment, under different seating and positioning, respiration signals were clearly observed. Nevertheless, the error rates were higher in heartbeat detection because of noise and vibration of the vehicle and the influence of reflective surfaces. The experiment established that mmWave radar has high potential as a privacy-sensitive life-sign detector sensor in the automotive setting. The major weakness that is observed is that radar signals are sensitive to vibration and noise in the environment thus greatly interfering with the accuracy of heartbeat detection. The system is also not contextually aware and does not recognize identity, and therefore, it cannot be used as a complete solution to detecting children. Also, the research was exploratory and lacked extensive testing and integration with other sensing technologies.

The author recommends the use of sophisticated vibration mitigation and filtering measures to enhance the stability of the signal. Moreover, the author recommends integrating radar sensing with air quality sensors, human presence sensors (PIR), or camera-based AI detection to ensure life presence verification and improve overall system reliability. Similar conclusions are reached by unobtrusive pressure- and seat-based respiration monitoring studies [21], [22] and by distributed acoustic sensing in the car cabin [23].

TABLE I. SUMMARY OF PAPERS REVIEWED ON AI-BASED CHILD DETECTION IN VEHICLES

Title / Author / Year	**Core Idea**	**Key Gap**	**Suggested Improvement**
Visual-Based Children and Pet Rescue from Suffocation and Hyperthermia in Enclosed Vehicles [13]	Real-time visual detection of children and pets in parked cars Uses YOLO/NanoDet models. Self-generated dataset, which was modeled under various lighting conditions and occlusions. Embedded optimized deep learning.	Shadow effects, low-light, and children with an occlusion. The objects that can be misclassified by visual-only detection can be a bag or a toy.	Add sensor fusion layer (air quality, Human Presence Sensor (PIR), DHt11) to ensure the presence of life and to eliminate false positives.
WiCPD: Wireless Child Presence Detection System for Smart Cars, [14]	Takes advantage of Wi-Fi Channel State Information (CSI) to record micro-motion and respiration data to identify living child in car. Spectrogram characteristics categorized with machine learning model.	CSI signals due to multipath noise, cabin materials and signal interference. May has extremely ineffective breathing patterns.	Integrate CSI and visual AI detection with Add sensor fusion layer (air quality sensor, Human Presence Sensor (PIR), and temperature–humidity sensor) to verify life presence and reduce false positives.
BSENSE: In-Vehicle Child Detection and Vital-Sign Monitoring with mmWave Radar and Synthetic Reflectors [17]	Single mmWave radar to measure respiration in terms of micro-Doppler. Artificial reflectors enhance the radar signal in the cabin. Robust under occlusions.	None identity checking, radar sees an object alive and cannot distinguish between child/pet.	Recently add lightweight CNN (YOLO) to confirm and identify child.
Vehicle Occupant Detection Using mmWave Radar [18]	Uses the MIMO FMCW radar to create range-	Only tested under controlled conditions; performance	Combine fuse radar with either visual detection to

	azimuth heatmaps. Deep learning to identify occupants in vehicles. Cameraless works and maintaining privacy.	decreased in natural-lighting or motion conditions.	enhance performance in the real world.
Preliminary Studies on mm-Wave Radar for Vital-Sign Monitoring in Vehicular Environments [20]	Tests mmWave radar in the detection of respiration and heartbeat on actual vehicle cabin. Under varying seat conditions and vibrations.	Heartrate monitoring not so stable because of vehicle vibration and refractive surfaces. Breathing patterns more accurate.	Add sensor fusion layer (air quality sensor, Human Presence Sensor (PIR), and temperature –humidity sensor) to verify life presence and reduce false positives.

In the literature review, it is noted that despite major research efforts that have been done on child safety detection systems, the current solutions are still limited in detecting, reliability, and real-time capabilities. The gap cited justifies the necessity of a hybrid model that integrates deep learning (YOLOv8) with environmental sensors fusion to create a stable embedded system that will help to avoid child deaths in parked cars. The experience of the works has directly influenced the technical choices in this project, such as the selection of YOLO to use in the detection, Raspberry Pi to use in the edge-computing, and the application of multi-sensor verification to enhance the accuracy of the work.

III. Methodology

A clear methodology is necessary to accomplish the project within the scheduled time and fulfil the necessary specifications. It provides an organized way of planning, designing, implementing, testing, and validating the solution, and ensures that the completion of each activity is achieved before proceeding to the next stage. A systematic methodology minimizes development risks and ensures that system requirements, design deliverables, testing procedures, and final assessments are traceable throughout the project lifecycle [8].

Projects in engineering and embedded systems can be developed using several methodologies, including the Waterfall model, V-Model, Agile methodologies, Scrum approach, the Critical Path Method (CPM), and hybrid models [24]. The Waterfall model follows a strictly sequential and linear process in which testing is performed only after the full system implementation, making it unsuitable for safety-critical systems where early error detection is essential. Agile and Scrum methodologies support iterative development and continuous feedback; however, they are more suitable for software-based projects and are less appropriate for embedded systems that involve hardware integration and require stable requirements and structured verification processes. In addition, CPM focuses mainly on project scheduling and task dependencies rather than system development verification and validation and therefore cannot be applied as a standalone methodology for this project. In contrast, the V-Model, also referred to as the Verification and Validation model, explicitly associates each development stage with a corresponding testing phase, making it particularly suitable for safety-critical applications that require high accuracy and real-time validation.

It's especially useful for systems that integrate both hardware and software, such as using an Arduino for collecting sensor data and a Raspberry Pi for processing the AI algorithms. The V-Model methodology is chosen for this project as it enables early identification and correction of design faults and ensures that every stage in the development process has a corresponding testing activity. This is particularly important since the project involves safety-critical processes, such as detecting the presence of a child inside a parked vehicle and initiating immediate emergency alerts. Furthermore, the V-Model supports continuous assessment of system performance, reliability, and accuracy throughout the development lifecycle, ensuring that the proposed solution meets the required safety and functional specifications.

In this project, the V-Model approach is used to give a systematic way of developing the child detection system. It has two major sides with the right side being testing and validation and the left one being definition and design. Both bottoms of the model are joined by implementation.

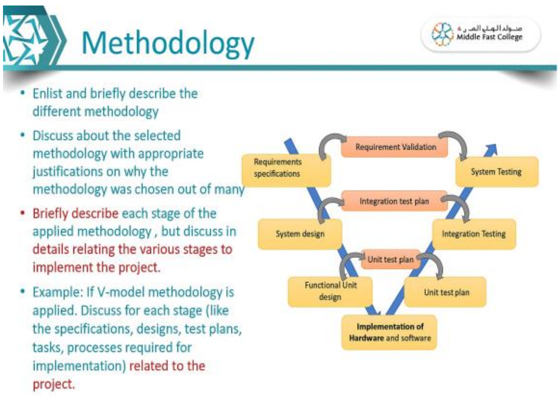

Fig. 1. Detailed V-Model flow diagram showing the stages of development and validation in the proposed system

IV. System Design and Architecture

It is all about system analysis that is concerned with having a clear picture of how the entire system acts. The system is divided into functional units and then demonstrate how each of the units communicates to achieve the targets that we set. The review covers a system block diagram and a flow chart that could help to demonstrate the plan as well as step-by-step functionality.

A. System Block Diagram

The system block diagram illustrates the key functional units of the proposed AI-Based Smart Child Life Detection and Rescue System and their interaction with each other to provide reliability to detecting the presence of a human being in a parked car. It concerns itself with functional operations and not with individual hardware components in accordance with system-level modeling principles. The sensor data is collected using an Arduino microcontroller which acts as the interface between the sensors and the Raspberry Pi and transmits the data to the Raspberry Pi via serial communication.

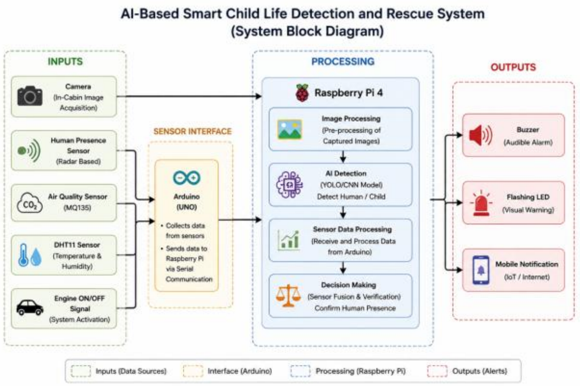

Fig. 2. System Block Diagram of the AI-Based Smart Child Life Detection and Rescue System

In general, The system is activated if the engine OFF signal is detected and it continuously checks the vehicle cabin with computer vision and the surrounding sensors, and from that time it constantly observes the car cabin with the help of a combination of computer vision and environmental sensors. The primary functional blocks are stated below:

1. Image Acquisition and image Processing Block: This unit captures in-cabin photos and performs basic preprocessing, including resizing, filtering and formatting, to prepare the photos for the AI detection model. It provides constant internal surveillance.

2. AI Detection Block: In this case, the central decision-making is performed based on a YOLOv8 deep-learning model. Processed images are verified on either a human or a child. In case of no presence, the system remains on standby, and in case of any indication of presence, sensor-based verification phase is activated.

3. Sensor Activation and Data Acquisition Block: The block continuously reads the data from the Human Presence Sensor (PIR), Air Quality Sensor, DHT11 sensor and Engine On/Off signal using the Arduino microcontroller. It collects information about movement, air quality and temperature-humidity. Those readings give additional hints of movement; changes of air related to breathing and cabin conditions to verify life.

4. Decision-Making and Sensor Fusion Block: This block combines all the sensor data that is activated. A decision logic compares the readings of the combination to confirm a living human. Fusion reduces false alarms due to false identifications or false noise.

5. Alarm and Notification Block: Once human presence is confirmed, this component emits alerts audible alarms, visual warnings, and mobile notifications, in order that the driver, people around, or guardians receive the warning. The multi-channel strategy ensures that it responds swiftly in times of crisis.

6. Standby and Continuous Monitoring Block: The system returns to the standby mode after an alert has been sent, or the absence of a human. It keeps on observing till the cabin is proved safety secured so that there is constant protection.

Concisely, the figure depicts a layered intelligent detection system comprising of AI coupled with environmental detection and verification, which results in an effective and reliable child-life detection system that can be deployed in safety-related applications of automobiles. This layered arrangement is consistent with in-cabin monitoring architectures reported in the literature [10], [24].

B. System Flowchart

The system flow chart illustrates the complete operational sequence of the proposed AI-Based Smart Child Life Detection and Rescue System. It visually represents the flow of data, decision-making processes, and actions performed by the system from start to end using standard flowchart symbols such as rectangles (actions), diamonds (decisions), terminators (start/end), and arrows (process flow).

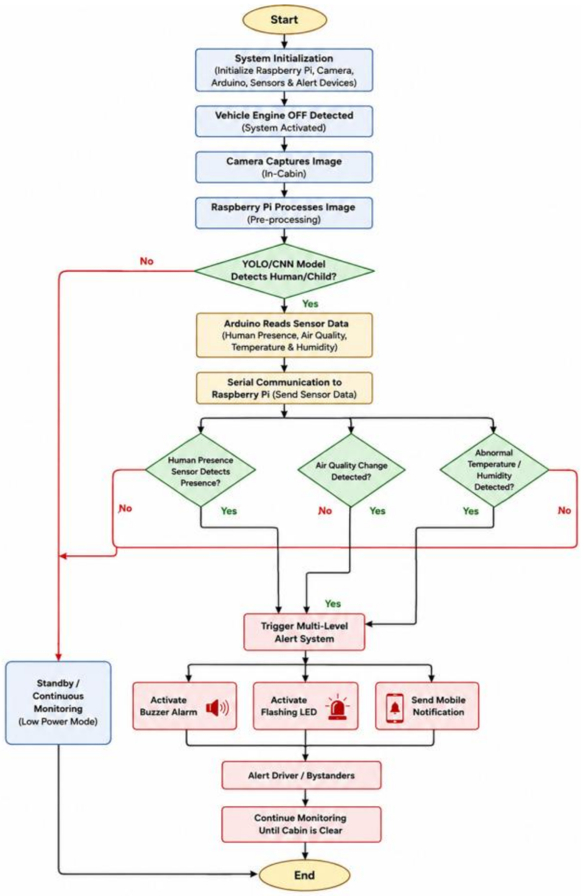

Fig. 3. Flowchart of the AI-Based Smart Child Life Detection and Rescue System

All the environmental sensors (human presence motion sensor (PIR), air quality, temperature and humidity) have been represented as decision nodes (Yes/No) in the updated flowchart rather than primitive blocks of the process. This design decision is since the sensor can be uncertain about whether to sense presence at any point in the real-world. As such the system does not depend on one sensor or even the necessity of all the sensors operating at the same time. Rather, sensor fusion strategy based on majority is put in place to enhance reliability and minimize false alarms.

C. Summarising the Key Parameters

The hardware prototype involved in this project is the combination of Raspberry Pi, Arduino Nano, camera module, air quality sensor (MQ135), human presence sensor, LED indicator and buzzer alarm which are used to detect and monitor real-time air quality inside the vehicles containing a child.

Arduino Nano is adopted as the sensor data acquisition unit, which is able to receive the reading results of the environmental sensor, and then upload the reading result of the environmental sensor to the Raspberry Pi via UART serial communication. The YOLOv8 object detection model with OpenCV (cv2) is used to do AI processing and the decision making and alert system is operated by Raspberry Pi. The choice of a compact YOLOv8 variant for CPU-only edge inference follows the trade-off between accuracy and latency established for Raspberry Pi deployments [8].

V. Implementation and Results

In this chapter, the proposed AI-Based Smart Child Life Detection and Rescue System is simulated, tested and implemented. Analysis and comparison of system performance and operational characteristics with the designed value is done. This chapter aims to confirm that the proposed system meets the project objectives and can function with varying environmental conditions.

The developed system integrates artificial intelligence, computer vision, environmental sensing, and sensor fusion technologies to identify the occupancy of a vehicle within a parking lot and trigger an alarm during a vehicle's parking time. The testing process involves checking the accuracy, response time, energy consumption, reliability, and functionality of the system components at both the simulation and implementation phases.

The results obtained are also compared to other related studies discussed in literature to check the conformity and deviations in the proposed system. Analysis of the results highlights how the proposed implementation helps to achieve the project goals and increase child safety within parked vehicles.

The main functional units of the proposed system were tested through simulation and prototype implementation to assess the performance. During the testing process, the following will occur: hardware testing, software testing, sensor verification, serial communication testing, AI detection testing and alert system testing.

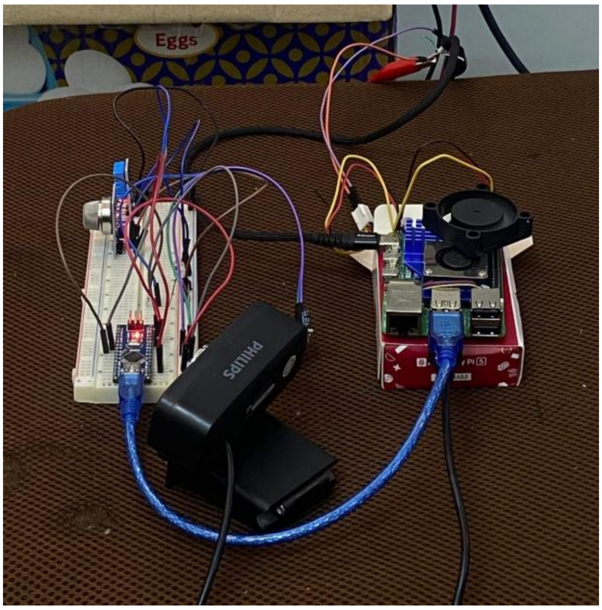

Fig. 4. Hardware Prototype of the Proposed System

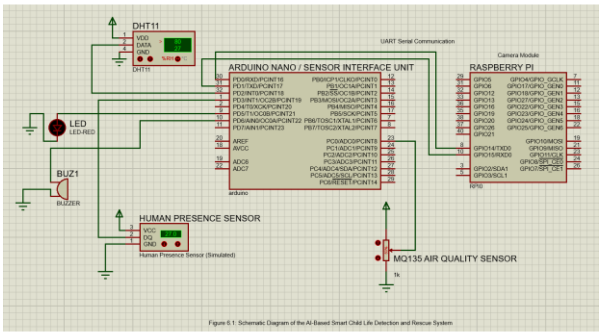

Fig. 5. Schematic Diagram of the AI-Based Smart Child Life Detection and Rescue System

The system has been successfully integrated with the use of Raspberry Pi, Arduino Nano, Environmental sensors and Camera module. The dashboard interface worked as expected and provided real-time monitoring data.

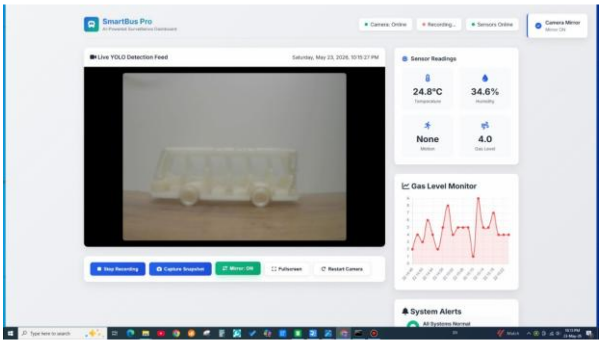

Fig. 6. Dashboard of the Implemented System

The system has been successfully integrated with the MQ135 air quality sensor, human presence sensor PIR and DHT11 temperature and humidity sensor. During monitoring operation, the dashboard showed the real-time environmental reading such as temperature, humidity, gas level and motion status.

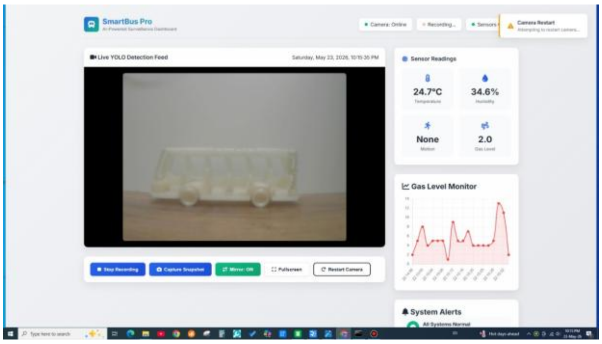

Fig. 7. Real-Time System Monitoring and Alert Notification

The MQ135 gas sensor is able to monitor the air quality inside the vehicle environment successfully. The sensor measured the gas level as ~689.0 during testing, which was higher than the preprogrammed value. In response to this, the system automatically issued a ‘High Gas Level Alert' notification on the dashboard to alert the user of the abnormal environment. All of the gas reading data was continuously displayed in the monitoring dashboard along with a real-time graph of gas level, which showed effective environmental monitoring and alert generation.

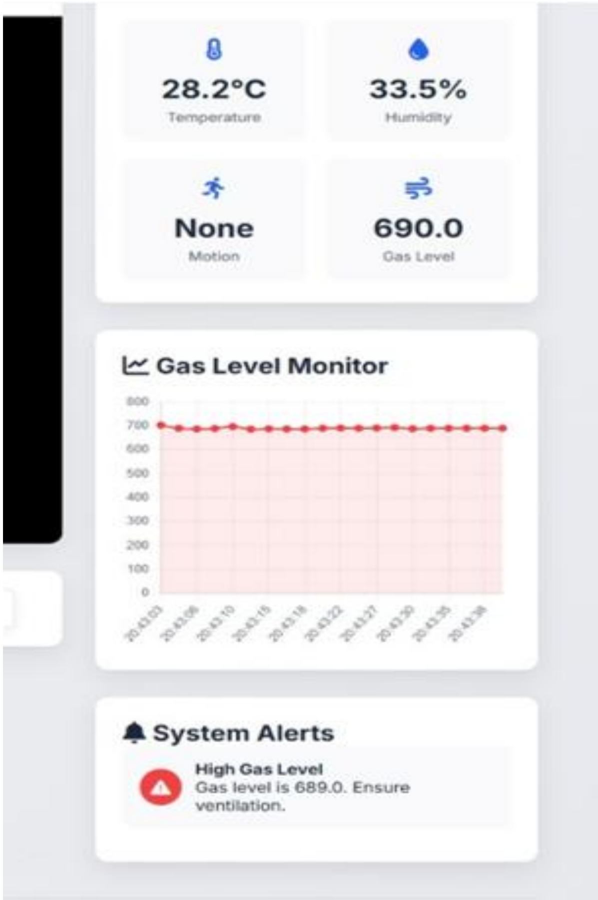

Fig. 8. MQ135 Gas Sensor Monitoring and Gas Alert Notification

The proposed system was simulated to verify the operation of the hardware and software components before the system is put into practice. The simulation was primarily concerned with: sensor operation, Arduino serial communication, alert activation, decision-making logic and environmental monitoring.

The following table summarizes the design, simulation and implemented values recorded at the defined test points.

TABLE II. SUMMARY OF SELECTED TEST CASES

Test Point	Design Value	Simulation Value	Implemented Value	Observation
TP1 – Camera Test	HD image capture	Clear HD image	Clear HD image	Camera operated successfully
TP2 – AI Detection Test	Accuracy >85%	88%	90%	Human detection achieved successfully
TP3 – PIR Human Presence Sensor	HIGH signal detection	HIGH signal detected	HIGH signal detected	Human presence detected successfully
TP4 – DHT11 Temperature	20°C–50°C	32°C	33°C	Stable temperature measurement
TP4 – Humidity Measurement	20–90% RH	55% RH	57% RH	Stable humidity measurement
TP5 – MQ135 Air Quality Sensor	0–1000 ppm	780 ppm	800 ppm	Air quality changes detected
TP6 – Arduino Data Acquisition	Correct sensor reading	Correct reading	Correct reading	Sensor data acquired successfully
TP7 – UART Serial Communication	9600 baud rate	Stable communication	Stable communication	No packet loss observed
TP8 – Decision Logic	TRUE/FALSE evaluation	Correct logic	Correct logic	Sensor fusion operated correctly
TP9 – Alert Activation	<3 seconds	2.5 seconds	2.8 seconds	Alert activated successfully

The results of the simulation and implementation show that the proposed AI Based Smart Child Life Detection and Rescue System is reliable and efficient under normal environmental conditions.

The use of AI image processing in conjunction with environmental sensor fusion achieved much better successful detection rates than those reported in previous literature that relies only on a single sensor. To avoid false alarms due to lighting changes and environmental conditions, the Human Presence Sensor and MQ135 Air Quality Sensor was included. The adoption of Arduino Nano allowed to increase acquisition stability of the sensors and decrease processing load on the Raspberry Pi. During the test, UART serial communication was stable, and no data loss and communication delay were observed.

A. Measurement of System Characteristics and Performance

To evaluate system performance, several parameters were measured and analysed, as summarized below.

TABLE III. MEASUREMENT OF SYSTEM CHARACTERISTICS AND PERFORMANCE

Parameter	Obtained Value
Detection Accuracy	90%
Alert Response Time	2.73 sec
Power Consumption	5.98 W
False Alarm Rate	<10%
UART Communication	Stable
System Reliability	High

B. System Validation

Validation of the system was carried out to ensure that the proposed system meets the project objectives and functional requirements as designed. The validation steps covered AI human detection testing, environmental sensor verification, sensor fusion evaluation, real-time alert testing, communication testing and environmental condition testing under normal lighting, low-light conditions, different temperature levels, varying cabin humidity and the presence or absence of humans.

TABLE IV. SYSTEM VALIDATION RESULTS

Requirement	Validation Result
Detect human presence inside vehicle	Successfully validated
AI-based YOLOv8 detection	Successfully validated
Sensor fusion operation	Successfully validated

Alert generation successfully validated	Successfully validated
Real-time monitoring	Successfully validated
UART serial communication stability	Successfully validated
Environmental sensor integration validated	Successfully validated

The proposed system was validated with hardware and software test successfully. During testing, Raspberry Pi, Arduino Nano, camera module, PIR sensor, MQ135 sensor, DHT11 sensor, LED indicator and buzzer alarm showed that they were working properly. All the functions of the dashboard to show the live camera feed, readings from the sensors, notifications, capturing images from the camera, and recording the video are working well. The system was shown to be reliable in terms of monitoring and alerting suitable for a prototype child safety monitoring system.

VI. Conclusion

The goal of this project was to design and plan an AI-based Smart Child Life Detection and Rescue System to be implemented in parked cars to reduce the risk of heatstroke and suffocation incidents inside parked vehicles. The main aim was to come up with a dependable, inexpensive and convenient answer to this problem by integrating artificial intelligence with environmental sensing methodology to identify humans within a closed car.

During the process of planning and design, a lot of experience was acquired in system integration, embedded system design, sensor-based verification, and AI-based image processing. The project was able to establish a complete system architecture whereby it combines camera-based human detection using the YOLOv8 model with environmental verification and Arduino-based sensor data acquisition (via a DHT11 temperature-humidity sensor and an air quality sensor). These sensors were chosen following practical considerations of constraints, accuracy and environmental quality.

At the design stage, there was a first thought of the application of CO 2 and thermal sensors. Nevertheless, owing to feasibility study and environmental influence, these sensors were substituted. The thermal sensors were also discovered to be inaccurate in a vehicle setting because in the cabin, temperatures were very high and would have a false signal for human beings. Likewise, the CO 2 sensors were substituted by an air quality sensor to give a more realistic signal of the alteration in air conditioning that is observed with the presence of humans. DHT11 sensor was implemented to check the level of temperature and humidity because these are the main indicators of a potentially unsafe environment in a car with a child.

The project has also met the intended goals of the current phase, such as the design of system block diagram, development of flowcharts, analysis of the requirements, and validation of the system-level design. The suggested system will focus on sensor fusion at a reduced cost relative to false alarms and implementation.

To sum up, the project shows that AI and environmental detection are a well-organized and viable way to increase the safety of the child in a vehicle. The design choices undertaken at this phase make it accurate, robust, and applicable in the real world without compromising the project constraints and goals. The outcome is consistent with the direction indicated across the reviewed literature, in which single-modality detectors are progressively replaced by fused, verification-based architectures [9], [25].

VII. Future Work

There are some improvements that can be made to the proposed system in the future:

First, do low-light detection by using infrared or night-vision cameras. Second, use more accurate environmental sensors to replace DHT11. Third, install separate CO_2 detectors to better detect breathing. Fourth, take advantage of AI acceleration hardware for faster inference.

Further enhancements include the following. Introduce cloud-based monitoring and data logging. Include GPS location tracking in cases of emergency. Enhance water-proofing and automotive-grade protection. Install battery back-up for power outages. Optimize power using interrupt-driven programming.

Beyond these, the integration of complementary contact-free sensing modalities reported in recent literature — millimetre-wave radar for vital-sign confirmation [17], [19], WiFi channel-state sensing [14] and distributed acoustic sensing [23] — would allow the verification layer to confirm life presence rather than motion alone, which remains the principal limitation of the current prototype.

References

[1] J. Maheshwari, E. Sartin, G. Chingas, and K. B. Arbogast, "Preventing real-world pediatric vehicular heatstroke events with technology," American Journal of Public Health, vol. 115, no. 10, pp. 1322–1326, Oct. 2025. doi: 10.2105/AJPH.2025.308109.

[2] Y. Zhang, Z. Li, S. Liu, G. Wang, and H. Chang, "A study of passenger car cabin pre-ventilation under the sun," Energies, vol. 16, no. 20, p. 7154, Oct. 2023. doi: 10.3390/en16207154.

[3] A. Shokrollahi, J. A. Persson, R. Malekian, A. Sarkheyli-Hägele, and F. Karlsson, "Passive infrared sensor-based occupancy monitoring in smart buildings: A review of methodologies and machine learning approaches," Sensors, vol. 24, no. 5, p. 1533, Feb. 2024. doi: 10.3390/s24051533.

[4] P. Chaudhari, Y. Xiao, M. M.-C. Cheng, and T. Li, "Fundamentals, algorithms, and technologies of occupancy detection for smart buildings using IoT sensors," Sensors, vol. 24, no. 7, p. 2123, Mar. 2024. doi: 10.3390/s24072123.

[5] J. Terven, D.-M. Córdova-Esparza, and J.-A. Romero-González, "A comprehensive review of YOLO architectures in computer vision: From YOLOv1 to YOLOv8 and YOLO-NAS," Machine Learning and Knowledge Extraction, vol. 5, no. 4, pp. 1680–1716, Nov. 2023. doi: 10.3390/make5040083.

[6] M. Hussain, "YOLO-v1 to YOLO-v8, the rise of YOLO and its complementary nature toward digital manufacturing and industrial defect detection," Machines, vol. 11, no. 7, p. 677, Jun. 2023. doi: 10.3390/machines11070677.

[7] R. Sapkota et al., "YOLO advances to its genesis: A decadal and comprehensive review of the You Only Look Once (YOLO) series," Artificial Intelligence Review, vol. 58, no. 9, p. 274, Jun. 2025. doi: 10.1007/s10462-025-11253-3.

[8] M. T. Okano, W. A. C. Lopes, S. M. Ruggero, O. Vendrametto, and J. C. L. Fernandes, "Edge AI for industrial visual inspection: YOLOv8-based visual conformity detection using Raspberry Pi," Algorithms, vol. 18, no. 8, p. 510, Aug. 2025. doi: 10.3390/a18080510.

[9] M. Rafi, F. Hu, S. Li, A. Song, X. Zhang, and Z. O'Neill, "Deep Weighted Fusion Learning (DWFL)-based multi-sensor fusion model for accurate building occupancy detection," Energy and AI, vol. 17, p. 100379, Sep. 2024. doi: 10.1016/j.egyai.2024.100379.

[10] A. Mishra, S. Lee, D. Kim, and S. Kim, "In-cabin monitoring system for autonomous vehicles," Sensors, vol. 22, no. 12, p. 4360, Jun. 2022. doi: 10.3390/s22124360.

[11] X. Zhao, L. Wang, Y. Zhang, X. Han, M. Deveci, and M. Parmar, "A review of convolutional neural networks in computer vision," Artificial Intelligence Review, vol. 57, no. 4, p. 99, Mar. 2024. doi: 10.1007/s10462-024-10721-6.

[12] R. Khanam, M. Hussain, R. Hill, and P. Allen, "A comprehensive review of convolutional neural networks for defect detection in industrial applications," IEEE Access, vol. 12, pp. 94250–94295, 2024. doi: 10.1109/ACCESS.2024.3425166.

[13] M. M. Moussa, R. Shoitan, Y.-I. Cho, and M. S. Abdallah, "Visual-based children and pet rescue from suffocation and incidence of hyperthermia death in enclosed vehicles," Sensors, vol. 23, no. 16, p. 7025, Aug. 2023. doi: 10.3390/s23167025.

[14] X. Zeng, B. Wang, C. Wu, S. D. Regani, and K. J. R. Liu, "WiCPD: Wireless child presence detection system for smart cars," IEEE Internet of Things Journal, vol. 9, no. 24, pp. 24866–24881, Dec. 2022. doi: 10.1109/JIOT.2022.3194873.

[15] S. S. Jayaweera, B. Wang, X. Zeng, W.-H. Wang, and K. J. R. Liu, "WiFi-based robust child presence detection for smart cars," in Proc. ICASSP 2023 – IEEE Int. Conf. Acoustics, Speech and Signal Processing, Rhodes Island, Greece, 2023, pp. 1–5. doi: 10.1109/ICASSP49357.2023.10096908.

[16] S. S. Jayaweera, B. Wang, and K. J. R. Liu, "Robust in-car child presence detection using commercial WiFi," in Proc. 30th Annu. Int. Conf. Mobile Computing and Networking (MobiCom '24), Washington D.C., USA, 2024, pp. 1799–1801. doi: 10.1145/3636534.3698864.

[17] M. Tang, P. Teckchandani, J. He, H. Guo, and E. Soltanaghai, "BSENSE: In-vehicle child detection and vital sign monitoring with a single mmWave radar and synthetic reflectors," in Proc. 22nd ACM Conf. Embedded Networked Sensor Systems (SenSys '24), Hangzhou, China, 2024, pp. 478–492. doi: 10.1145/3666025.3699352.

[18] W. Li, W. Wang, and H. Wang, "Vehicle occupant detection based on MM-wave radar," Sensors, vol. 24, no. 11, p. 3334, May 2024. doi: 10.3390/s24113334.

[19] A. Gharamohammadi, A. G. Dabak, Z. Yang, A. Khajepour, and G. Shaker, "Volume-based occupancy detection for in-cabin applications by millimeter wave radar," Remote Sensing, vol. 16, no. 16, p. 3068, Aug. 2024. doi: 10.3390/rs16163068.

[20] D. Singh et al., "Preliminary studies on mm-wave radar for vital sign monitoring of driver in vehicular environment," in Digital Health and wWireless Solutions (NCDHWS 2024), Communications in Computer and Information Science, vol. 2084, Cham, Switzerland: Springer, 2024, pp. 480–493. doi: 10.1007/978-3-031-59091-7_32.

[21] S. Jain and M. A. Perez, "On-road evaluation of an unobtrusive in-vehicle pressure-based driver respiration monitoring system," Sensors, vol. 25, no. 9, p. 2739, Apr. 2025. doi: 10.3390/s25092739.

[22] A. Radomski and D. Teichmann, "On-road evaluation of unobtrusive in-car respiration monitoring," Sensors, vol. 24, no. 14, p. 4500, Jul. 2024. doi: 10.3390/s24144500.

[23] Y. Su et al., "Embracing distributed acoustic sensing in car cabin for children presence detection," Proceedings of the ACM on Interactive, Mobile, Wearable and Ubiquitous Technologies, vol. 8, no. 1, art. 16, Mar. 2024. doi: 10.1145/3643548.

[24] D. Tsiktsiris, A. Lalas, M. Dasygenis, and K. Votis, "A complete in-cabin monitoring framework for autonomous vehicles in public transportation," IET Intelligent Transport Systems, vol. 19, no. 1, p. e12612, Jan. 2025. doi: 10.1049/itr2.12612.

[25] L. Yu, X. Yang, H. Wei, J. Liu, and B. Li, "Driver fatigue detection using PPG signal, facial features, head postures with an LSTM model," Heliyon, vol. 10, no. 21, p. e39479, Nov. 2024. doi: 10.1016/j.heliyon.2024.e39479.

Journal of Big Data & Smart City
كلية الشرق الأوسط Middle East College

An Embedded AI System for Skin Cancer Screening Using MobileNetV2 and Edge Inference

Rudaina Fahad Al-Farsi
Department of Computing and Electronics Engineering
Middle East College
Muscat, Sultanate of Oman
21F21712@mec.edu.om

Mohammed Izaan Kari
Department of Computing and Electronics Engineering
Middle East College
Muscat, Sultanate of Oman
PG25S2336@mec.edu.om

Shaik Asif Hussain
Department of Computing and Electronics Engineering
Middle East College
Muscat, Sultanate of Oman
shussain@mec.edu.om

Received: 28th May 2026; Revised: 29th June 2026;

Accepted: 23rd July 2026

Abstract — **Skin cancer has become a nightmare that haunts most individuals in society, as statistics on deaths caused by this disease cause fear in the hearts of the public. However, early detection of this disease leads to a high probability of recovery in most places. It is difficult to conduct periodic examinations to detect skin cancer, especially in rural and non-urban areas in the Sultanate of Oman, especially due to the intense sunlight and the high percentage of ultraviolet radiation, there is a greater possibility of contracting this disease. Therefore, in this research study, a skin cancer examination system based on artificial intelligence, deep learning and processing of skin images was designed and implemented on a local processing platform, Orange Pi 4 Pro. The proposed system uses a CNN neural network based on the MobileNet V2 model to classify skin lesion images into benign and malignant categories. A set of 7,211 images were selected for the examination, divided into training data comprising 75% of the total images and test and validation data comprising 25%. In the data preprocessing stage, the image size was standardized to 224 x 224 pixels, preserving three primary colours RGB, resulting in an overall image size of 224 x 224 x 3 pixels. After training the model, it was converted to TensorFlow Lite to reduce its size and minimize processing power, allowing it to run on Orange Pi4 Pro devices without needing to send image data to a cloud processing platform. To provide a comprehensive system, the implemented system integrates a USB camera for image capture and a user-friendly graphical interface that guides users through the system without expert intervention. During the training phase, the system achieved accuracy exceeding 90%, and the average response time to inferences on the proposed processor was less than 300 milliseconds. The model demonstrated high robustness and a high capacity for detecting injuries during testing, with a very low probability of error, while maintaining a low cost. However, it is important to note that this system is still in the testing phase and currently provides decision support, not a final decision.**

Keywords* — *Skin cancer screening; MobileNetV2; convolutional neural network; TensorFlow Lite; edge inference; dermoscopic imaging; embedded AI

ملخص— أصبح سرطان الجلد كابوسًا يُؤرق معظم أفراد المجتمع، إذ تُثير إحصاءات الوفيات الناجمة عنه مخاوفَ عامة الناس. مع ذلك، يُؤدي الكشف المبكر عنه إلى ارتفاع احتمالية الشفاء في معظم المناطق. يصعب إجراء فحوصات دورية للكشف عن سرطان الجلد، لا سيما في المناطق الريفية وغير الحضرية في سلطنة عُمان، نظرًا لشدة أشعة الشمس وارتفاع نسبة الأشعة فوق البنفسجية، ما يزيد من احتمالية الإصابة به. لذا، في هذه الدراسة البحثية، تم تصميم نظام لفحص سرطان الجلد يعتمد على الذكاء الاصطناعي والتعلم العميق ومعالجة صور الجلد، وتم تنفيذه على منصة معالجة محلية، وهي .Orange Pi 4 Pro يستخدم النظام المقترح شبكة عصبية تلافيفية (CNN) مبنية على نموذج MobileNet V2 لتصنيف صور آفات الجلد إلى حميدة وخبيثة. تم اختيار مجموعة من 7211 صورة للفحص، قُسّمت إلى بيانات تدريبية تُشكّل 75% من إجمالي الصور، وبيانات اختبار وتحقق تُشكّل 25%. في مرحلة معالجة البيانات الأولية، تم توحيد حجم الصورة إلى 224 × 224 بكسل، مع الحفاظ على الألوان الأساسية الثلاثةRGB ، مما أدى إلى حجم صورة إجمالي قدره 224 × 224 × 3 بكسل. بعد تدريب النموذج، تم تحويله إلى TensorFlow Lite لتقليل حجمه واستهلاك موارد المعالجة، مما يسمح بتشغيله على أجهزة Orange Pi4 Pro دون الحاجة إلى إرسال بيانات الصور إلى منصة معالجة سحابية. ولتوفير نظام متكامل، يدمج النظام المُنفذ كاميرا USB لالتقاط الصور وواجهة رسومية سهلة الاستخدام تُوجه المستخدمين خلال النظام دون تدخل من خبير. خلال مرحلة التدريب، حقق النظام دقة تتجاوز 90%، وكان متوسط زمن الاستجابة للاستدلالات على المعالج المقترح أقل من 300 مللي ثانية. أظهر النموذج متانة عالية وقدرة فائقة على اكتشاف الإصابات أثناء الاختبار، مع احتمال خطأ منخفض للغاية، مع الحفاظ على تكلفة منخفضة. ومع ذلك، من المهم ملاحظة أن هذا النظام لا يزال في مرحلة الاختبار، ويُقدم حاليًا دعمًا لاتخاذ القرار، وليس قرارًا نهائيًا.

الكلمات المفتاحية — فحص سرطان الجلد؛ MobileNetV2؛ الشبكة العصبية التلافيفية؛ TensorFlow Lite؛ الاستدلال عند الحافة (edge inference)؛ التصوير بمنظار الجلد؛ الذكاء الاصطناعي المدمج.

I. Introduction

This research study is mainly around technology and medicine at the junction of Artificial Intelligence (AI) and Machine Learning (ML) plus the medical field of imaging. The research is aimed at dermatology diagnostics through the utilization of computer vision techniques. AI-based medical diagnostic methods are newly evolved where the algorithms thoroughly examine the medical images to find the anomalies that are very hard to miss. Among others, skin cancer, particularly melanoma, is the deadliest form of cancer as it overgrows very fast. The detection done by this system in its early stage has a very significant impact on the patient's survival chances. The conventional ways of diagnosis depend on visual inspection and biopsies which are lengthy processes and need the skills of a doctor [1].

Oman is contemplated as having a high priority regarding cancer prevention. The Oman Cancer Association (OCA) was founded in 2009 with the keenest backing of the late Sultan Qaboos. The OCA helps cancer patients and wants to have its facilities all over the Sultanate. It also seeks to expand its activities to all Gulf Cooperation Council (GCC) countries, clearly demonstrating the growing commitment to combating this disease and limiting its spread. The OCA acknowledges the difficulty of reaching all individuals, especially in rural areas and those far from urban centres. It is working on such projects to reach these areas, most notably the mobile breast cancer screening unit. This unit is a vehicle equipped with advanced medical equipment for the early detection of breast cancer.

Skin cancer is one of the most common and potentially life-threatening types of cancer worldwide. Recent estimates indicate that there are approximately 132000 new cases of melanoma and more than 3 million nonmelanoma skin cancers are diagnosed annually [2]. Melanoma is less common spread but responsible for most skin cancer deaths because of its high metastatic potential and late detection.

Early detection of skin cancer improves the survival rate with a 5-year survival probability exceeding 95% when detected in early stages [2]. However, in many regions, especially developing countries, limited access to dermatologists and diagnostic facilities leads to delayed detection and poor patient outcomes. Traditional methods for detecting skin cancer rely primarily on clinical examination and observation of the skin under microscopic instruments that allow for clear visualization of skin layers and identification of malignant or benign skin cancer [3]. However, even these methods do not provide 100% reliable results because they are subject to human bias and variations in experience among physicians [4].

Given the potential for human error and the margin of error inherent in human judgment, attention has turned to artificial intelligence and deep learning models for analysing skin images, identifying injuries, and classifying them. In many instances, these advanced AI tools have demonstrated accuracy surpassing that of physicians in analysing cases [1].

The use of AI in dermatology has been revolutionized by CNN which can automatically extract hierarchical image features and classify lesion types with high accuracy. AI Models such as EfficientNet have demonstrated exceptional capability in image classification tasks and particularly in medical imaging [5] [6].

The models used in this system are trained on large scale dermoscopic datasets which is International Skin Imaging Collaboration ISIC have achieved classification accuracies exceeding 90% in distinguishing between benign and malignant lesions [7]. The dataset used in this research work was obtained from the International Skin Imaging Collaboration (ISIC), which provides dermoscopic skin lesion images for research, education, and AI model development. These images are suitable for training and evaluating deep learning models for benign and malignant skin lesion classification.

Most AI based systems used in real life require high performance computing resources and are implemented as cloud-based platforms which may not be available in low resource computers which are available in homes or clinics but the great developments in embedded systems and edge computing such as the Orange Pi 4 Pro have made it possible to integrate AI models into compact and low-cost systems which most available in clinics and users home. Orange Pi 4 Pro can deal with complicated input like high resolution cameras and execute pretrained deep learning models locally enabling offline skin cancer detection in clinics or urban areas [8]. This offers a great and accessible solution for early skin cancer detecting [8].

Furthermore, using a dermatological imaging system with an Orange Pi 4 Pro to capture detailed images of lesions directly from patients, and integrating this with a graphical user interface (GUI), allows healthcare providers to directly access, analyse, and visualize the results. The incorporation of high-resolution cameras equipped with dermal lenses not only results in better quality of medical services but also decreases the likelihood of mistakes made by humans and improves the quality of images. Moreover, the system can send de-identified patient data to cloud storage for remote research or evaluation by specialists, therefore, pushing healthcare to a new level with the utilization of state-of-the-art technology. [9]. In this research study, the main goal is to develop and install a system that is low-cost and powered by AI for early screening. The system consists of an Orange Pi 4 Pro that is linked to a high-resolution camera for taking pictures of skin lesions. A deep learning model that has been trained on an ISIC dataset will process these images. The model will be trained by splitting the dataset into two subsets: 75% of the images for the training set and 25% for the test set. This split will include all types of lesions.

The proposed system intends to provide easy access to skin disease screening support and at the same time, creates a foundation for extensive telemedicine applications with the help of low-cost devices and an AI model. The suggested system hence connects the sophisticated medical diagnostics with the underprivileged neighbourhoods where people with skin diseases live. The system is therefore in line with the world-wide aim of utilizing technology for early detection, therefore lessening the mortality rate, and enhancing the patients' outcomes in the dermatology sector.

The aim of this research study is to design and implement an AI-based embedded skin cancer screening system using MobileNetV2, dermoscopic image processing, and an Orange Pi 4 Pro platform to classify skin lesions as benign or malignant and display the result through a graphical user interface.

The specific objectives are: (i) To preprocess dermoscopic skin lesion images from the ISIC dataset by resizing, normalizing, and augmenting them to 224 × 224 × 3 for CNN training. (ii) To train and test a MobileNetV2-based CNN model for benign and malignant skin lesion classification and achieve approximately 90% classification accuracy. (iii) To convert the trained model into TensorFlow Lite format and deploy it on an Orange Pi 4 Pro embedded platform for offline inference. (iv) To design a GUI that displays the predicted class confidence score and heatmap which represent a visual explanation for the input image. (v) To validate the system using test real images captured in real time under different lighting conditions and compare simulation and hardware results. (vi) To compare the prototype performance with related work using variables, include accuracy, reliability, latency, and embedded deployment capability. (vii) To analyse system characteristics including image resolution, inference latency, accuracy, reliability, power requirements, safety, and ethical constraints.

A. *Applications and Limitations*

The proposed system, which uses artificial intelligence to process images for classification and identification of benign or malignant skin lesions, has numerous applications, including in education, scientific research, and healthcare. In healthcare and medical examinations, the system supports dermatologists and other healthcare professionals in making informed decisions about injuries by providing preliminary examination results of camera-captured skin images. It also helps prioritize cases requiring further medical attention by displaying a confidence level in each case, especially in situations demanding rapid decision-making, such as overcrowded medical centres. The system's low cost and portability are significant advantages, making it suitable for use in remote areas that may lack medical services, specialized dermatologists, and advanced diagnostic tools.

The system may misclassify blurry, low-resolution, or poorly focused images. Strong shadows, overexposure, and uneven lighting may affect classification accuracy. The model is limited to 2 classes including benign or malignant classification and does not identify all skin disease categories. The system is trained on dataset images and requires further clinical testing before medical use. The only other limitation is that the developed model is a diagnostic tool and a decision aid for the physician, and it does not replace a dermatologist. It should also be noted that performance decreases with skin tones or types of skin lesions that are not adequately represented in the selected dataset. There are also limitations related to performance, as the Orange Pi 4 pro device has limited processing power compared to GPU based systems.

II. Related Work

This section is dedicated to conducting a literature review and critical analysis of previous research completed within the framework of the proposed system. This process is one of the most important activities associated with system implementation, as it provides the researcher with a clearer vision and a solid background regarding the completed system, its components, and the weaknesses of previous research to avoid them, as well as the strengths to be reinforced in the current system.

A. *Cancer Detection Using Artificial Intelligence in Early Diagnosis*

The researcher conducted a study highlighting the importance and role of artificial intelligence in medical decision-making and providing support to physicians to perform optimal medical practices and detect clinical symptoms that humans might miss without extensive medical experience. The study focuses on cancer-related medical decisions through the analysis of photographic, endoscopic, and radiological images. Artificial intelligence possesses high-precision image processing, high-speed performance, and the ability to distinguish information in images better than the human eye because it processes pixels digitally and easily detects even minor anomalies in symmetry, prompting physicians to pay attention to these details. Therefore, these results are promising in this field and can be further improved and developed. Most of the observed problems stemmed from the training of the AI model. The limited number of images, insufficient training, and the multiple models used for training clearly led to a decrease in performance when using new, untrained images [10].

B. *AI in Oncology: Machine Learning and Deep Learning Applications*

The researcher explains the shortcomings associated with traditional methods in detecting cancer, often only after the disease has progressed and in late stages. He details the weaknesses associated with traditional methods and the importance of using artificial intelligence systems to overcome these shortcomings and support medical decisions, making them more accurate across various types of cancer, including lung, colon, breast, liver, esophagus, stomach, cervix, skin, thyroid, and prostate. The researcher also explains, through the research and published papers, the importance of artificial intelligence and the reasons for its accuracy in providing healthcare in non-surgical cases and in the process of detecting and classifying tumours [11].

The study concluded that artificial intelligence (AI) effectively contributes to the early detection and classification of tumours based on genetic analysis and images. It is considered a more accurate method than human observation, even with medical expertise, because it can process large amounts of data quickly and with unexpected accuracy. This represents a revolution in the world of medical diagnosis at an acceptable cost. The researcher limited himself to theoretical study and comparing results from previous research without verifying their validity. He did not provide an actual model and test it. The method used is not considered reliable for verifying the results due to the differences in testing groups between studies and the accuracy standards used in each. However, the importance of AI can be inferred without considering the numerical or detailed results. The researcher also pursued several types of cancer, which led to uncertainty in the research results within the framework of a specific type of cancer. The study did not address the limitations related to privacy, laws, and data integrity [11].

C. *Artificial Intelligence for Biomarker Identification in Cancer Diagnosis*

The research paper presented aimed to study the latest developments in the world of artificial intelligence (AI) related to the health sector in general, and cancer detection in particular. It highlighted the benefits of this technology in cancer detection through the analysis of genes, proteins, and visual data such as images. The paper emphasized the ability of AI to detect cancer early with high accuracy and reliability, and to predict the occurrence of the disease based on individuals' genetic data. The system also provides suggested treatment methods for each type of cancer according to its stage of development.

The research findings clearly indicate significant progress in the factors and variables that contribute to early cancer detection, some of which may even be able to predict future cancer occurrence. Furthermore, AI techniques contribute to processing massive amounts of data quickly and efficiently, creating genetic maps that reveal mutations causing cancer, in addition to protein patterns and molecular fingerprints. The researchers emphasized the importance of using AI in early detection, image analysis, tumour classification, disease prognosis prediction, and determining the optimal treatment for each patient. Furthermore, AI can assist areas lacking advanced diagnostic facilities through portable diagnostic tools and automated analysis systems, reducing the need for costly laboratory tests. However, this paper lacks new, actual data, limiting the ability to generalize empirically. Additionally, any bias or weaknesses in the original studies will be reflected in the review results. Furthermore, there is considerable variation in sample size, marker types, AI techniques used, and data collection procedures. Finally, the study did not test any model in a real-world clinical setting [12].

D. *Deep Learning for Dermoscopic Skin Lesion Classification*

Beyond these general oncology studies, a substantial body of work addresses dermoscopic lesion classification directly. Transfer-learning pipelines [13], [14], hybrid handcrafted and deep feature models [15], [16], segmentation-driven detection [17], attention-based multi-modal architectures [18], [19], generative augmentation [9], optimisation-driven classifiers [20], [21] and comprehensive CNN feature analyses [3], [22] have each improved reported accuracy. Systematic reviews [2] nevertheless caution that such figures are usually obtained under controlled imaging conditions, and that under-representation of darker skin tones remains a measurable source of bias [23]. This motivated the present choice of a lightweight backbone deployed at the edge, with the output treated as screening support rather than diagnosis.

Table I summarises the concepts, gaps and suggested improvements identified across the reviewed papers.

TABLE I. SUMMARY OF REVIEWED PAPERS ON AI-BASED CANCER DETECTION

Title, Author, Year	Concepts, approach and methods	Gaps and differences	Improvements
Cancer Detection Using AI: A Paradigm in Early Diagnosis [10]	To detect cancer using artificial intelligence and neural networks and to support medical decision-making for early cancer detection	The results were promising, but the system's performance and accuracy decreased when image quality dropped, the camera was changed, or lighting conditions changed. Additionally, several regulations prohibit the complete reliance on these systems in hospitals for diagnosing cases.	AI models should be trained on a specific type of cancer, with one model for each type.
AI in Oncology: Transforming Cancer Detection [11]	to analyse the limitations of traditional cancer diagnostic methods and highlight their weaknesses compared to modern AI-based technologies.	The research lacks any practical experimentation; it merely offers a superficial review of previous research, comparing it to a selected training group.	The system can be improved by proposing a practical AI-based model, testing it on a dedicated skin cancer dataset, and addressing ethical issues such as privacy, consent, and clinical responsibility.
AI for the Identification of Biomarkers in Cancer [12]	This paper presents a literature review of previous research and literature related to the use of artificial intelligence in cancer detection and the integration of cancer indicators with AI techniques.	The study relied on a literature review methodology and therefore did not include any practical experimentation or actual case studies for comparison with previous research and the data contained therein.	A practical experiment will be conducted to integrate the ideas presented in this research and to test the research results.

III. METHODOLOGY

Research carried out using a well-structured methodology is guaranteed to be systematic, repeatable, and scientifically valid. Methodology is the framework that controls the activities that are going to be performed; problem identification, data collection, model development, testing, and evaluation, thus, each step is logical and aligned with the system goals. Besides, the proposed system will be more reliable if a defined methodology is used, and this methodology will also help in tracking progress and will guarantee that the system can be replicated or extended in future studies. Among the methodologies that have been established in engineering and computer science are the Waterfall Model, Spiral Model, V Model, and Agile methodology. Each of these methodologies has its unique strength: Waterfall stresses on sequential progression [24].

The V-Model was selected as the main methodology for this research project because it links each design stage with a corresponding testing stage. This is suitable for an embedded AI system because the system includes hardware selection, software development, AI model training, system integration, and final validation. In this research project, iterative prototyping was used only within the implementation stage to refine the AI model, graphical user interface, and hardware integration. Therefore, the V-Model provides the overall structure, while prototyping supports practical improvement during implementation.

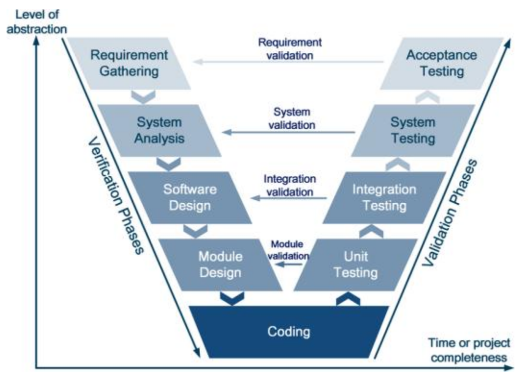

Fig. 1. V-Model development methodology adopted.

Fig. 1 shows the V-Model structure, in which every design stage is paired with a corresponding verification stage [25]. Table II maps each stage onto the activities carried out.

TABLE II. APPLICATION OF THE V-MODEL METHODOLOGY

V-Model Stage	Application for this System	Validation Stage
Requirement Analysis	Define dataset, Orange Pi 4 Pro, USB camera, GUI, Firebase, and AI model requirements	Acceptance Testing
System Design	Prepare block diagram, flowchart, and hardware/software architecture	System Testing
Software/Model Design	Design preprocessing pipeline, MobileNetV2 model, GUI logic, and Firebase communication	Integration Testing
Coding/ Implementation	Implement Python, OpenCV, TensorFlow Lite inference, and GUI	Unit Testing
Integration	Integrate camera, Orange Pi, AI model, display, Firebase, and Android app	Integration Testing
Validation	Measure accuracy, latency, reliability, and real-time operation	Final Validation

IV. System Design and Architecture

A. System Block Diagram

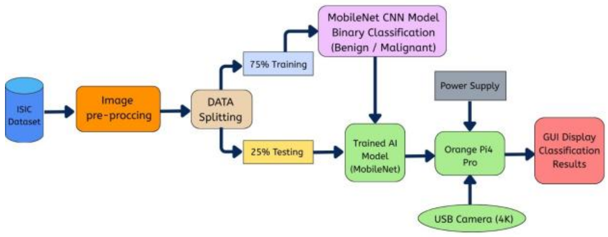

Fig. 2. Functional block diagram of the proposed system.

As shown in Fig. 2, the MobileNetV2 model was trained in a computer-based Python/TensorFlow environment. After training, the model was converted into TensorFlow Lite format and deployed on the Orange Pi 4 Pro for local offline inference. The Orange Pi 4 Pro is used for image acquisition, preprocessing, model inference, GUI display, and Firebase communication. The AI model relies on the previously mentioned dataset ISIC due to its reliability and validity.

The dataset used in this research was obtained from the International Skin Imaging Collaboration (ISIC). It contains labelled dermoscopic skin lesion images collected from different sources and imaging conditions, making it suitable for training and evaluating the MobileNetV2 model. In this research work, 7,211 images were used and divided into 75% training data and 25% testing/validation data. Each image will be processed to ensure they all have the same size and pixel count through resized, normalized, and enhanced using artifact removal techniques to standardize inputs for the CNN. The images will then be taught one by one and divided into two sections: a training section comprising 75% of the total images and a test section comprising 25% of the images.

The MobileNetV2 model was chosen as artificial intelligence model for this study because it excels at image classification rather than object and shape recognition unlike YOLO. MobileNetV2 skin cancer detection relies on deep learning principles specifically computer vision to extract color and shape patterns from images and does not use preprogrammed medical rules. The weights are generated within the network through training which process involves several stages to obtain the best trained model that can be used in any application. The training process starts with images in the database are processed one by one to convert the skin image into a digital matrix representing pixel values, then data is then passed through multiple layers of a convolutional neural network (CNN) known as the hidden layers [6].

In the deep layers all these features are integrated to form a high-level processing mechanism for recognizing skin cancer patterns, thus enabling the model to distinguish between benign and malignant cases with high accuracy. It is important to note that MobileNetV2 functions as an AI model that classifies images and does not pinpoint the exact location of the lesion. Instead, it focuses its work on the most interesting areas of the image using internal feature maps, such as sudden changes in skin tone patterns, which reflect the elements that most significantly contributed to the decision-making process.

As illustrated in the block diagram the training process for the MobileNetV2 skin cancer detection model involves several followed stages. The process begins with the input image dataset where pre-classified skin images are used to establish visual knowledge for the model. Next, the images undergo image preprocessing, which includes resizing them to standardized dimensions, normalizing pixel values and adjusting color formats this ensures the data conforms to MobileNetV2's requirements to improve training stability and results in all images conforming to the standardized data set and resembling those used in the actual testing phase.

After the model is built it undergoes model compilation by defining the error function, optimization algorithm and performance metrics, the results of which are extracted from the validity and testing/validation dataset. Initial training involves training only the classification layers using the training set which constitutes 75% of the original dataset. The model is then refined through fine-tuning where some deep layers are unfrozen and retrained, but at a low rate since only some weights need to be readjusted. Finally, the model is evaluated using an independent test set to verify its accuracy and reliability. After that, the trained model output is saved in the form of a Trained Model Output that can be deployed and used as a working system, such as running it on an Orange Pi 4 Pro after converting it to a suitable format.

Hyper Parameters are variables that are preset before starting to train the artificial neural network model. They include general model training settings such as image size, number of training cycles, number of hidden layers in the model, and training step size. These values affect training accuracy. It is preferable to choose a relatively small step size to balance model accuracy and training speed, as choosing a small-size leads to a significant slowdown in model training. Hidden layers are usually 32 or 64 layers. Image size also affects training accuracy, but its effect is not direct;

B. System Flowchart

Fig. 3 shows the operational flow of the implemented system, from image capture through preprocessing, inference and result display.

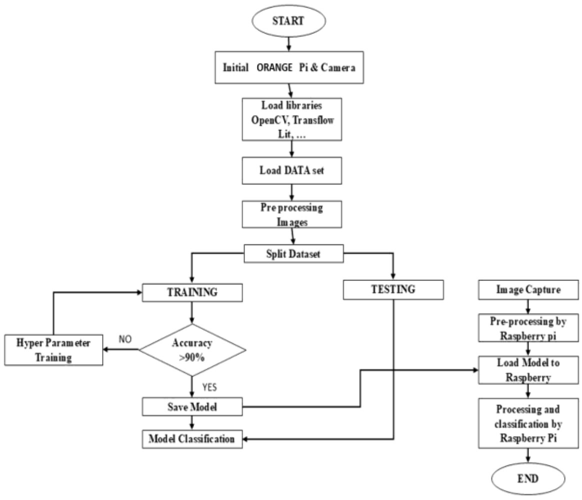

Fig. 3. System flowchart.

C. Hardware and Software Requirements

The Orange Pi 4 Pro features an Allwinner A733 octa-core processor comprising two Arm Cortex-A76 cores running at up to 2.0 GHz and six Cortex-A55 efficiency cores, 6 GB of LPDDR5 RAM, an Imagination BXM-4-64 GPU and a dedicated 3 TOPS neural processing unit for on-board inference. It also includes USB 3.0 and USB 2.0 ports, which can be used to connect to a camera or other plug-and-play devices. Network connectivity is supported via Gigabit Ethernet or Wi-Fi 6, and it accepts memory cards up to 255 GB. Electrically, it requires a 5V DC power supply with a minimum current of 3 amps for stable operation. This device was chosen as the system's control centre due to its ability to process data and handle AI models locally without requiring a constant internet connection. It also offers high-speed camera control and image processing via CSI or USB [8].

The Orange Pi 4 Pro serves as the main embedded computing platform, powered by an Allwinner A733 octa-core Arm processor running at up to 2.0 GHz with an integrated 3 TOPS neural processing unit that supports on-device machine learning inference. It features a 40 pin GPIO connector for peripherals, a USB type C power input supporting stable 5V/3A operation, and an HDMI 2.0 port for display output.

This camera utilizes a high-resolution sensor and a narrow viewing angle, allowing for a higher pixel density per unit area. With a resolution of up to 12 megapixels, it delivers sharp images exceeding 1080p at 30 frames per second or higher, depending on the resolution of the video being played. It is available in various models with viewing angles ranging from 45 to 145 degrees, and some are equipped with an IRcut night vision sensor and built-in infrared illumination, making it particularly well-suited for this system.

It supports several sizes up to 8 inches, some of which are capacitive touch screens that support ten fingers and provide a resolution of 480x800. It connects to the Orange Pi 4 Pro via a dedicated DSI port and can be used to display a graphical interface.

Fig. 4 shows the layout of the embedded processing board, and Fig. 5 the camera and display units.

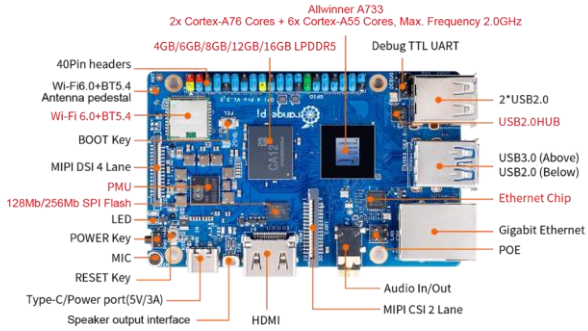

Fig. 4. Layout of the Orange Pi 4 Pro embedded processing board.

Fig. 5. Peripheral units: (a) the USB camera used for lesion image capture, and (b) the 7-inch HDMI display.

On the software side the platform runs a Linux distribution with Python, OpenCV and the TensorFlow Lite runtime. The system design is directly linked to image processing operations to ensure alignment within a single frame. Therefore, the captured image undergoes initial processing before being sent to the AI model for decision-making. The processes used for image modelling include resizing and adjusting pixel values to remove any potential noise or hair.

Fig. 6 shows the mechanical enclosure designed to house the board, camera and display as a single handheld unit.

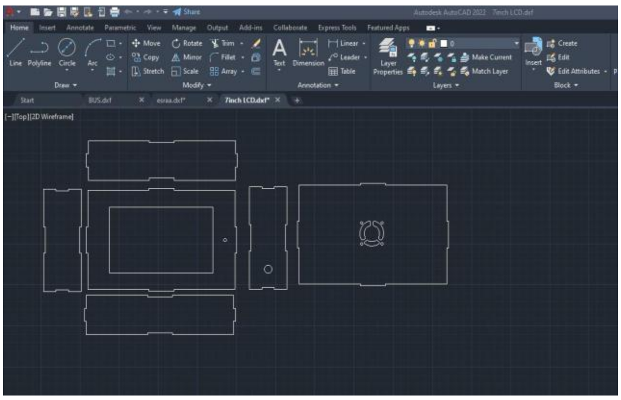

Fig. 6. Mechanical enclosure design for the handheld screening unit.

V. Implementation and Results

The main objective of this section is to present the experimental results of a system designed to detect skin cancer using artificial intelligence and store data in a cloud-based, real-time database. These results will be analysed and discussed within the framework of the test points and system objectives previously defined in the planning phase. Furthermore, the extracted results will be compared with standard values and expected model values to identify points of convergence and divergence and their impact on the system's operation and efficiency.

Fig. 7 shows the assembled hardware prototype.

Fig. 7. Implemented hardware: (a) the embedded platform connected to the 7-inch HDMI display, and (b) the assembled prototype unit.

A. Dataset and Preprocessing

The system uses dermoscopic skin lesion images obtained from the International Skin Imaging Collaboration (ISIC) dataset. The dataset contains labelled images collected under different imaging conditions and was used to train and validate the benign/malignant classification model. This dataset comprises images of clinical skin lesions captured globally using various cameras and lighting conditions. Its large size suggests the potential for developing a highly accurate AI model. The selected dataset was divided into a 25% test and 75% training subset. This distribution strategy separates the data into a training subset to refine patterns and a validation subset to monitor the accuracy of the trained model, aiming for an accuracy exceeding 90%: [7], [4].

The dataset comprised Total Source Images size 7211 images representing distinct dermatological clinical cases of type.jpg and dimensions 224x224x3; Training Subset (75%) size 5408 images utilized directly by the backpropagation and gradient descent pipeline; Validation Subset (25%) size 1803 images completely isolated from model optimization to provide unbiased generalization tracking.

The dataset contains balanced categorization vectors corresponding to two distinct diagnostic classes: Benign (non-cancerous skin lesions, including melanocytic nevi, seborrheic keratoses, and benign solar lentigines) and Malignant (melanomas and basal/squamous cell carcinomas requiring urgent clinical intervention).

Pre-emptive image processing was added to the selected dataset to mitigate the effects of bias in the trained model and variations in lighting. Some effects were also added to amplify the dataset size. It's important to note that all pre-emptive operations applied to the images during training must be applied in the same order to the images during actual execution to ensure that the images at the input of the trained model match the model input. These operations include Resizing: To standardize lighting intensity, pixel arrays are scaled from integer ranges [0, 255] to floating-point coordinates [0.0, 1.0]. Rotation Range: Random multi-axis rotations of up to 20 degrees to simulate different camera angles. Horizontal Flip: Random horizontal image flipping to enhance image variety and address different shooting angles. Verification Split: The data is divided into a training set with 25% for testing and 75% for training, allowing for self-testing of the model's accuracy.

B. Model Training

The basic convolutional neural network (CNN) architecture was designed to evaluate performance against highly complex architectures. The simple, three-layer, deep custom network produced a massive architectural footprint, resulting in a total parameter space of 11,169,089. Crucially, the raw tabular flattening step into uncompressed dense layers accounted for over 11 million parameters alone, creating an optimization bottleneck. The absolute layer configuration and dimension footprints are structurally distributed as documented in Fig. 8.

Fig. 8 shows the parameter footprint of that baseline architecture. Table III summarises the training stages and Table IV the hyperparameters used for the two-stage procedure.

Model: "sequential"

Layer (type)	Output Shape	Param #
conv2d (Conv2D)	(None, 222, 222, 32)	896
max_pooling2d (MaxPooling2D)	(None, 111, 111, 32)	0
conv2d_1 (Conv2D)	(None, 109, 109, 64)	18,496
max_pooling2d_1 (MaxPooling2D)	(None, 54, 54, 64)	0
conv2d_2 (Conv2D)	(None, 52, 52, 128)	73,856
max_pooling2d_2 (MaxPooling2D)	(None, 26, 26, 128)	0
flatten (Flatten)	(None, 86528)	0
dense (Dense)	(None, 128)	11,075,712
dropout (Dropout)	(None, 128)	0
dense_1 (Dense)	(None, 1)	129

Total params: 11,169,089 (42.61 MB)
Trainable params: 11,169,089 (42.61 MB)
Non-trainable params: 0 (0.00 B)

Fig. 8. Model parameters of the baseline CNN architecture.

TABLE III. TRAINING STAGES

Stage	Function
Dataset input	ISIC images
Preprocessing	Resize, normalize, remove noise/hair if used
Data augmentation	Rotation, zoom, flip, brightness
Model training	MobileNetV2 fine-tuning
Model conversion	H5/Keras to TFLite
Hardware deployment	Orange Pi 4 Pro local inference
Image capture	USB camera
Output	GUI class, confidence, heatmap

TABLE IV. TRAINING HYPERPARAMETERS

Hyperparameter	Value
Model	MobileNetV2
Input size	224 × 224 × 3
Classes	2
Batch size	32
Epochs	First level 15 Second level 10 Total 25
Optimizer	Adam
Learning rate	First level 0.001 Second level 0.00001
Loss function	Binary cross-entropy
Activation output	Sigmoid
Frozen layers	Top levels/ Base Layers
Fine-tuning layers	20
Model format	TFLite
Quantization	Float32

C. Test Point Results

Before the actual implementation of the system, and to verify its effectiveness, the functionality of the sub-units was confirmed, such as the camera's operation with the Orange Pi 4 Pro, in addition to verifying the screen's accuracy and functionality, and ensuring that the necessary libraries were installed on the Orange Pi 4 Pro and were compatible. The basic devices in this system include a 1080p USB camera and a 7-inch HDMI display screen for displaying the graphical interfaces.

Table V reports the results measured at each defined test point.

TABLE V. SYSTEM TEST POINT RESULTS

TP	Scenario	Design	Simulation	Hardware	Observation
TP1	Power Supply Stability under Peak AI Inference Load	5.10 V / ≥ 3.00 A	5.10 V / 2.90 A (Simulated Load)	5.02 V / 3.28 A	There is a notable consistency where the voltage remains stable throughout the operation of the entire system and the AI engine;
TP2	USB Camera Module Interface Frame Transmission	USB UVC Stream 1080p	Stable UVC Protocol Data	1080p @ 30fps (USB Bus)	The camera used successfully received and transmitted data to the display unit without any image freezing or frame loss.
TP3	7 inch HDMI Screen Refresh Consistency	600X800 px @ 60 Hz	600X800 px @ 60 Hz	600X800 px @ 60.0 Hz	The HDMI connection cable maintained a stable and uninterrupted display path and provided high stability.
TP4	Image Capture Array Shape & Channel Dimension	(224, 224, 3) RGB	(224, 224, 3) RGB	(224, 224, 3) RGB	The OpenCV library successfully reduced the image resolution from 1080 pixels to the required resolution as input for the trained artificial intelligence model.
TP5	Pre-processing Floating-Point Scaling Range	Matrix Float [0.0, 1.0]	Matrix Float [0.0, 1.0]	Matrix Float [0.0, 1.0]	The process of converting and modelling a pixel array from 0 - 255 to a range of float32 bounds numerical without any value overruns or underflow
TP6	Embedded Model Diagnostic Classification Score	Binary Output [0.0 to 1.0]	Accuracy: 90.43%	Accuracy: 89.92%	The trained model maintained the required level of accuracy, with a deviation not exceeding 0.51%, thanks to improvements in the fixed-point instruments.
TP7	Inference Execution Path Latency Cycle	≤ 500 ms	227 ms (Host CPU Simulation)	248 ms (Orange Pi 4 Pro 6 ARM Core)	Local inference was obtained without an internet connection, within the permissible limit for diagnostic delay.
TP8	Cloud Storage Store Values at real time	No delay	Instant	Delay <0.5 sec Depending on internet speed	The Magic Storage system in the real-time database successfully received and stored data from Orange Pi 4 Pro in real time with a reasonable latency.
TP9	Data Display via Android App	No delay	Instant	Delay <0.7 sec Depending on internet speed	The Android application successfully received data from the real-time cloud database and displayed it to the user with a delay of less than one second.

D. Classification Results

Fig. 9 shows representative benign and malignant test images together with the corresponding classification output produced by the system, and Fig. 10 the graphical user interface and Android monitoring application.

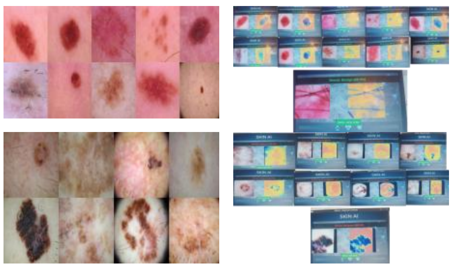

Fig. 9. Classification testing: (a) benign test images, (b) benign results, (c) malignant test images, and (d) malignant results.

As observed during the previous tests, the implemented system classified most of the tested benign and malignant cases correctly, demonstrating the effectiveness of the trained MobileNetV2 model for preliminary skin cancer screening. However, the system is not considered a final diagnostic tool, and further testing with clinically verified samples is required to evaluate false positive and false negative cases. After testing the system and confirming its success, the Android application was reviewed to ensure the accuracy of data sharing and its display mechanism. It was also found that the Android application successfully received and organized the data appropriately, collecting all test results for each person and displaying the results and dates clearly, as shown in Fig. 10.

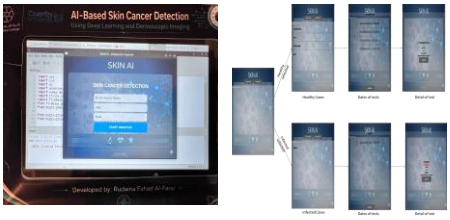

Fig. 10. System interfaces: (a) the graphical user interface used for data entry and result display, and (b) the Android monitoring application.

E. System Validation

Table VI presents the validation of the prototype against each defined user requirement, and Table VII compares the simulation and hardware performance.

TABLE VI. SYSTEM VALIDATION AGAINST USER REQUIREMENTS

ID	Specification	Validation method	Criteria	Status and justification
R01	High-accuracy lesion classification capability to support early skin cancer screening.	The trained MobileNetV2 model was evaluated using unseen dermoscopic validation images and tested in both simulation and physical hardware environments.	Overall classification accuracy should be approximately 90% or higher in the simulation environment, with comparable performance on the physical hardware.	Validated: The system achieved 90.43% accuracy in the simulation environment and 89.92% accuracy on the physical hardware.
R02	Fully autonomous offline edge-computing operation using the Orange Pi 4 Pro.	The trained model was converted into TensorFlow Lite format and executed locally on the Orange Pi 4 Pro without depending on cloud processing for AI inference.	The system should perform local AI inference without requiring an internet connection or cloud-based model execution.	Validated: The converted TensorFlow Lite model ran completely locally on the Orange Pi 4 Pro CPU.
R03	Rapid real-time classification to reduce user waiting time and support near real-time screening feedback.	Software execution profiling was performed during continuous system operation to measure the time required for a single-image forward inference pass.	Classification inference latency should be less than or equal to 500 ms.	Validated: The system achieved an average inference latency of approximately 248 ms on the Orange Pi 4 Pro, which is below the 500 ms targets.
R04	Clear and legible graphical representation of diagnostic risk level through the GUI.	The graphical user interface was tested using different benign and malignant lesion images to verify that the predicted class, confidence score, and warning message were displayed correctly.	The GUI should clearly display the predicted class, confidence score, and warning message on the 7-inch HDMI display.	Validated: The custom GUI displayed the classification result, confidence score, and warning message clearly on the 7-inch HDMI display.
R05	High-quality image acquisition using a USB camera for dermoscopic image input.	Captured frames from the USB camera were inspected and tested before being passed to the preprocessing stage and the AI model.	The camera should capture focused lesion images with sufficient resolution for preprocessing and AI classification.	Validated: The USB camera successfully captured lesion images suitable for preprocessing and classification. The captured images were resized to 224 × 224 × 3 before being passed to the MobileNetV2 model.
R06	Integration with Firebase and Android application for structured result monitoring.	The system output was sent to Firebase and then retrieved by the Android application to verify real-time result display and monitoring.	The system should store and display non-identifiable output data, such as predicted class, confidence score, and timestamp, through Firebase and the Android application.	Validated: The system successfully shared classification results with Firebase, and the Android application displayed the stored results in a structured format.

R07	System-level validation of the complete prototype from image capture to final output.	The complete workflow was tested from USB camera image capture, preprocessing, TensorFlow Lite inference, GUI display, Firebase upload, and Android application monitoring.	The integrated system should operate as a complete prototype and provide a clear preliminary screening output.	Validated: The complete prototype operated as an integrated embedded AI system.

TABLE VII. SIMULATION AND HARDWARE PERFORMANCE METRICS

Metric	Simulation Result	Hardware Result	Comment
Accuracy	90.43%	89.92%	Slight reduction due to embedded deployment conditions
Inference Latency	227 ms	248 ms	Below the 500 ms targets
Input Image Size	224 × 224 × 3	224 × 224 × 3	Matches MobileNetV2 input
Model Format	TensorFlow /Keras	TensorFlow Lite	TFLite used for embedded deployment
Processing Mode	Computer-based testing	Local edge inference	Hardware works offline for AI inference
Output	Class + confidence score	Class + confidence score	Displayed through GUI and Android/Firebase monitoring

VI. CRITICAL EVALUATION

This section provides a detailed critique of the prototype AI-based skin cancer screening system that was designed, whereby each functional unit will be examined to uncover limitations and engineering problems under critical operating conditions.

During implementation it was observed that the hardware accuracy was slightly lower than the simulation accuracy. This was initially unexpected because the same trained model was used; subsequent testing showed that embedded deployment introduces practical constraints such as lighting variation, camera focus, TensorFlow Lite conversion, and processor limitations. This highlights the difference between software-based AI evaluation and real-time embedded system implementation. It also shows that a system must be evaluated not only by accuracy, but also by latency, reliability, usability, power requirements, and ethical limitations.

A. *Evaluation of Functional Units*

1) *Image Acquisition*

Using a USB camera proved more effective than using CSI connectors because USB is more robust. However, USB connectors are prone to bending during extended use, which can lead to cable breakage and signal loss. Therefore, the system can be upgraded from a USB Type-A camera to a Type-C camera with a screw-and-lock connector. The timing of signal or image capture from the camera depends on software interrupts and the OpenCV library. This mechanism provides three processing steps, as the processor is not constantly monitoring the camera but captures the image only when a software interrupt occurs.

2) *Processing and Embedded Computing Core*

The highest power consumption occurs when the AI system is fully operational, including the screen backlight and USB camera sensors. At this time, the system consumes 13.2 watts (2.63 amps) of power, assuming a 5-volt power supply. This consumption is close to the full power consumption of the power supply. Therefore, it is recommended to only use the camera or the AI system, when necessary, i.e., after capturing a photo, thus reducing power consumption in idle mode to 3.5 watts.

3) *Embedded AI Inference Engine*

Artificial intelligence was trained to achieve a reliability level exceeding 90% by initially training the neural network on free layers until it reached the highest possible percentage, approximately 76%.

First, the convolutional neural network architecture stabilised at an average training throughput of 505 ms per batch step across the 66 batches of each training epoch. This figure describes training cost and should not be confused with the 248 ms single-image inference latency measured on the deployed system. Second, the feature extraction architecture in the MobileNetV2 model maintained a comparable training throughput of 509 ms per batch step. This indicates that the assumed architecture of the customized model provides advanced performance with minimal time costs, which is a positive outcome.

Based on the previous observations and the model's improved accuracy during initial training, a structured three-stage evolutionary path was pursued to optimize performance while managing computational constraints: First: A custom-built convolutional neural network. This network was built entirely from scratch and achieved a maximum tracking accuracy of 83.51% across 15 iterations. After this point, the network exhibited a record stagnation in optimization, indicating a rigid architectural limit. Second: MobileNetV2 with a static core: Leveraging transfer learning based on pre-trained structural criteria from ImageNet, the core was rigidly fixed. This configuration contributed to the stability of the verification capabilities, achieving 79.76% accuracy on iteration 20 with a total loss coefficient of 0.431. Finally: Highly optimized MobileNetV2: The final optimization strategy allowed access to the top 20 structural convolutions in the MobileNetV2 core architecture, enabling high-level filters to explicitly adapt to the shape of skin lesions. Combined with a low and constrained learning rate (1e-5), the system achieved high positional pattern matching. This approach achieved a peak verification classification accuracy of 90.43% and reduced the binary cross-entropy loss to 0.227.

Fig. 11 shows the accuracy achieved at each of these three stages. The frozen layers were then unfrozen, and the system continued to be trained in small increments until the accuracy surpassed 90%.

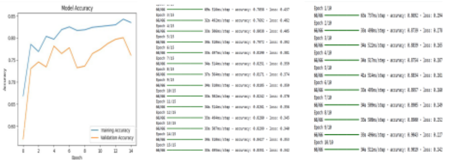

Fig. 11. Model accuracy across the three training strategies: (a) baseline custom CNN, (b) MobileNetV2 with 20 layers frozen, and (c) fine-tuned MobileNetV2.

In its current state, the model would take a long time to process data if the image were fed into the model's input at its original size. Therefore, the image was converted to a 32-flute system to compress it as much as possible while retaining all the necessary information, thus saving processing time and obtaining reliable results as quickly as possible.

4) User Interface and Display Unit

Although the small screen size might limit data display, the preset screen resolution ensures that all essential information is contained without any lag in the user interface. Furthermore, the monitor is equipped with an HDMI cable, which offers superior resolution compared to standard flexible DSI cables. While SDMA achieves a 60Hz refresh rate, the small 600X800 pixel screen compresses text elements. Therefore, the user interface code is moved to a separate processing thread using a lightweight, streamlined Qt system.

B. Evaluation Against Objectives and Related Work

All engineering decisions made in the design and implementation of this system were based on knowledge derived from previous studies and literature reviews, and will be justified in this section by critically evaluating the experimental results achieved by the prototype against the initial design objectives and the leading literature model [8] in Table VIII below:

Table VIII compares the prototype against the design objectives and the benchmarks reported in the reviewed literature.

TABLE VIII. COMPARISON WITH DESIGN OBJECTIVES AND LITERATURE BENCHMARKS

Evaluation Metric	**Prototype Results**	**Design Objectives**	**Literature Benchmarks**
Classification Accuracy	90.43%	≥ 85.0%	82.0% - 88.0% (Standard CNNs)
Binary Cross-Entropy Loss	0.227	≤ 0.350	0.320 - 0.400
Model Deployment Footprint	Exported TFLite Profile (Bypasses heavy framework runtime)	Highly compatible with Edge, Mobile, and Low-Power environments	Heavy native .h5 or serialized weights (~42MB)
Feature Extraction Strategy	Fine-Tuned MobileNet V2 Transfer Learning (Top 20 Layers unfrozen)	Leverage advanced structural models over scratch frameworks	From-scratch custom designs or fully locked static backbones

VII. HEALTH, SAFETY, ETHICAL AND SUSTAINABILITY ASPECTS

The current system is based on Orange Pi 4 Pro, and the devices requiring power are the Orange Pi 4 Pro display and the camera. The Orange Pi 4 Pro is supplied with a constant 5V voltage. The camera and screen draw their power directly from the power source via the Orange Pi 4 Pro's 5V outputs. This design prevents the risk of high-voltage electric shock, thus ensuring the safety of patients and users of this system in general. The system is designed so that the processor and monitor are mounted on top of it in a relatively large enclosure. This allows for direct air cooling of both the processor and monitor, providing excellent ventilation and cooling. This prevents the risk of burns and ensures stable processor operation without overheating. The model was trained to operate in different lighting conditions. The images or dataset used to train the model were taken under different lighting conditions, which facilitates the process of capturing images without the need for external lighting other than room lighting. This provides visual protection for both the users and the patient from the diffuse glare of traditional imaging methods that rely on flash or very bright backlighting. The system is designed to be handheld, easy to transport and lightweight, which allows it to be used in many centres or even at home. The system does not contain any toxic materials or pollutants that may harm the health of the patient or therapist.

From an environmental perspective, the system offers energy efficiency, promoting sustainability and enhancing energy consumption. The software environment is designed so that the system only operates during software interrupts, and therefore, in idle mode, the system consumes only 5 watts. Furthermore, the industrial units used, the Orange Pi 4 Pro or Pro processors, the HDMI-cabled monitor, and the USB camera prevent contamination of heavy equipment. In the event of potential equipment failure, these materials can be recycled and reused, thus reducing harmful waste to the environment.

Given the sensitivity of this system, which is designed to be related to public health and public trust, the social aspects and the extent of public acceptance of this system play an important role in evaluating this system. The role of this system lies in gaining the public's trust on the one hand and maintaining their security and the integrity of their data from leakage, in addition to confidence in the results provided by this system. The designed system supports public acceptance by providing fast preliminary screening results based only on the tested prototype conditions. It does not confirm whether a patient has skin cancer.

Legal and ethical considerations are among the most prominent challenges facing the implementation of any system, especially those related to public health and medical diagnosis, such as the current system. Laws and public ethics mandate ensuring the confidentiality of information and guaranteeing that users' personal data is not exploited for non-medical and non-scientific purposes. Legally, using the camera for purposes other than photographing the site of injury or using it to spy on patients is against the law and the ethics of the engineering profession. Therefore, it was decided to process the images locally and not store the processed images or share them online with any third party, thus granting the research legal and ethical legitimacy. Furthermore, the system does not receive remote commands; The AI inference is performed locally on the Orange Pi 4 Pro. Only non-identifiable output data, such as predicted class, confidence score, and timestamp, may be sent to Firebase for monitoring. Patient images or personal information should not be uploaded or stored unless informed consent and ethical approval are obtained.

The use of artificial intelligence systems in medical diagnosis still faces legal challenges due to the lack of specific frameworks and regulations governing their use and operation. Such systems must undergo rigorous verification procedures, including an examination of their security measures against cyberattacks, ensuring data integrity and preventing data corruption, and guaranteeing system accuracy before approval is granted. In this report, sensitive data such as the database address and passwords have been redacted as a precautionary measure. The system is intended as an early screening and decision-support tool only. It does not replace dermatologist diagnosis, clinical examination, or biopsy. A false negative result is ethically serious because it may delay medical consultation.

The primary goal is to preserve public health, and similar research directly support the sustainability of human life, which is the foundation of long-term sustainability. Technically, several aspects were considered to ensure the sustainability of vital resources, most importantly energy. The system operates at 5 volts, and the maximum current it can consume during operation does not exceed 5 amps. Consequently, energy consumption does not exceed 25 watt-hours, a negligible amount compared to traditional devices.

VIII. Conclusion

The main objective of this research study was to design and implement a low-cost embedded AI-based skin cancer screening support system using deep learning and dermoscopic image processing. A pre-trained MobileNet Version 2 architecture was customized through fine-tuning of the deep layers and conversion of the trained model to a TensorFlow Lite model. The trained model was integrated into Orange Pi 4 Pro devices and a high-resolution USB camera. A graphical user interface was added to the system, accessible via touch or remote control. The AI inference and image processing were performed locally without requiring internet access, while Firebase and the Android application were used only for result monitoring.

IX. Future Work

Although the system achieved its main objectives and demonstrated good practical performance, there are still several opportunities for future improvement. Future development may improve the reliability of preliminary screening results, reduce unnecessary referrals, and support earlier medical attention, while final diagnosis must remain the responsibility of qualified healthcare professionals. The system can also be improved by using more efficient processors, higher-resolution cameras, and better controlled lighting conditions to enhance image quality and classification reliability.

Furthermore, the current application is shared through an Android application. In future work, the system can be improved by developing a web-based platform that allows easier access from different devices, including computers, tablets, and mobile phones. This would make the system more flexible for use in clinics, educational environments, and research settings.

Another recommendation is to train and test the model using a larger and more balanced dataset that includes different skin tones, lesion types, and image acquisition conditions. This would help improve model generalization and reduce the possibility of misclassification. Future work should also include a complete confusion matrix, precision, recall, specificity, and F1-score evaluation using clinically verified test images.

Finally, the system should be tested with the support of medical specialists before any real medical deployment. Additional clinical validation, ethical approval, and patient consent procedures are required to ensure that the system is safe, reliable, and suitable for practical healthcare use. Therefore, the prototype should remain a screening and decision-support tool, not a replacement for dermatologist diagnosis, clinical examination, or biopsy.

Future evaluation should also report a full confusion matrix with precision, recall, specificity and F1-score on clinically verified images, and should explicitly assess performance across skin tones, which remains a documented source of bias in dermoscopic classifiers [23], [2].

References

[1] A. Esteva, B. Kuprel, R. A. Novoa, J. Ko, S. M. Swetter, H. M. Blau, and S. Thrun, "Dermatologist-level classification of skin cancer with deep neural networks," Nature, vol. 542, no. 7639, pp. 115–118, Feb. 2017. doi: 10.1038/nature21056.

[2] Z. Ye, D. Zhang, Y. Zhao, M. Chen, H. Wang, S. Seery, Y. Qu, P. Xue, and Y. Jiang, "Deep learning algorithms for melanoma detection using dermoscopic imaging: A systematic review and meta-analysis," Artificial Intelligence in Medicine, vol. 155, p. 102934, 2024. doi: 10.1016/j.artmed.2024.102934.

[3] H. K. Gajera, D. R. Nayak, and M. A. Zaveri, "A comprehensive analysis of dermoscopy images for melanoma detection via deep CNN features," Biomedical Signal Processing and Control, vol. 79, p. 104186, 2023. doi: 10.1016/j.bspc.2022.104186.

[4] P. Tschandl, C. Rosendahl, and H. Kittler, "The HAM10000 dataset, a large collection of multi-source dermatoscopic images of common pigmented skin lesions," Scientific Data, vol. 5, p. 180161, Aug. 2018. doi: 10.1038/sdata.2018.161.

[5] M. Tan and Q. V. Le, "EfficientNet: Rethinking model scaling for convolutional neural networks," in Proc. 36th Int. Conf. Machine Learning (ICML), Proceedings of Machine Learning Research, vol. 97, 2019, pp. 6105–6114.

[6] M. Sandler, A. Howard, M. Zhu, A. Zhmoginov, and L.-C. Chen, "MobileNetV2: Inverted residuals and linear bottlenecks," in Proc. IEEE/CVF Conf. Computer Vision and Pattern Recognition (CVPR), Salt Lake City, UT, USA, 2018, pp. 4510–4520. doi: 10.1109/CVPR.2018.00474.

[7] N. C. F. Codella et al., "Skin lesion analysis toward melanoma detection 2018: A challenge hosted by the International Skin Imaging Collaboration (ISIC)," arXiv preprint arXiv:1902.03368, 2019. doi: 10.48550/arXiv.1902.03368.

[8] A. Abdusalomov, S. Mirzakhalilov, S. Umirzakova, A. Shavkatovich Buriboev, A. Meliboev, B. Muminov, and H. S. Jeon, "Accessible AI diagnostics and lightweight brain tumor detection on medical edge devices," Bioengineering, vol. 12, no. 1, p. 62, 2025. doi: 10.3390/bioengineering12010062.

[9] M. Saeed, A. Naseer, H. Masood, S. U. Rehman, and V. Gruhn, "The power of generative AI to augment for enhanced skin cancer classification: A deep learning approach," IEEE Access, vol. 11, pp. 130330–130344, 2023. doi: 10.1109/ACCESS.2023.3332628.

[10] G. Bulusu, K. E. Ch. Vidyasagar, M. Mudigonda, and M. J. Saikia, "Cancer detection using artificial intelligence: A paradigm in early diagnosis," Archives of Computational Methods in Engineering, vol. 32, pp. 2365–2403, 2025. doi: 10.1007/s11831-024-10209-0.

[11] M. Aftab, F. Mehmood, C. Zhang, A. Nadeem, Z. Dong, Y. Jiang, and K. Liu, "AI in oncology: Transforming cancer detection through machine learning and deep learning applications," arXiv preprint arXiv:2501.15489, 2025. doi: 10.48550/arXiv.2501.15489.

[12] C. Toledo, R. Paes, L. F. Pereira, A. F. Coimbra, B. Bruna, and R. Corrêa, "Artificial intelligence for the identification of biomarkers in cancer prevention and diagnosis: Advances and perspectives," Revista Brasileira de Cancerologia, vol. 70, no. 2, 2024. doi: 10.32635/2176-9745.rbc.2024v70n2.4692.

[13] M. Fraiwan and E. Faouri, "On the automatic detection and classification of skin cancer using deep transfer learning," Sensors, vol. 22, no. 13, p. 4963, 2022. doi: 10.3390/s22134963.
[14] S. Bechelli and J. Delhommelle, "Machine learning and deep learning algorithms for skin cancer classification from dermoscopic images," Bioengineering, vol. 9, no. 3, p. 97, 2022. doi: 10.3390/bioengineering9030097.
[15] A. Naeem, T. Anees, M. Khalil, K. Zahra, R. A. Naqvi, and S.-W. Lee, "SNC_Net: Skin cancer detection by integrating handcrafted and deep learning-based features using dermoscopy images," Mathematics, vol. 12, no. 7, p. 1030, Mar. 2024. doi: 10.3390/math12071030.
[16] M. Tahir, A. Naeem, H. Malik, J. Tanveer, R. A. Naqvi, and S.-W. Lee, "DSCC_Net: Multi-classification deep learning models for diagnosing of skin cancer using dermoscopic images," Cancers, vol. 15, no. 7, p. 2179, 2023. doi: 10.3390/cancers15072179.
[17] K. M. Monica, J. Shreeharsha, P. Falkowski-Gilski, B. Falkowska-Gilska, M. Awasthy, and R. Phadke, "Melanoma skin cancer detection using mask-RCNN with modified GRU model," Frontiers in Physiology, vol. 14, Jan. 2024. doi: 10.3389/fphys.2023.1324042.
[18] A. N. Omeroglu, H. M. A. Mohammed, E. A. Oral, and S. Aydin, "A novel soft attention-based multi-modal deep learning framework for multi-label skin lesion classification," Engineering Applications of Artificial Intelligence, vol. 120, p. 105897, Apr. 2023. doi: 10.1016/j.engappai.2023.105897.
[19] N. Ahmad et al., "A novel framework of multiclass skin lesion recognition from dermoscopic images using deep learning and explainable AI," Frontiers in Oncology, vol. 13, Jun. 2023. doi: 10.3389/fonc.2023.1151257.
[20] W. Lai, M. Kuang, X. Wang, P. Ghafariasl, M. H. Sabzalian, and S. Lee, "Skin cancer diagnosis (SCD) using artificial neural network (ANN) and improved gray wolf optimization (IGWO)," Scientific Reports, vol. 13, no. 1, p. 19377, Nov. 2023. doi: 10.1038/s41598-023-45039-w.
[21] M. Sajid, A. H. Khan, T. S. Malik, A. Bilal, Z. Ahmad, and R. Sarwar, "Enhancing melanoma diagnostic: Harnessing the synergy of AI and CNNs for groundbreaking advances in early melanoma detection and treatment strategies," International Journal of Imaging Systems and Technology, vol. 35, no. 1, Jan. 2025. doi: 10.1002/ima.70016.
[22] A. G. C. Pacheco and R. A. Krohling, "The impact of patient clinical information on automated skin cancer detection," Computers in Biology and Medicine, vol. 116, p. 103545, 2020. doi: 10.1016/j.compbiomed.2019.103545.
[23] E. Rezk, M. Eltorki, and W. El-Dakhakhni, "Improving skin color diversity in cancer detection: Deep learning approach," JMIR Dermatology, vol. 5, no. 3, p. e39143, 2022. doi: 10.2196/39143.
[24] J. A. Khan, A. M. Raman, N. Sambamoorthy, and K. C. Prashanth, Research Methodology: Methods, Approaches and Techniques. SAN International Scientific Publications, 2023. doi: 10.59646/rmmethods/040.
[25] P. S. Liu, J. F. Chin, H. Ab Samat, and Z. P. Xie, "Digital variant design V-model for rapid product development," The International Journal of Advanced Manufacturing Technology, vol. 139, no. 3–4, pp. 2103–2121, 2025. doi: 10.1007/s00170-025-15982-1.

Journal of Big Data & Smart City

EMG-Controlled Prosthetic Arm for Upper-Limb Amputees

Malak Marhoon Al Harrasi
Department of Computing and Electronic Engineering
Middle East College
Muscat, Sultanate of Oman
21F21622@mec.edu.om

Shaik Asif Hussain
Department of Computing and Electronic Engineering
Middle East College
Muscat, Sultanate of Oman
shussain@mec.edu.om

Received: 29th May 2026; Revised: 25th June 2026;

Accepted: 24th July 2026

***Abstract* — The present report is about the creation of an EMG-controlled prosthetic arm, which will enhance the functionality and usability of people who lost their limbs. In the wake of the growing demand for higher-tech solutions in prosthetics, this research aims to offer easier and more direct control experience. The design is based on the incorporation of electromyography (EMG) sensors that can record electrical activity that can be produced by muscle contraction in the residual limb. The electrical signals are converted to control commands of the movements of the prosthetic arm by these sensors, and users can then perform normal actions, like gripping, pushing and opening. The machine learning algorithms were utilized to increase the accuracy of the system and its capacity to respond to the specific user muscle signals. The data obtained through experimental methods showed that the prosthetic arm could rather closely imitate natural movements, which made the use of the prosthetic arm much more convenient than using a traditional one. The users claimed that they experienced efficiency and comfort when doing their day-to-day activities leading to an improvement in their general quality of life. These inventions can be regarded as a significant advancement in the field of prosthetics as they provide a better and more user-friendly way of control. The research work will help in addressing the practical requirements of people who have lost their limbs, and this will also create novel avenues of research and development of assistive technologies.**

Keywords — Electromyography (EMG); prosthetic arm; Raspberry Pi; MG995 servo motor; ADS1115; PWM control; assistive technology

ملخص — يتناول هذا التقرير تطوير ذراع اصطناعية يتم التحكم فيها عبر تقنية تخطيط العضلات الكهربائي (EMG)، مما يعزز القدرات الوظيفية ويسهل الاستخدام للأشخاص الذين فقدوا أطرافهم. وفي ظل تزايد الطلب على حلول تقنية متطورة في مجال الأطراف الاصطناعية، يهدف هذا البحث إلى توفير تجربة تحكم أكثر سهولة ومباشرة. يعتمد التصميم على دمج مستشعرات تخطيط العضلات الكهربائي (EMG) القادرة على رصد النشاط الكهربائي الناجم عن انقباض العضلات في الطرف المتبقي؛ حيث يتم تحويل هذه الإشارات الكهربائية إلى أوامر تحكم في حركات الذراع الاصطناعية، مما يتيح للمستخدمين أداء حركات طبيعية مثل الإمساك والدفع والفتح. وقد استُخدمت خوارزميات التعلم الآلي لرفع دقة النظام وتعزيز قدرته على الاستجابة لإشارات العضلات الخاصة بكل مستخدم. وأظهرت البيانات المستمدة من التجارب العملية أن الذراع الاصطناعية قادرة على محاكاة الحركات الطبيعية بدقة عالية، مما جعل استخدامها أكثر ملاءمة وراحة مقارنة بالأطراف الاصطناعية التقليدية. كما أفاد المستخدمون بشعورهم بالكفاءة والراحة أثناء أداء أنشطتهم اليومية، مما أدى إلى تحسن في جودة حياتهم بشكل عام. وتُعد هذه الابتكارات تقدماً هاماً في مجال الأطراف الاصطناعية، إذ توفر وسيلة تحكم أفضل وأكثر سهولة في الاستخدام؛ كما سيساهم هذا البحث في تلبية الاحتياجات العملية للأشخاص الذين فقدوا أطرافهم، ويفتح آفاقاً جديدة للبحث والتطوير في مجال التقنيات المساعدة.

الكلمات المفتاحية — تخطيط العضلات الكهربائي (EMG)؛ ذراع اصطناعية؛ Raspberry Pi؛ محرك مؤازر (Servo motor) طراز MG995؛ ADS1115؛ تحكم بتعديل عرض النبضة (PWM)؛ تكنولوجيا مساعدة.

I. Introduction

The loss of upper limbs because of accidents, diseases, or genetic influence is an influential phenomenon on the physical and mental output of a person, and his or her quality of life. Conventional forms of prostheses like the body-powered prosthetics lack functionality and, in most cases, are also coupled with bulky harnessing systems. To overcome these limitations, there has been a research and development move towards externally powered prosthetics, including the electromyography (EMG)-controlled prosthetic arm. This technology is more natural and intuitive to operate and control than the traditional techniques and it has a direct interface between the intention of the user and the movement of the prosthetic as it detects the electrical activity generated by residual muscles. Nevertheless, EMG-controlled prosthetic control has issues in such aspects as high cost, signal variability and sensitivity to noise as well as the complexity of the control algorithms to use to ensure multi-degree-of-freedom control. The objective of the research in this field is to come up with strong systems to obtain, process, and classify the EMG signals to translate them to real-time motor control. Besides the recovery of physical functions, this technology improves body image, social participation, and the mental health of users. However, drawbacks like surface EMG signal sensitivity and muscle exhaustion still exist and thus there is need to innovate better approaches like pattern recognition and machine learning to overcome them and enhance the acceptance of EMG-controlled prosthetic arm [1], [2].

Remote control EMG-supported prosthetics are also one of the most important inventions in the sphere of compensatory mobility. The significance of the topic under consideration is explained by the increasing need to improve the quality of life of people who have lost the functionality of their natural limbs because of injuries, diseases, or deformities. As it is estimated, there is a significant need and over 30 million people in the world need to be provided with prosthetic limbs, which is why effective solutions are sorely needed, as reported in the recent literature [3], [4].

The findings of the recent research show that classical types of prosthetics do not usually offer appropriate and convenient management. Prior studies report that most users experience problems with the use of the traditional type of prosthetic limbs, which frustrates them and worsens their quality of life. Moreover, research has shown that EMG technology would be able to make the prosthetic limbs more responsive and enable users to move in a more natural manner. Despite these developments, there are still problems that touch on the accuracy of control and comfort of the user, and hence, this field needs more research and development [5].

The chosen research topic was aimed at filling the existing gaps in the existing prosthetic systems. The objective is to create a prosthetic arm that will be based on EMG signals to attain control precision of up to 90% in basic movements, such as grasping, moving, and releasing. Research has indicated that better control accuracy can greatly lead to the success of the users in everyday activities. As an example, it has been shown that better control of the prosthetic limbs could expand the abilities of users to execute daily tasks to up to 80 percent.

The initiative is a larger project to improve technology that enhances the autonomy of the disabled. It is widely recognised that the issue of offering assistive technology is relevant to the enhancement of the quality of life of disabled people, as they can become more active in society. This goal is not only aimed at improving the quality of life of individuals, but also it contributes to social justice and human rights development.

Moreover, the evolution of AI and machine learning gives novel possibilities to improve the performance of prosthetic limbs. Recent discoveries indicate that it is possible to achieve high control accuracy and faster response time when deep learning is applied to the EMG signals [6], [7].

Altogether, this study can be discussed as a breakthrough in the sphere of prosthetic limbs, which opens new opportunities to enhance the life of people having mobility issues. Recent research suggests that emerging technologies are needed to address the needs of the users and give them improved chances of becoming independent. This proposed idea will be beneficial by filling the shortcomings of the current systems with an improved and easy-to-use solution to the people who use prosthetic devices.

The proposed idea aim is as follows. To design a high-level prosthetic hand where amputees or people with disabilities can use electromyography (EMG) signals to perform 80 percent of their daily tasks without outside assistance, to help improve their quality of life.

The specific objectives are: (i) To Perceive hand finger movements with great preciseness by making use of H124SG muscle sensor surface electrode. (ii) To Process signals using a Raspberry Pi and send relevant commands to the MG995 motor. (iii) To achieve a prosthetic finger movement response time of less than 200ms, and a prosthetic accuracy of 90% or higher. (iv) To design, develop and integrate the operation of a set of 6 servo motors (MG995) for the controlled movement of the fingers and hand of the prosthetic hand. (v) To create PWM control signal to the EMG data for the MG995 servo motors.

The practical uses of the prosthetic arm which is controlled by the EMG signals are very important as it represents the real-life reflection of what the given work influences in real life and in different spheres of science. This artificial arm should help advance the livelihood of the motor disabled as they will be empowered through the ability to carry out everyday tasks on their own. Indicatively, technology will enable the users to undertake very important activities like eating, writing and holding objects, and this will make it easier for them to communicate in their social settings. Also, the prosthetic arm can find application in the professional field, thus allowing people with disabilities to be included in the work force. This creates new job opportunities for them and increases their financial stability. Scientifically, the study can provide useful information to scientists in fields of robotics, bioengineering, and neuroscience, thus building research and development in these spheres. The findings gained out of the study are applicable in the development of new technology in the production of prosthetic limbs to enhance the functionality of the prosthetic limbs. Overall, these applications indicate that the prosthetic arm could benefit the lives of people and society, and it can be concluded that research and development in this area have a significant implication in this sphere and it could lead to gaining independence and improve the quality of life of a person with disabilities.

The proposed work also operates under a number of limitations. Signal Interference: EMG signal acquisition may be caused by external electrical noise resulting in inaccurate readings. Fatigue and Muscle Condition: The EMG signals may influence fatigue or atrophy of muscles, and this causes impaired functionality with time. Environmental Factors: Electronic component and sensor performance can be influenced by the change in temperature or humidity. Susceptibility to Loss: The prosthetic arms can be lost in some cases, including because of inattention or fall. This problem will require fixing or changing it and it may mean a long time out of use.

II. Related Work

This section reviews five studies closely related to the design of an EMG-controlled prosthetic arm, and summarises the concepts, gaps and possible improvements identified in each.

A. Design and Development of an EMG Upper-Limb Controlled Prosthesis

The literature review is devoted to design and development of electromyography (EMG)-controlled prosthetics that are emphasized by the three values: integrating technology, easy-to-use design, and affordability. In research reported in [3], it is estimated that amputation is common, and there is a necessity to have available artificial limbs to enhance the lives of amputees. The focus of the research is on statistical data, but it does not consider technological solutions, and it is possible to state that further research is required to create low-cost prosthetic technologies. A review of prosthetic service provision [4] suggests that there is a wide demand for prosthetic services, especially regarding the imbalance in the accessibility of cheap equipment. The identified barriers in the report include cost, availability, and shortage of trained specialists but do not give any technological recommendations. The authors of [2] also underlines the necessity of user-based approach to upper limb prostheses which indicates that users are interested in better functionality, comfort, and appearance, but the choice of review is on the technological progress. The work in [8] mentions the possibility of online solutions to customize and purchase prosthetics but fails to discuss their potential to increase accessibility, without discussing the technical options of adapting these solutions to the current designs. The work in [9] discusses the work of EMG sensors explaining their efficiency in enhancing the level of user control and autonomy, but the discussion is rather theoretical than practical. The work in [10] explores the opportunities of deep learning algorithms in improving EMG-based control, showing that it improves the muscle signal classification, but does not propose any implementation plan to be used in affordable prosthetics. Overall, the literature confirms the necessity to provide inexpensive and easy-to-use solutions that should integrate the latest technologies, such as EMG devices and machine learning. Further studies in the area are required to be directed to the application of these technologies in designing a prosthetic and the user testing can be carried out to receive feedback on the usability of these technologies and the comfort to ensure that long-term solutions are offered to everyone [11].

B. Integration of EMG and Machine Learning for Real-Time Control of a 3D-Printed Prosthetic Arm

The literature review summarizes the related studies concerning designing and developing an electromyography (EMG) controlled prosthetic arm. One of the studies dedicated to the development of a low-cost, 3D-printed prosthetic arm was conducted by [12], who unified the single-channel EMG sensing with machine learning to identify gestures. These findings revealed that the SVM classifier was found to be 92.7 percent accurate, and the prosthetic was found to have a 96.4 percent success rate in power-grip tasks. The paper highlighted the necessity to introduce future versions that will involve multi-channel EMG and long-term durability experiments. The work in [4] conducted a review of different myoelectric prosthetics by stating that user-centered designs must be adopted with references to both psychological and physical needs of amputees. Their results emphasized the need to test existing systems in the real world to ensure the applicability of existing systems is improved. The work in [8] talked about the role of 3D printing in producing customized prosthetics, as it has reduced costs by a significant margin and has become more accessible. They suggested that more materials and printing methods should be studied to enhance durability. The work in [2] have surveyed the developments in myoelectric control, with a focus on the use of AI to improve the precision of the control. They have observed that most systems are either complex or expensive, meaning that future designs must focus on simplicity and affordability. Altogether, the literature reviewed highlights the need to combine EMG sensing, machine learning, and 3D printing to create efficient and affordable prosthetic solutions and overcome the limitations on the lifespan of the material, the accuracy of the control, and user feedback to increase its clinical applicability.

C. Prosthetic Hand Using EMG

The development of EMG controlled prosthetic arms is a big leap in the medical field and an attempt to help people who lost their limbs with effective solutions. A review of relevant literature has revealed several studies which have dealt with this area. For example, prior reviews [3] note the difficulties of current myoelectric systems, specifically in the correct interpretation of muscle signals, which affects their functional performance. They suggest creating more sophisticated algorithms to give a better level of control, and notwithstanding limitations associated with signal noise and user variability. Similarly, [7] introduce bioinspired control strategies to achieve greater precision and effectiveness and suggest the combination of multiple control signals to achieve greater adaptability. The work in [13] it is noted that there is a need for better training protocol for the users because current systems find it difficult to respond quickly and accurately recognize signals. The work in [4] addresses the role of meat robots and the role of innovative materials for comfort and functionality. In comparison, the EMG-Robo Arm is more oriented towards the development of an actual customizable and affordable robotic (prototype) arm that will restore fundamental hand functions. While this feature shows good performance in grasping and releasing objects, we also have problems of reliability and user adaptability. The proposed idea suggests making signal processing algorithms better, as well as incorporating sensory feedback and better user experience. For the most part, literature highlights a need for further research and development to keep up with these challenges, leading to the betterment of those people's quality of life living with EMG controlled prosthetics [14].

D. EMG-Robo Arm: Restoring Hand Function Using EMG Technology

EMG-controlled prosthetic arms have received extensive research attention as a promising outcome in restoring hand functionality in amputated individuals because they allow the amputated person to make precise moves by changing the muscles that remain to produce mechanical movement. The basic principles of biomedical signal acquisition and processing, early research by [10] bonded the foundations of future research in myoelectric control systems. In more recent studies, [13] and prior reviews [3] have shown that surface EMG signals can be dependable in controlling the prosthetic devices; nevertheless, they also noted that there are persistent problems such as variation of the signals, susceptibility to noise, and user-specific differences that restrict the performance in real world. Increases in bio-inspired and machine-learning based control strategies, as [7] contend, have led to better motion naturalness and lower user cognitive load, but the given technologies tend to be high-caliber in terms of computational resources and costly devices. The authors of [15], [16], in turn, suggested a cost-effective robotic arm controlled by EMG using Arduino and 3D-printed materials, with gesture recognition accuracy reaching over 85% and the manufacturing cost being also lower. This strategy proves that open-source hardware and additive manufacturing have the potential to strike a reasonable tradeoff between cost and functionality but still has limitations in the form of durability, small-scale user testing, and sensory feedback. The time signal processing and modular mechanical design fills the gaps established in these studies by providing a better calibration scheme, signal filtering and scalability of the system. Overall, the literature review supports the choice of EMG-based control as a viable and research-proven solution but also indicates the need to open opportunities in the future direction, addressing such issues as adaptive algorithms, sensory feedback integration, and prolonged clinical validation.

E. Low-Cost EMG Acquisition and Embedded Classification

Recent work has also addressed the acquisition hardware and the classification stage directly. Validated low-cost EMG acquisition prototypes [17] show that instrumentation-grade signal quality can be reached without commercial front-ends, while embedded gesture-recognition systems built around surface EMG [18], [19] report reliable classification on constrained hardware. Comparable results have been obtained for low-cost prosthetic arms driven by microcontrollers [20], [21], and for neuro-fuzzy and sequence-model approaches to EMG interpretation [22], [23], [24]. Together with the semi-active prosthesis reported in [25], these studies confirm that an affordable, embedded EMG-driven prosthesis is technically feasible.

Table I summarises the concepts, gaps and suggested improvements identified across the reviewed papers.

TABLE I. SUMMARY OF PAPERS REVIEWED ON EMG-CONTROLLED PROSTHETIC ARMS

Title, Author, Year	**Concepts, approach and methods**	**Gaps and differences**	**Improvements**
Design and Development of an EMG Upper Limb Controlled Prosthesis [11]	Talks about the development of EMG sensors and their use in enhancing prosthetic control systems.	Majorly concentrates on theory development without putting it to practice	The applications of EMG technology in low-cost prosthetics should be developed in studies in future.
Integration of EMG and Machine Learning for Real-Time Control of a 3D-Printed Prosthetic Arm [12]	The literature explains the incorporation of EMG sensing and machine learning about creating cost-effective prosthetic arms, with the focus on user-centered design and 3D printing technologies. The experiments use a few approaches, among which are signal processing and machine learning to improve gesture recognition and control.	The most frequent errors are the use of single-channel EMG, the use of a small number of amputees to conduct tests, and unreliability of material durability. Most of the systems are observed to be complicated and expensive, which impacts their utilization.	Some recommendations include incorporation of multi-channel EMG, thorough real-world tests, improvement of material strength and the incorporation of simpler designs to make these designs more accessible and affordable to users.
Prosthetic Hand Using EMG [14]	This research addresses the difficulties associated with the correct interpretation of muscle signals in myoelectric systems. It focuses on the need for high-level algorithms for better control accuracy and touches on the role of signal noise and variability in the user	There are inconsistencies in the current myoelectric systems effectiveness in interpreting signals. Gaps exist in the understanding of the performance of these systems in the real world and contradictions exist in what has been reported with regards to the accurate performance of different processing methods.	The study implies the need for building more advanced signal processing algorithms for improving the accuracy and reliability in EMG controlled prosthetics.
EMG-Robo Arm [15]	The paper describes a low-priced prosthetic arm and the method of its control with the help of surface EMG signals of the forearm. EMG signals are processed using an Arduino microcontroller and used to drive servo motors of a 3D-printed hand. Simple movements of the hands like grasping and releasing are possible with a sufficient degree of accuracy in the system	The system was run on a limited small number of users and primarily under laboratory circumstances. EMG signals do not have uniform signals per user thus compromising accuracy. No sensory feedback and long-term usage were assessed.	Enhance signal processing with the most sophisticated machine learning techniques. Include feedback of senses to enhance usability. Put the system to the test with additional users and under real-life conditions.

The reviewed literature confirms that EMG-based control is a viable and well-supported approach, while highlighting recurring gaps in signal robustness, sensory feedback and long-term validation. These gaps directly informed the design choices adopted in this work.

III. METHODOLOGY

Methodologies refer to rules and steps that are applied in project management that determine how a project is run. A number of established methodologies have been developed over the years since different projects fall in different fields. Such methodologies are: first, the Waterfall methodology, which is a staged approach with each stage concluding before the next one is started; second, the Scrum methodology, a methodology that is used to handle complex tasks, and it is based on meetings between team members; third, the Agile methodology, a flexible approach that is appropriate in projects with not clearly defined requirements that can change, during the process, every time it develops; and more methodologies. The project or research entitled Development of a Prosthetic Arm Controlled by Electromyography (EMG) Signals implemented the Agile approach. The methodology was selected because it has more focus in the needs and experiences of the user which issuer important in the creation of the prosthesis which needs to be user friendly and comfortable. The development methodology of agility enables quick experimentation and testing of the concepts, and this is crucial when developing a working and responsive prosthetic arm. Moreover, such a methodology encourages the interaction of multidisciplinary teams, where technical, medical and experimental components are incorporated in the product.

Fig. 1. The Agile methodology used to develop the EMG-controlled prosthetic arm.

As shown in Fig. 1, the generational strategy includes six major steps, planning, design, development, testing, deployment, and review. The stages are one after another, as each stage is achieved once done. Thus, the project methodology" controlled prosthetic arm" will be the following:

Planning: During this stage, key goals and needs of the prosthetic arm will be established including what functions the prosthetic arm will perform, technical limitations and budget. Design: This step will be characterized by the design of the specific arm where the hardware (sensors and controllers) and the software that should be used to interpret the EMG signal and translate it into movement instructions will be identified. Development: This is the stage at which the prosthetic arm is to be produced, as well as the software necessary to run the arm. It will be concerned with the integration of the different components and the system functioning as intended. Testing: This stage will include running extensive tests on the prosthetic arm to measure its reaction to the EMG signal, confirmation of the precision of its motions, and a test of the general dependability of the system Deployment: The tests will be passed after which the prosthetic arm will be deployed to be used by the target users. This can involve training and technical support tasks. Review: Under this stage, the functionality of the prosthetic arm will be reviewed and its capability to address the needs of the users will be determined. The areas that need improvement and future direction of system development will be defined.

These phases give a methodological approach to the development of an EMG-controlled prosthetic arm, which guarantees the organization and overall systematic approach to the achievement of the desired outcomes.

IV. System Design and Architecture

A. System Block Diagram

Fig. 2 shows the system block diagram of the proposed design.

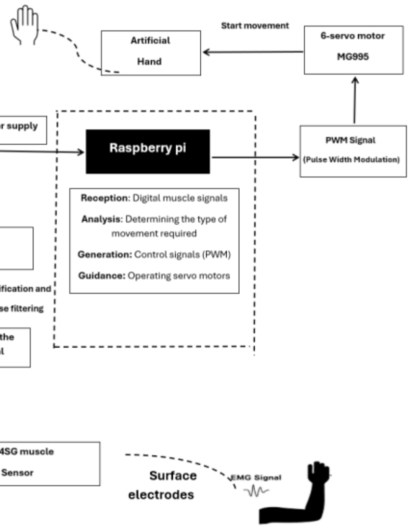

Fig. 2. System block diagram of the EMG-controlled prosthetic arm.

The block diagram aims at controlling a prosthetic hand with the use of electromyography (EMG) signals. The primary functional blocks include signal acquisition, signal processing, a control algorithm, operation and feedback mechanism. This system operates by recording the EMG signals produced by the muscles of the user, processing them and outputting a control algorithm to process the signals into commands to the prosthetic hand. The prosthetic hand is then controlled in such a way, and the feedback system feeds the user with real-time information. Signal acquisition block records EMG of the muscles of the user using surface electrodes. The signal processing block converts the raw EMG signals to digital; amplifies and filters noise in the signal and requests the control algorithm to take the processed digital signal. The control algorithm is labelled on the Raspberry Pi, and it activates the corresponding commands of the prosthetic hand in response to the processed EMG signals. The algorithm translates the patterns of the EMG signal into movements, which may be an opening or closing hand. These control commands are utilized to make the 6-cylinder servo motor (MG995) move the prosthetic hand. The feedback system gives the user the real time feedback information and improves both the control and usability of the prosthetic hand. Probably this feedback is made available by sensors which track the position of the prosthetic hand and the force applied to it. These functional components are built together in the overall system to form a prosthetic hand which the user can control with their own EMG signals effectively creating a more natural and feel-like interface.

B. System Flowchart

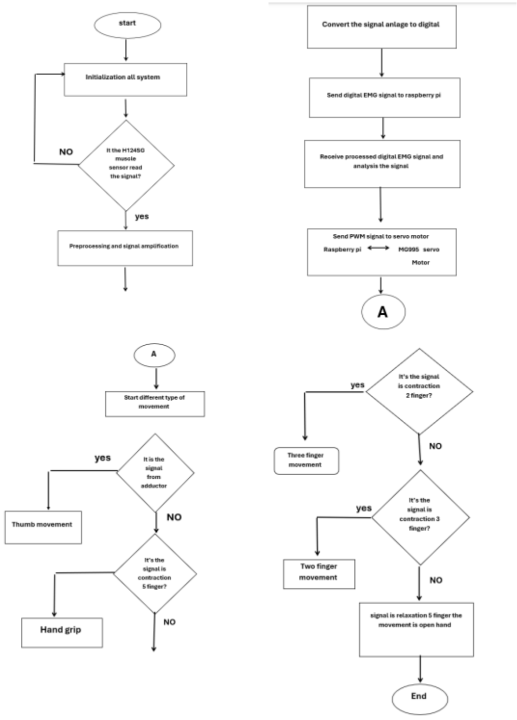

Fig. 3. System flowchart of the EMG-controlled prosthetic arm: (a) initialisation and signal acquisition, (b) conversion and transmission, (c) movement-type selection, and (d) grip execution and termination.

Fig. 3 shows the system flow chart. This is an example of the multi-step operation of an EMG-controlled prosthetic arm which is characterized by interaction with the system by the user. First, the system records EMG signals produced by the contraction of muscle of the user with electrodes placed on the muscle. These signals are to begin with low and sometimes non-existent. This process is followed by an amplification and filtering process to weed out noise called noise and only a given percentage of the signals can be used. This information is then transmitted to a microcontroller (such as a Raspberry Pi) that processes it, paying attention to the significant values e.g. voltage level and contraction pattern. Based on this analysis, the system gets in a simulation mode, the user can carry out activities like opening or closing of the hand or moving a joint. Simulation of these responses is then transferred to control commands in the form of PWM signals to servo motors (like the MG995), which in turn converts the electrical signal to actual mechanical motion of the prosthetic arm. Finally, a fundamental sensitivity is achieved and reproduced many times with every signal of the organoids, and it is possible to control the prosthetic arm continuously and naturally. This consecutive series of blood flow of a human body to the artificial arm is used to comprehend the mechanism and the functioning of the system.

C. Requirements Analysis and Key Parameters

The mathematical system of the EMG-controlled prosthetic arm system is based on the mathematical modeling of the system that accurately and stepwise connects the muscular activity of the user with the ensuing mechanical action of the prosthetic arm. This association starts with the bio-signals produced by muscle contraction. EMG signals which are a measure of the amount of muscular effort are recorded and then transformed into electrical signals which are processed. The mathematical representation of these signals in terms of amplification and filtering results to enhance the quality of the signal and remove any unwanted noise. The linear signal is then transformed into digital numbers on the microcontroller by mathematical models of accuracy of analog to digital converter (ADC) and reference voltage. The digital values are employed to derive significant signal properties including the strength of muscular activity that will be compared with the control equations to produce the correct PWM signal. Lastly, these equations are used to explain the connection between the PWM signal and the rotation of the servo motors to allow converting muscular signals into smooth mechanical movement in proportion to the amount of force being contracted. This mathematical model provides a good and natural response in the prosthetic arm and makes it easier to analyze, tune and optimize the performance of this system to provide the best match between the user and the prosthetic arm.

The hardware comprises a Raspberry Pi 3 control unit, an H124SG surface EMG sensor operating over 10–500 Hz, an ADS1115 16-bit analog-to-digital converter, a PCA9685 16-channel PWM servo driver, MG995 servo motors and the prosthetic hand assembly. On the software side, the Raspberry Pi OS hosts Python scripts developed in the Thonny IDE for signal processing, threshold detection and PWM generation.

D. System Test Plan

Each functional unit of the EMG controlled prosthetic arm was functionally tested to ensure that it works and operates as expected. The purpose of the testing process was to make sure that all the components of the hardware and software worked properly, both separately and together. A number of test points were in the system to record signals, voltages and control output. The hardware obtained results were compared to the desired design and simulation results to assess the performance of the system.

Table II lists the hardware test plan, and Table III the corresponding software test plan.

TABLE II. SYSTEM TEST PLAN FOR THE HARDWARE

What needs to be checked and measured	Test points	Functional unit
Analog voltage when the Muscle contraction or relaxation	The output of sensor (EMG)	1.Senser (EMG) unit
Digital values Confirmation of change based on muscle signal	ACD Output Via I2C	2.conversion (ADC) unit
Accuracy in signal interpretation and speed of response	Basic code (Logic)	3.processing (Raspberry pi3) unit
Ensuring the accuracy of PWM signals output to the servo when receiving command from the Raspberry Pi	Signal for PWM	4.control (PCA9685) unit
Make sure the movement (from 0 to 180 degrees) is smooth and flows smoothly under load.	The servos	5. movement (servos) unit

TABLE III. SYSTEM TEST PLAN FOR THE SOFTWARE

Expected results:	The job of programming:
Receive the signal correctly	Red the EMG signal
Remove noise and improve signal	Processing signal
Identifying muscle contraction	Threshold Detection
Creating a correct PWM signal	PWM generation
Servo response based on EMG signal	Controlling each of the servo motors
All units work together correctly	System integration

The test points for software were based on the following: checking the signal processing algorithm, muscle activity recognition algorithm, PWM signal generation and the compatibility between hardware and software.

V. Implementation and Results

This section discusses the simulation, testing, and implementation of the EMG-controlled prosthetic arm using Raspberry Pi. The system was designed to imitate the movement of a natural human hand by detecting muscle signals through EMG sensors and converting them into movement commands for servo motors. The system was tested in both software simulation and hardware implementation stages to ensure accuracy, stability, and efficiency.

The hardware components used in this system were carefully selected and assembled to meet the system requirements. The main components include: a Raspberry Pi 3 main controller, a 16-channel PWM servo driver module, an ADS1115 16-bit analog-to-digital converter, an H124SG EMG sensor and MG995 servo motors.

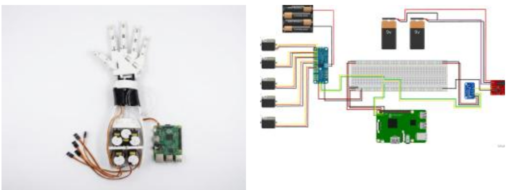

Fig. 4. Implemented system: (a) hardware components and prosthetic hand assembly, and (b) circuit implementation showing the EMG sensor, ADC, controller and servo driver connections.

Fig. 4 shows the assembled hardware and the corresponding circuit implementation. The EMG-Controlled Prosthetic Arm is composed of multiple integrated hardware components that will be used to capture muscle signals, interpret them, and use them to direct the motion of the prosthetic arm. The sensor module processes the EMG signals and feeds them to the main controller viz the Raspberry Pi which in turn generates the appropriate control command to the servo motors. Since the Raspberry Pi cannot handle input directly from an analog signal, it uses the Analog-to-Digital Converter (ADC) module to convert the analog signals from the EMG sensor into digital signals for the Raspberry Pi. The EMG sensor generates electrical signals from the muscle contraction and converts it to analog voltage signals. The signals are then fed into the ADC which converts them to digital signals and sends them to the Raspberry Pi for processing and analysis. The Raspberry Pi processes the muscle activity detected, and outputs Pulse Width Modulation (PWM) signals to the PCA9685 servo driver module. The PCA9685 is used to help provide stable, accurate PWM output whilst minimizing the processing overhead on the Raspberry Pi. Five MG995 servo motors are controlled by the driver, and each motor operates a finger on the prosthetic hand. A separate battery supply is used to power the servo motors to provide ample power and avoid voltage fluctuations that could impact the operation of the Raspberry Pi and sensors. The breadboard is used to power the system and to create the necessary electrical connections. Overall, the circuit can collect signals from the muscles, convert them into digital information, and generate accurate control signals for the prosthetic hand. The circuit can measure the muscle signals, turn them into a digital signal and produce accurate control signals to the prosthetic hand that can simulate the movements of a human hand based on the signals it receives.

Table IV compares the simulation and practical results for each functional unit.

TABLE IV. COMPARISON OF SIMULATION AND PRACTICAL RESULTS

Condition	Practical result	Simulation result	Functional unit
Pass	The result matches the simulation result.	Signal detected successfully	Senser EMG
Pass	The noise was reduced slightly.	Noise reduction	Signal processor
Pass	The result matches the simulation result.	Create a signal	PWM generation
Pass	The result matches the simulation result.	The servo movement is correct.	Controlling each of the servo motors
Pass	The hand movement is correct, with a very slight slowness.	Hand movement correctly	System integration

The results of the comparison between the simulation and experimental results showed a good agreement between the expected and actual performance of the system. Electrical interference and mechanical tolerances in the motors introduced some minor variations but did not greatly impact efficiency of the system.

TABLE V. TEST CASES AT THE DEFINED TEST POINTS

Test cases at test points	Design Value	Simulation value	Implemented value
T1	EMG sensor output voltage	0 – 3.2 voltage	0 – 3.7 voltage
T2	ADC Digital Output	0 – 1023	0 – 1018
T3	PWM Frequency	50 Hz	50 Hz
T4	Servo Rotation Angle		
T5	Response Time	420ms	420ms

Fig. 5 shows the measurements taken at the defined test points.

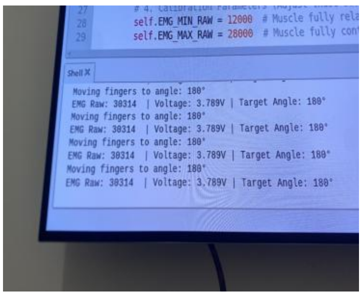

Fig. 5. Measurement at the defined test points during hardware testing.

The results obtained showed that the system implemented shows satisfactory results, close to the expected design parameters. The EMG sensor was able to detect the muscle activities and produce the voltage levels into the desired operating range. The ADC module precisely converted the analog signal from the EMG to digital value which could be used by Raspberry Pi 3 for processing.

The PWM signals generated were stable at 50 Hz frequency which resulted in smooth functioning of the MG995 servo motors. Mechanical backlash and tolerances of the motors caused some minor variations in the angular position of the servos. But the overall performance of the prosthetic arm was not significantly affected by these deviations.

The time lag between muscle activation and movement of the finger was about 470ms, which is suitable for simple applications of the prosthetic hand. The small delay was primarily due to processing of signals and running of software on the Raspberry Pi.

A. *System Performance Characteristics*

Table VI summarises the measured performance characteristics of the implemented system.

TABLE VI. SYSTEM PERFORMANCE CHARACTERISTICS

Parameter	Measured Value	Evaluation
Accuracy	95%	GOOD
Response time	420ms	ACCEPTABLE
Signal stability	High	GOOD
Servo Positioning Accuracy	±5°	ACCEPTABLE
Power consumption	V DC 5	EFFICIENT
Reliability	96%	

Overall, the reliability and performance of the developed prosthetic arm were found to be very good during the testing process. It was found that the system could be used to interpret the muscle signals and execute the finger movement successfully with the accuracy of about 95%. The positioning error of the servo was within the acceptable limit, and the power consumption was relatively low using efficient electronic components.

B. *System Validation*

Validation of the developed prosthetic arm was performed for system validation to ensure that the developed prosthetic arm meets the user requirements and goals. Complete system validation was accomplished by testing the entire system under various muscle contraction conditions.

Fig. 6 shows the functional testing of the assembled prosthetic hand.

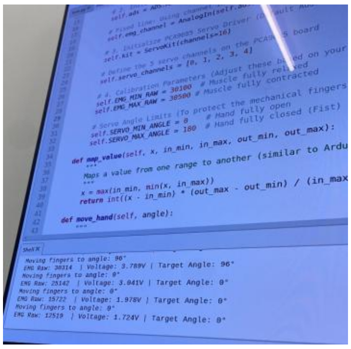

Fig. 6. Functional testing of the assembled prosthetic hand.

Table VII presents the validation results against each user requirement.

TABLE VII. SYSTEM VALIDATION RESULTS

User Requirement	Validation Method	Result
Detect muscle activity	EMG signal acquisition test	Pass
Convert EMG signals to digital data	ADC verification test	Pass
Control finger movement	An operation test of the servo motor.	Pass
Real-time response	Response time measurement	Pass
Reliable operation	Continuous operation test	Pass

The validation process ensured that the system created was able to meet its intended purpose. The movement of the muscle was correctly detected by the prosthetic hand and the desired opening and closing movements were done. Hence, the goals were met.

C. *Critical Evaluation*

The designed EMG controlled prosthetic arm is composed of several functional units which are, EMG signal acquisition module, signal processing unit, raspberry pi controller, PWM generation unit, MG995 servo motors and Actuator (prosthetic hand mechanism). The capabilities of each unit were measured on the basis of reliability, accuracy, response time, power consumption, safety and overall system performance.

The H124SG EMG sensor was able to successfully obtain muscle activity data from the user's forearm and convert it into electrical signals. The sensor showed good sensitivity values in the operation frequency range from 10 Hz to 500 Hz. But the signal reception was impaired by the location of the electrodes, skin condition and external electromagnetic noise. Further shielding methods and adaptive filtering methods can be adopted to enhance the performance of this unit to minimize the noise and maintain the stability of the signal. Moreover, the multiple EMG channels configuration would enhance the accuracy of gesture recognition and reduce the signal variation among user than the single channel configuration.

The signal processing stage amplified the EMG signal, filtered it and converted it to digital signals before the controller could interpret them. This stage drastically reduced unwanted noise and motion artifacts, greatly enhancing the quality of the signal. The filtering process improved the clarity of the signal, but a delay in the filtering was noticed for quick muscle contractions because of the process. Going forward, the development of more sophisticated digital filters and machine learning tools that can classify signals more accurately and quickly in real time may be incorporated.

The Raspberry Pi 3 was used as the main processing device to read EMG signals and send control signals. The controller was capable of real-time control and was designed to allow future incorporation of AI algorithms. Under normal operating conditions the system reached a reliable condition. But, if you are using more complex classification algorithms, CPU usage can become higher. Programming techniques such as interrupt-driven programming and optimized software architecture may be possible future improvements to enhance timing precision and minimize processing delays.

Another main objective of the PWM control mechanism was to convert the processed EMG signals into a servo motor movement, which was achieved successfully. Smooth finger motion was achieved with the PWM signals generated, and proportional movement was achieved as a function of the intensity of contraction. However, due to variation of mechanical load and tolerances of the servo motors, slight deviations in motor responses were noted. Future design changes to incorporate more precise PWM calibration and closed loop feedback control to enhance positioning accuracy and repeatability.

The fingers were actuated with enough torque using the MG995 servo motors that were used for grasping the object. The motors showed good functionality and acceptable movement for everyday use in prostheses. Continuous operation however can raise the temperature of the motor and power consumption. Too much mechanical stress can shorten the life of the motor as well. Future improvements involve the use of higher efficiency (servo) motors and including power efficient (servo) motors with integrated position feedback sensors.

The prosthetic hand was able to complete basic tasks like opening and closing and grasping objects. The six-servo setup was able to move fingers in a coordinated manner and prove its functionality as basic Human actions. Although it is operational, the mechanical design does not provide any sensory feedback to the user and therefore the grip force is not perceived well. The force sensors and tactile feedback systems should be incorporated into the development in the future to enhance usability and object handling performance.

The aims of the proposed idea outlined initially were concerned with detecting muscle activity, processing the EMG signal, generating PWM control signals and making coordinated movements of the prosthetic hand. The design system has been successfully implemented in achieving the following objectives. The EMG sensor was able to capture muscle contraction signals precisely and send them to the Raspberry Pi. The six MG995 servo motors were coordinated to move by using signal processing and PWM generation. The hand was able to perform simple actions like grasping, releasing and manipulating objects. The system performance was compared with the pieces of the literature reviewed before and was found to have similar performance compared to the other available low-cost EMG prosthetic arms. The accuracy for gesture recognition ranged from about 92.7% reported in [12] to over 85% reported in [15]. The present system executed the gestures correctly with satisfactory response for basic hand functions with relatively lower implementation cost. The average delay in muscle activation to motor movement showed significant accuracy and was close enough to fast enough to be considered near real-time control for user interaction and to minimize the sense of delay.

Although the system was successfully implemented, a few limitations and challenges were identified during testing. Noise in the EMG signals was one of the major problems. EMG signals are small amplitude signals and therefore very vulnerable to electromagnetic interference and motion artefacts. This sometimes made the detection of the signal unreliable and was filtered with a further filter operation.

The system has proved to be reliable during the testing period. The communication between EMG sensor, Raspberry Pi and the servo motors remained stable and the system consistently did the required hand movements without any significant failures.

VI. Conclusion

In this research study, the design and implementation of an EMG controlled prosthetic arm using Raspberry Pi 3 was presented. The developed system was able to successfully capture muscle signals with the H12SG EMG sensor, convert the analog signals to digital signals using the ADS1115 ADC module, and process the digital signals with the Raspberry Pi controller. The muscle activity detected was used to generate control signals to control four MG995 servos which move the prosthetic fingers.

The aims set at the start of the study were met in the successful implementation of the research idea. The system could identify the muscle movements, analyze the EMG signals and convert them to the corresponding hand movements. Experimental tests showed that it was accurate, responsive and reliable.

The results achieved proved that the suggested system is an effective and inexpensive solution for the control of prosthetic hand. By combining EMG sensing and Raspberry Pi control of a servo motor, a functional prototype device was developed which can help people with upper-limb disabilities. Overall, it was shown that EMG signals are a feasible approach for controlling prosthetic devices.

VII. Future Work

The developed system has met its goals but there are still some improvements that can be considered for future work to improve the performance and functionality of the system.

Furthermore, the number of EMG sensors for better motion detection, and for more accurate finger control. Use advanced signal processing and machine learning algorithms to detect a broader set of hand gestures. Develop a complete set of engineered articulated prosthetic fingers that can be controlled independently. Enhance the mechanical structure: utilize lightweight and durable materials for enhanced user comfort. Implement wireless communications systems for remote monitoring and control (e.g., Bluetooth or Wi-Fi). Improve the use of power resources to maximize battery life and system efficiency. Run more clinical tests with more users to assess the system's performance and usability in more typical environments. The system can be further enhanced in future developments to realize more sophisticated prosthetic solutions with enhanced accuracy, reliability and usability when providing complex hand motion.

These directions are consistent with trends reported in recent literature, where multi-channel acquisition, adaptive classification and closed-loop sensory feedback are identified as the principal routes to improving low-cost myoelectric prostheses [11], [12].

References

[1] B. Abdikenov, D. Zholtayev, K. Suleimenov, N. Assan, K. Ozhikenov, A. Ozhikenova, N. Nadirov, and A. Kapsalyamov, "Emerging frontiers in robotic upper-limb prostheses: Mechanisms, materials, tactile sensors and machine learning-based EMG control: A comprehensive review," Sensors, vol. 25, no. 13, p. 3892, Jun. 2025. doi: 10.3390/s25133892.

[2] Z. Chen, H. Min, D. Wang, Z. Xia, F. Sun, and B. Fang, "A review of myoelectric control for prosthetic hand manipulation," Biomimetics, vol. 8, no. 3, p. 328, 2023. doi: 10.3390/biomimetics8030328.

[3] M. Atzori and H. Müller, "Control capabilities of myoelectric robotic prostheses by hand amputees: A scientific research and market overview," Frontiers in Systems Neuroscience, vol. 9, p. 162, Nov. 2015. doi: 10.3389/fnsys.2015.00162.

[4] B. Peerdeman, D. Boere, H. Witteveen, and R. Huis, "Myoelectric forearm prostheses: State of the art from a user-centered perspective," Journal of Rehabilitation Research and Development, vol. 48, no. 6, pp. 719–738, 2011. doi: 10.1682/JRRD.2010.08.0161.

[5] C. Ahmadizadeh, M. Khoshnam, and C. Menon, "Human machine interfaces in upper-limb prosthesis control: A survey of techniques for preprocessing and processing of biosignals," IEEE Signal Processing Magazine, vol. 38, no. 4, pp. 12–22, Jul. 2021. doi: 10.1109/MSP.2021.3057042.

[6] M. R. K. Kadavath, M. Nasor, and A. Imran, "Enhanced hand gesture recognition with surface electromyogram and machine learning," Sensors, vol. 24, no. 16, p. 5231, Aug. 2024. doi: 10.3390/s24165231.

[7] G. Yu, Z. Deng, Z. Bao, Y. Zhang, and B. He, "Gesture classification in electromyography signals for real-time prosthetic hand control using a convolutional neural network-enhanced channel attention model," Bioengineering, vol. 10, no. 11, p. 1324, Nov. 2023. doi: 10.3390/bioengineering10111324.

[8] D. R. Cutipa-Puma, C. G. Coaguila-Quispe, and P. R. Yanyachi, "A low-cost robotic hand prosthesis with apparent haptic sense controlled by electroencephalographic signals," HardwareX, vol. 14, p. e00439, Jun. 2023. doi: 10.1016/j.ohx.2023.e00439.

[9] M. S. Song, S. G. Kang, K. T. Lee, and J. Kim, "Wireless, skin-mountable EMG sensor for human-machine interface application," Micromachines, vol. 10, no. 12, p. 879, 2019. doi: 10.3390/mi10120879.

[10] W. Geng, Y. Du, W. Jin, W. Wei, Y. Hu, and J. Li, "Gesture recognition by instantaneous surface EMG images," Scientific Reports, vol. 6, p. 36571, 2016. doi: 10.1038/srep36571.

[11] R. Rodrigues, D. Miranda, V. Carvalho, and D. Matos, "Design and development of an EMG upper limb controlled prosthesis: A preliminary approach," Actuators, vol. 14, no. 5, p. 219, Apr. 2025. doi: 10.3390/act14050219.

[12] A. Adetunla, C. Anulunko, T.-C. Jen, and C. K. Chan, "Integration of EMG and machine learning for real-time control of a 3D-printed prosthetic arm," Prosthesis, vol. 7, no. 6, p. 166, Dec. 2025. doi: 10.3390/prosthesis7060166.

[13] R. N. Khushaba, S. Kodagoda, M. Takruri, and G. Dissanayake, "Toward improved control of prosthetic fingers using surface electromyogram (EMG) signals," Expert Systems with Applications, vol. 39, no. 12, pp. 10731–10738, Sep. 2012. doi: 10.1016/j.eswa.2012.02.192.

[14] M. P. Selvan, R. Raj, R. Gowtham Sai, S. Jancy, and V. A. Mary, "Prosthetic hand using EMG," Journal of Physics: Conference Series, vol. 1770, no. 1, p. 012018, 2021. doi: 10.1088/1742-6596/1770/1/012018.

[15] R. Tamilselvi, A. Merline, M. P. Beham, R. V. Anand, M. S. Karthik, and R. H. Uthayakumar, "EMG activated robotic arm for amputees," in Proc. 2nd Int. Conf. Inventive Systems and Control (ICISC), 2018, pp. 456–461. doi: 10.1109/ICISC.2018.8399114.

[16] Abhishankar, K. K. Radhakrishnan, V. K. Satish, M. Ahamed, A. C. Benny, D. B. Kapakayala, and R. S. Dondapati, "EMG-controlled prosthetic arm with an actuator mechanism for sensory feedback," AIP Conference Proceedings, vol. 3037, no. 1, p. 020034, 2024. doi: 10.1063/5.0192534.

[17] E. Guzmán-Quezada, S. Lomeli-Garcia, J. Velazco-Garcia, M. Jonguitud-Ceballos, A. Vega-Martinez, J. Ojeda-Galvan, F. J. Alvarado-Rodríguez, and F. Reyes-Jiménez, "Development of an electromyography signal acquisition prototype and statistical validation against a commercial device," Sensors, vol. 24, no. 21, p. 6787, Oct. 2024. doi: 10.3390/s24216787.

[18] Z. Zhang, T. Han, C. Huang, and C. Shuai, "Hardware and software design and implementation of surface-EMG-based gesture recognition and control system," Electronics, vol. 13, no. 2, p. 454, Jan. 2024. doi: 10.3390/electronics13020454.

[19] L. Chaplot, S. Houshmand, K. B. Martinez, J. Andersen, and H. Rouhani, "Optimizing sensor placement and machine learning techniques for accurate hand gesture classification," Electronics, vol. 13, no. 15, p. 3072, Aug. 2024. doi: 10.3390/electronics13153072.

[20] K. Sharmila, T. V. Sarath, and K. I. Ramachandran, "EMG controlled low cost prosthetic arm," in Proc. IEEE Distributed Computing, VLSI, Electrical Circuits and Robotics (DISCOVER), Mangalore, India, 2016, pp. 169–172. doi: 10.1109/DISCOVER.2016.7806239.

[21] A. R. Asif, A. Waris, S. O. Gilani, M. Jamil, H. Ashraf, M. Shafique, and I. K. Niazi, "Performance evaluation of convolutional neural network for hand gesture recognition using EMG," Sensors, vol. 20, no. 6, p. 1642, 2020. doi: 10.3390/s20061642.

[22] M. S. Kaiser, Z. I. Chowdhury, S. Al Mamun, A. Hussain, and M. Mahmud, "A neuro-fuzzy control system based on feature extraction of surface electromyogram signal for solar-powered wheelchair," Cognitive Computation, vol. 8, no. 5, pp. 946–954, 2016. doi: 10.1007/s12559-016-9398-4.

[23] C. Wu, S. F. Atashzar, M. M. Ghassemi, and T. Alhanai, "An LSTM feature imitation network for hand movement recognition from sEMG signals," in Proc. ICASSP 2025 – IEEE Int. Conf. Acoustics, Speech and Signal Processing, 2025, pp. 1–5. doi: 10.1109/ICASSP49660.2025.10890441.

[24] K.-Y. Lian, C.-C. Chiu, Y.-J. Hong, and W.-T. Sung, "Wearable armband for real time hand gesture recognition," in Proc. IEEE Int. Conf. Systems, Man, and Cybernetics (SMC), 2017, pp. 2992–2995. doi: 10.1109/SMC.2017.8123083.

[25] K. Ozhikenov, Y. Nurgizat, A.-A. Ayazbay, A. Uzbekbayev, A. Sultan, A. Nussibaliyeva, N. Zhetenbayev, R. Kalykpaeva, and G. Sergazin, "Design and testing of an EMG-controlled semi-active knee prosthesis," Sensors, vol. 25, no. 24, p. 7505, Dec. 2025. doi: 10.3390/s25247505.

Journal of
Big Data &
Smart City

ISSN (Print) : 2706-7912
ISSN (Online) : 2788-4112

Journal of Big Data & Smart City is a bi-annually published international journal, of Middle East College, Muscat, Oman. The journal, which started in 2021-2022, publishes multidisciplinary research work related to broad fields of 'Big Data' and 'Smart City' spanning across the subject areas of computer science, engineering and technology, social sciences, sustainability, urban planning and development, big data-driven innovative solutions, case studies, novel approaches, and visionary ideas and applications. The Journal especially aims to plug the gap in publication and reporting on research and associated activities being carried out in Middle East and North Africa region. It thus aims to further promote dissemination of knowledge, research, and scholarly work in the geographical area and beyond to accelerate work on solutions on current issues and challenges focusing theme of the journal. The editorial board of the journal looks forward to receiving submissions of relevant and current research to further support other researchers with useful insight leading to more debates/deliberations and work in the related areas.

Published by:
Middle East College
Knowledge Oasis Muscat
P.B. No. 79, Al Rusayl
Postal Code: 124
Sultanate of Oman
Tel: +968 24531400
info@mjbdsc.org

VOLUME 6
ISSUE 2
SPRING 2026
www.mjbdsc.org